UNIVERSITY OF ALBERTA

NUMERICAL SIMULATION OF THE EFFECTS OF INDUSTRIAL MPLEXES ON CONVECTIVE RAIN SHOWERS

BY

Shucai Guan

A THESIS SUBMITTED TO THE FACULTY OF GRADUATE STUDIES AND RESEARCH IN PARTIAL FULFILMENT OF THE REQUIREMENTS FOR THE DEGREE OF DOCTOR OF PHILOSOPHY IN METEOROLOGY

DEPARTMENT OF GEOGRAPHY

Edmonton, Alberta

Spring, 1995

UNIVERSITY OF ALBERTA

RELEASE FORM

NAME OF AUTHOR: Shucai Guan

TITLE OF THESIS: Numerical simulation of the effects of industrial complexes on convective rain showers

DEGREE: Doctor of Philosophy

YEAR THIS DEGREE GRANTED: Spring 1995

Shucai Guan

Shucai Guan

3A, 9004-112 St.

Edmonton, Alberta

Canada T6G 2C5

Dec. 22, 1994

UNIVERSITY OF ALBERTA

FACULTY OF GRADUATE STUDIES AND RESEARCH

The undersigned certify that they have read, and recommend to the Faculty of Graduate Studies and Research for acceptance, a thesis entitled: NUMERICAL SIMULATION OF THE EFFECTS OF INDUSTRIAL COMPLEXES ON CONVECTIVE RAIN SHOWERS, submitted by Shucai Guan in partial fulfilment of the requirements for the degree of DOCTOR OF PHILOSOPHY in METEOROLOGY.

G. W. Reuter

G. W. Reuter, Supervisor

E. L. Jackson for H. G. Leighton

H. G. Leighton, External Examiner

J. Ronald Eyton

J. R. Eyton

S. S. Shen

Edward Lozowski

E. P. Lozowski

J. D. Wilson

J. D. Wilson

15 December, 1994

Abstract

An axisymmetric cloud model is used to investigate the evolution of convective clouds and associated rain showers that develop in a calm atmosphere over a large industrial complex with cooling towers. The complex has a continuous release of sensible waste heat, water vapour and anthropogenic cloud condensation nuclei that affect the cloud convection. The simulated convection is in fair agreement with observations for a particular cloud developing over a large oil refinery. Sensitivity experiments are run for two different soundings to quantify how the convection and rainfall depend on the magnitude of the waste energy loss, the area of the source region, the degree of pollution, and other parameters. The Factor Separation Method is applied to quantify the relative contributions of the heating, moisturizing and pollution as individual factors to the convective rain shower, as well as the relative contributions due to the mutual interactions among two or three of these factors. The major findings are the following.

1) Without sustained waste heat input the model convection ceases. The model convection becomes progressively more intense and developed more rain as the rate of total waste energy heat released from the industrial complex is increased. Doubling the total waste energy amount from its control case value causes a 15-fold increase in 3-h rainfall values. However, reducing the control case value of total waste energy release by 20% leads to much weaker convection

without rain

2) The triggering of cumulus clouds is reduced when the waste energy is released as latent heat rather than sensible heat. As the relative contribution of sensible heat increases, so does the intensity of the circulation and the rainfall.

3) The cloud formation depends on the area of the heat source: a wider source tends to delay and to weaken the convection. Specifically, when the area is doubled the simulated cloud appears 2.5 min later and the 3-h rainfall is reduced by 88%. Moreover, the maximum total kinetic energy is reduced by 26%.

4) Model convection is only slightly sensitive to the horizontal distribution of the sensible and latent heat fluxes within the source region.

5) Pollution has only a minor effect on the development of the model cloud and rainfall. Heavy pollution increases accumulated rainfall by 1.8%, whereas light pollution conditions indicate an even smaller rainfall enhancement of 0.2%.

6) For typical magnitudes of sensible heat, latent heat and industrial pollution conditions, the model results suggest that sensible heat is the most important individual contributor for cloud development and rainfall. The contributions arising from interaction between the heat source and the pollution effects are significant for typical atmospheric conditions.

Acknowledgments

I would like to present my sincere thanks and appreciation to Dr. G. W. Reuter, my supervisor, for his patient advice and his valuable guidance during his supervision of this thesis. I am also thankful to Drs. E. P. Lozowski and J. D. Wilson for their suggestions on a draft of this thesis. Thanks are extended to Drs. H. G. Leighton, S. Shen, and J. R. Eyton for serving on my examining committee.

The help and friendly attitude of Mr. Terry Thompson, Ms. Laura Smith, Mr. Victor Chung, Ms. Lingyan Xin and others are very much appreciated.

Financial support for this research was provided by Atmospheric Environment Service and Natural Sciences and Engineering Research Council of Canada.

Table of contents

List of Tables

List of Figures

Appendix 1

Chapter 1

Introduction

1.1 Research topic

Large industrial complexes such as clusters of electrical power plants and oil refineries release large amounts of waste energy into the atmosphere. The waste energy is usually emitted through natural-draft cooling towers as both sensible and latent heat. In addition to the enhanced fluxes of heat and moisture, the fossil-fuelled combustion of power plants emits significant amounts of pollutants such as sulphur dioxide. Once in the atmosphere the sulphur dioxide is converted into sulphate aerosols that can act as very efficient cloud condensation nuclei (CCN) due to their affinity for water (Hobbs, 1993).

There are concerns about the effects of the waste heat, moisture and abundant CCN on the possible triggering of cumulus convection (Hanna and Gifford 1975, Kramer et al. 1976). In a conditionally unstable atmosphere, even a small disturbance might result in cloud formation and the release of much larger amounts of latent energy stored within the atmosphere itself. Once convection has been triggered, it might become organized and in some circumstances might develop into a local storm with significant rainfall or hail, which can cause severe damage.

In this thesis, we will use a numerical cloud model to

quantify the effects of industrial complexes on convective clouds and rain showers. The investigation is designed to determine the relative roles of waste heat, vapour, and industrial pollution emitted from large industrial facilities in affecting convective rain showers. Before a more precise statement of the thesis problem is formulated, some pertinent literature will be briefly reviewed to provide some essential background. First, we discuss the essential features of numerical cloud models and their application to simulate moist convection. Second, we review modifications to weather and climate due to mankind's activities. Thereafter, the focus is moved toward observational and modelling studies of the atmospheric effects due to large industrial facilities.

1.2 Cumulus cloud models

A cumulus cloud model is a mathematical description of the complex interactions of dynamic, thermodynamic and cloud physical processes that occur in convective clouds. The air motions in and around clouds are difficult to describe mathematically, because of the latent heat accompanying phase transitions of the water substance, and the drag exerted on the air by the condensed water. The basic equations of a numerical cloud model are the equations of the conservation of momentum, mass and energy. These result in prognostic partial differential equations for the three components of the velocity vector, temperature, pressure (or density) and the water

substance in its various phases. Because these partial differential equations are nonlinear and highly coupled with each other, they have to be solved using numerical approximation techniques.

a. Dynamics

The depth of a cumulus cloud is of the same order of magnitude as its width, i.e., the aspect ratio of vertical to horizontal size is close to unity. This implies that the vertical component of the velocity vector is typically of the same magnitude as the horizontal wind speed. Likewise, vertical and horizontal accelerations have similar magnitudes. A consequence of this is that the equation for vertical motion is prognostic with an acceleration term. Also, the pressure is not in hydrostatic balance. The existence of pressure deviations from their hydrostatic mean values allows the equations of motions to support acoustic waves. Acoustic waves contain only small amounts of energy and do not significantly affect the dynamics of real clouds. However, due to small truncation errors in a numerical approximation of convective motion, sound waves can develop in the numerical model. Once formed, the sound waves grow exponentially and thereby jeopardize the numerical stability of the computational scheme. To prevent such spurious acoustic waves from growing unrealistically, they have to be resolved adequately. This requires the numerical time step for the integration method to

be extremely small (about 0.1 second for typical spatial resolution). However, such small time steps tend to provide an inaccurate solution for the grid-resolved flow due to the buildup of repeated truncation errors. In addition, time integrations with a small time step become computationally expensive.

There are two approaches to overcome this issue of a small time step. The one approach is the use of a time-splitting scheme: All terms of the equations involving perturbation pressure use a time step several times smaller than used for the other terms. Cloud models that use this time-splitting approach are termed fully compressible models. Examples of these models were developed by Klemp and Wilhelmson (1978), and Cotton and Tripoli (1978). The alternative to the time-splitting technique is to adopt the deep anelastic set of equations. The basic assumption of the anelastic equations is that the local rate of change of air density is negligible compared to its changes due to advection. A careful scale analysis shows that the deep anelastic assumption is indeed valid except for locations of extremely rapid heating such as during rapid discharge of electric lightning (Ogura and Phillips, 1962). Examples of cloud models based on the system of deep anelastic equations are the models developed by Clark (1973), Steiner (1973), Orville and Kopp (1977), and Schlesinger (1975, 1984).

b. Parameterization of microphysics in warm clouds

Even if the convective motion within the cloud is fully resolved by the model grid structure, the mechanisms controlling the detailed evolution of the water droplets cannot be modelled explicitly. The microphysical processes such as condensation, evaporation, collision and coalescence occur on scales far too small to be treated explicitly. Thus, microphysical processes have to be approximated by some formulation based on parameters that are available from the resolved scale. This approximation is termed the cloud microphysical parameterization scheme. Ideally, the parameterizations should capture the essence of the known microphysics in simple formulations of the processes with few free parameters. The problem is that, in some cases, the physics is not sufficiently well known, or is too complex to be fully captured in simple formulations.

The most popular approach to parameterizing the warm-cloud physics is to partition the condensed liquid water into two separate categories: cloud water and rainwater. Cloud water consists of all the small droplets with diameters less than 0.1 mm and it is assumed that these droplets move with the air (i.e., they have negligible terminal fall speeds). Rain water, on the other hand, consists of the large drops which have finite terminal fall speeds depending on their sizes. Kessler (1969) first developed a simple parameterization of the rate of autoconversion of cloud water

to rainwater that mimics the observed initial broadening of the cloud droplet spectrum into "embryonic" raindrops. Once embryonic raindrops are formed, Kessler hypothesized that the water content converted to rain is distributed in the inverse exponential distribution function formulated by Marshall and Palmer (1948). With a fixed size distribution of raindrops it is possible to deduce parameterizations for accretion of cloud water by falling raindrops, evaporation of raindrops, and an effective mass-weighted terminal fall speed of the rainwater. Most cloud models use bulk water parameterization schemes that are similar to Kessler's original formulation, differing only in the choice of different size distribution of raindrops or a different threshold value for the autoconversion of cloud water into rainwater.

One major shortcoming of Kessler's warm-rain parameterization scheme is that it is unable to distinguish between continental and maritime air masses. Continental cumuli differ from maritime cumuli in that maritime cumuli have a much narrower size spectrum of cloud droplets which is slower to broaden into embryonic rain. Berry (1968) extended Kessler's bulk-water parameterization scheme in that the rate of autoconversion of cloud water to rain was assumed dependent on the cloud droplet concentration and the dispersion of the cloud droplet distribution. In this thesis we will use both Kessler's and Berry's parameterization schemes for warm rain processes.

The cloud microphysics interact with the dynamics. For example, the presence of cloud water and rainwater changes the spatial distribution of the buoyancy. The cloud updraft becomes weakened due to the weight of the condensed water that yields "loading" to the upward motion. The condensed water which is removed from the upper parts of a rising cloud tower often accumulates at lower levels, eventually leading to the cell's decay (Srivastava 1967). An even more important consequence of the formation of cloud and rain is the thermodynamic effect due to release of latent heat during condensation and the cooling during vaporization of cloud and rain (e.g. Liu and Orville, 1969). Numerical results suggest that thermodynamic effects are far more important than water-loading effects, particularly, during the maturing and decaying stages of the cumulus lifetime, when the rain evaporates below the cloud base (Murray and Koenig 1972). The subcloud cooling causes downward acceleration that develops downdrafts. The downdrafts eventually lead to termination of the convective cell due to cutting off its moisture supply. The downdrafts often lead to enhanced convergence near the ground which stimulates the formation of new convective cells.

c. Applications of numerical cloud models

Numerical cumulus models require realistic initial and boundary conditions to simulate cumulus convection. The initial conditions for model variables are usually from an

observed environmental sounding, assuming horizontal uniformity. Convection is then triggered by adding a small initial perturbation in temperature, humidity or vertical motion. Alternatively, one can specify surface heat and moisture fluxes. Comparison studies between observed and numerically simulated convection suggest that cloud models are able to simulate convincingly the large-scale characteristics of convective clouds. Particularly good results are found for severe storms in midlatitudes. For example, Wilhelmson and Klemp (1981) were able to reproduce many observed characteristics of a severe supercell storm, such as the direction of its movement, the timing of splitting into two daughter storms, and the shape of the precipitation pattern. In fact, the agreement they found between simulations and observations was remarkable. Computer cloud models that simulate nature so closely can provide detailed insights to the dynamic processes of storm development that are not available from radar or aircraft observations. A good example for use of cloud models to better understand severe storm dynamics is the initiation and intensification of a pair of counterrotating vortices, typically 3-10 km across. Tornadoes are thought to develop by the intensification of the cyclonical mesovortex (Klemp et al., 1981). Model simulations have clarified under which atmospheric conditions the rotation amplifies and which processes are responsible for the transition of the storm to its tornadic phase.

Cloud models have succeeded in simulating convection in the tropics (e.g., Turpeinen and Yau, 1981) and multicellular storms (e.g., Wilhelmson and Chen, 1982). Their use has led to better understanding of the role of mesoscale lifting in organizing and sustaining convective storms (e.g., Schlesinger, 1982). Cloud models have also been able to simulate the interaction of neighbouring cells in an ensemble of cumulus clouds (Yau and Michaud, 1982). The simulations have suggested that formation of a new cell is closely associated with the convergence of downdrafts from neighbouring clouds.

The physical processes that lead to merging of neighbouring cells have also been investigated using cloud models (e.g., Orville et al., 1980; Turpeinen, 1982). The merger is mainly due to a large perturbation in the pressure field that causes a "bridging" between the merging clouds. Clark et al. (1986) found that a favourable perturbation pressure distribution arises from constructive interference of gravity waves, excited by each of the clouds. Furthermore, the presence of precipitation accentuates the cloud-related pressure anomalies in the subcloud layer. Thus, precipitating downdraft outflows and their interactions between neighbouring clouds play a key role in the merger process.

When coupling a cloud model with a detailed surface layer model, the simulated spatial and temporal distributions of cumulus clouds agree closely with observations (Smolarkiewicz

and Clark, 1985). Sensitivity tests of the separate effects of topography and surface fluxes suggest that the fractional cloud cover is mainly determined by the surface orography. However, variations in soil type and vegetation influence the spatial location of individual cells in the cloud ensemble.

Recently cloud models have been applied to simulate large mesoscale weather systems. Rotunno and Emanuel (1987) used a cloud model to investigate the formation of a hurricane. Their results show that a weak vortex can amplify into hurricane-like strength in an atmosphere which is neutral to cumulus convection. The dramatic amplification is fed solely by the air-sea interaction instability. Hedley and Yau (1991) used a cloud model to simulate wintertime explosive cyclogenesis over the midlatitude ocean. They found that the structure of the intense warm front observed ahead of the rapidly deepening cyclone required modelling by nonhydrostatic dynamics. This was crucial to simulate adequately the rapid formation of the extremely intense frontal structure, which aided in the rapid spin up of the cyclone.

Dudhia and Moncrieff (1989) simulated a line of multicell storms adjoined by a short segment of three supercells. A well-defined mesovortex was associated with the stratiform precipitation region, which only existed rearward of the line of multicell storms. The line of flanking supercells was not accompanied by trailing stratiform rain. The model results indicated that the updraft-generated cyclonic vorticity

produced within the supercell flanking line strongly influenced circulation. It greatly counteracted the anticyclonic flow occurring at upper levels and left a significant net cyclonic vorticity over an appreciable portion of the troposphere. Cloud models have also been used to better understand the dynamics of midlatitude squall lines. Model simulations reproduce realistically the observed multi-cell structure whereby new cells form in the unstable air ahead of the storm. These cells are then lifted and accelerated rearward over an evaporatively chilled cold pool (e.g. Fovell and Ogura 1988, 1989). Skamarock et al. (1994) simulated two squall lines in an environment characterized by shallow weak shear and an absence of large-scale forcing. In simulations without Coriolis forcing, the presence of line ends leads to mature symmetric systems characterized by a central region of strong convection, trailing flanks of weaker convection, and a strong centrally focused rear inflow. Simulations that include Coriolis forcing lead to asymmetric systems with significant system growth and migration to the right of the original system centerline. In both cases the evolution of the leading-line convection is primarily controlled by the surface cold pool expansion. The structure of the rear-inflow circulations in squall lines was further investigated by Weisman (1992). His results suggest that ambient convective available potential energy (CAPE) and the vertical wind shear together control the strength and structure of the rear-inflow

circulation. For environments characterized by weak shear and weak CAPE, the rear-inflow jet descends and spreads along the surface well behind the leading edge gust front, and the subsequent convective activity becomes weaker. However, for environments characterized by strong shear and strong CAPE, a line of deep convective cells is maintained along the gust front.

1.3 Mankind's impact on microclimates

Mankind's most profound influence on the atmosphere is probably its modification of local microclimates by the construction of large cities. The construction of buildings, roads and factories destroys existing microclimates and creates new ones. There are three main effects of urban structures discussed below:

1) Production of heat

Urban areas are warmer than the surrounding countryside due to the direct production of heat by combustion and the delayed release of heat stored during the day. The urban heat island effect is most pronounced under clear skies and light synoptic wind situations (Oke, 1973). The urban-rural temperature difference usually peaks during the night.

2) Modification of atmospheric composition

City atmospheres are liable to pollution in the form of smoke particles, sulphur dioxide and other gases, resulting from combustion. These pollutants provide abundant

condensation nuclei, increase cloudiness, and cut down the passage of sunlight. The character of domestic power demands causes city smoke pollution to have seasonal and diurnal cycles. Pollution and the associated fog, termed smog, reduce incoming sunshine, particularly when the sun's rays strike the smog layer at low angles.

3) Alteration of surface albedo and roughness

Urban structures affect the movement of air by producing channelling effects in street "canyons". Roughening the surface also produces turbulence which usually results in weaker city wind speeds compared to those of surrounding rural areas.

Urban influences on precipitation are more difficult to determine than thermal and wind effects. It is now fairly certain, however, that urban areas are responsible for local conditions that can trigger excesses of precipitation under marginal conditions (Changnon, 1981). The increase in precipitation amounts just downwind of urban areas is related to the high surface roughness of the urban area, which results in low-level convergence and thereby upward vertical velocities, as well as upward motions caused by the enhanced surface heating. Hjelmfelt (1982) conducted numerical simulation experiments of the urban heat island of St. Louis and produced rising air motion downwind of the city. Such a pattern was obtained because of the urban surface roughness convergence effect and the downwind shifting of the heat

island circulation by the large-scale flow. Hjelmfelt's results are consistent with the hypothesis that the increased summer rainfall in the St. Louis area comes from the enhanced heat fluxes and surface roughness (Huff and Vogel, 1978). The increase in urban precipitation has also been attributed to a large number of ice nuclei due to anthropogenic pollution.

1.4 Cloud convection affected by industrial facilities

This thesis deals with the unintentional effects on convective rainfall of an industrial facility for certain meteorological conditions. The facility in mind is either a large electrical power station, an oil refinery or a huge paper mill. Its spatial dimension is a few hundreds of meters and it is located on flat terrain. Commonly, such facilities require extensive cooling systems that release their uneconomic heat into the atmosphere. The waste heat released to the atmosphere is usually a combination of latent and sensible heat (through evaporative cooling towers), but can be in the form of sensible heat alone (through dry natural-draft towers).

Industrial facilities typically also emit significant amounts of pollutants into the atmosphere. As these pollutants often occur in the size range of a few tenths of a micrometer and are water soluble, they can act as CCN (Hobbs et al., 1970; Hindman et al., 1977a; Hobbs, 1993).

Possible atmospheric effects of large amounts of waste

energy and pollutants emitted over a small area are increasing fog and snowfall (Hanna and Gifford 1975; Kramer et al. 1976; Campistron 1987; Changnon et al. 1991). In this thesis we focus exclusively on the possible triggering and enhancing of convective rain showers due to waste energy and pollutants released into a conditionally unstable atmosphere. When the rising heat and vapour plume released from the cooling towers reach the condensation level, cloud condensation will increase the upward buoyancy, resulting in cumulus convection that will "feed" on the much larger amounts of latent heat stored within the conditionally unstable atmosphere itself. Thus the perturbation arising from the cooling system might sometimes trigger large convective clouds and related events such as strong winds, heavy rain, and lightning.

It is hard to quantify the effects of the waste heat emission on convective clouds, because of the big expense associated with detailed cloud observations in different atmospheric conditions. It is thus no surprise that only a few observational programs of "industrially spawned" cumuli have been undertaken. Stout (1962) documented preferential cumulus formation over industrial complexes. Extensive aircraft measurements were sampled through horizontal traverses of an isolated cumulus cloud which was obviously caused by the presence of a large oil refinery complex at Wood River in Illinois (Auer 1976). Auer documented the temperature, vertical velocity, and microphysical structure in a quasi-

stationary cumulus cloud and stated that his observations might permit evaluation of numerical cloud models.

Hobbs et al. (1970) reported that an industrial complex increased precipitation by more than 30%. They suggested that the increased precipitation was a consequence of the increased numbers of very efficient CCN emitted into the atmosphere by the industrial source, that is, the pollution increased the amount of the local rainfall. This suggestion was supported by Eagan et al.'s (1974) observation. Eagan et al. observed that clouds formed in the plume from a paper mill had a much broader spectrum of droplet size than those formed in the ambient air. The former clouds contained a significant number of droplets with diameters > 30 μm, as well as a large number of smaller droplets, so they thought that precipitable drops should form in them very efficiently by the coalescence mechanism.

It should be stressed that pollutants can also act as additional ice nuclei and thereby influence the mixed-phase microphysics (Hobbs, 1993). This might not only influence the production of precipitation, but could also modify the radiative properties of clouds. For a review of the effects of industrial pollution on cloud radiation we refer to Coakley et al. (1987), Radke et. al. (1990) and Hobbs (1993).

The alternative to expensive field observations is to use numerical models. Comparing the results from a series of carefully selected model experiments can determine the

sensitivity of convection to the strength and size of the waste energy source. Model experimentation can also play an important role in the planning the siting of new industrial facilities.

Early attempts to model "industrial cumuli" were made with a one-dimensional cloud model (Hanna 1976). This simple approach, however, cannot adequately predict the convective circulation as it does not allow for horizontal variation in cloud conditions. Three-dimensional cloud models are required to model an environmental wind field that varies realistically both in direction and speed with altitude. However, they require extensive computing resources. This, coupled with the fact that many numerical experiments with different input parameters are needed, has prohibited the actual use of three-dimensional simulations of industrial clouds. Instead, modellers have used two-dimensional slab-symmetric models that simulate conditions in a vertical plane, assuming that there is no variation of quantities in the orthogonal direction. Murray et al. (1978) used a slab-symmetric model to simulate Auer's (1976) observations of the "industrially spawned" cumulus that formed over the oil refinery complex of Wood River, Illinois. One of their major conclusions was that the careful use of time-dependent two-dimensional cloud models could provide an effective tool in siting and planning new industrial facilities. Using the same slab-symmetric model, Koenig et al. (1978) compared numerical experiments that had

different ratios of sensible to latent heat release to evaluate the relative importance of temperature increase versus vapour increase. For a fixed amount of total heat emission, the convection became more intense as the sensible heat component increased. An important implication of this finding is that a cooling system using only dry natural-draft towers may not be the optimal solution that minimizes local environmental disturbances.

Hane (1978) also used a slab-symmetric cloud model to quantify the atmospheric effects of nuclear energy centres that release large amounts of waste heat. The effects of excess water vapour from the nuclear energy centre upon an existing squall line convective element which passed over the centre and the initiation of convection by both sensible heat and latent heat consistent with that released by cooling towers in such centre are investigated. The simulated results suggested that the water vapour from a source characteristic of a nuclear energy plant was sufficient to cause discernible effects upon existing deep convection of the squall line type and that both sensible heat and latent heat released by the nuclear energy centre initiated deep convection in some cases representative of summer in the east-central and southeastern United States. Orville et al. (1981) used a slab-symmetric cumulus model to simulate heat emission from a power park for severe storm conditions. The power park emitted the larger waste heat over a larger area than the above complexes. They

found that the addition of waste energy had little impact on triggering severe storms. Furthermore, if all the waste energy was emitted as sensible heat, the severity of the simulated storm could be reduced. This finding is in sharp contrast with Hane's simulations that indicated that the preconditioning of boundary layer air (due to the destabilization and humidity increases from the cooling tower effects) usually enhances the convection.

Possible effects of changing the chemical composition of the air due to industrial pollutants have been studied with numerical models. Hindman et al. (1977b) used a simple dynamical model but with detailed treatment of warm microphysical processes. The input into their model was taken from an observed spectrum of droplet sizes sampled over a paper mill (Hindman et al., 1977a). Their model results indicated that the higher concentrations of large droplets in the plume from the large paper mill should not cause any significant changes in the rainfall, that is, the large and giant CCN emitted by the mill were not by themselves responsible for the increased rainfall measured in the vicinity of the mill. It should be mentioned that there is a rich literature of numerical modelling studies that deal with how cumulus clouds change the distribution of pollutants through transport and by enhancing some chemical reactions due to the large wet surface area of numerous cloud droplets (e.g. Tremblay and Leighton 1986). The focus of these studies is

usually on how the pollutants change the acidity of the precipitation, rather than how the pollutants affect the cumulus dynamics and precipitation amounts.

1.5 Statement of research problem

Most of the modelling studies focusing on industrially spawned clouds have used a model geometry that assumes slab-symmetry [illegible], it is well-known that the slab-symmetric assumption has some major shortcomings as the wind cannot flow around a cloud tower, thereby forcing the air to subside or rise (Schlesinger 1984). Veering of the environmental wind cannot be reproduced. Heat and moisture sources of finite dimensions also cannot be treated realistically. Hane (1978) discussed in detail the shortcomings of representing a finite heat source region with an infinite band of heat. He argued that this slab-symmetric arrangement may be adequate to study the initiation of convection, but would underestimate the rapidity with which clouds form and the intensity of the ensuing deep convection.

Based on linear theory, Reuter and Jacobsen (1993) showed that the contribution of diabatic heating towards the circulation is largest when the ambient wind is zero. In such a case, the heat plume remains intact and can build up strong upward buoyancy. In the absence of wind, the three-dimensional airflow triggered by an axisymmetric heat source can be modelled using an axisymmetric cloud model, in which the

equations are developed in cylindrical polar coordinates and all azimuthal derivatives are set to zero. Axisymmetric models require far less computing resources than fully three-dimensional models, yet at the same time they overcome some of the principal objections of the slab-symmetric assumption mentioned above.

The purpose of this thesis is to use a time-dependent axisymmetric cumulus model to quantify the sensitivity of the convection to the waste energy (emitted as sensible and latent heat) and pollutants. The atmospheric condition examined is a moist airmass with conditionally unstable stratification, static on the large scale (i.e., windless case). Furthermore, the convective condensation level has a temperature far above 0^0 C so that collision-coalescence is the dominant rain producing mechanism. In fact our model will not include ice phase processes. Pollution effects are included in our cloud model by adjusting the cloud microphysical parameterization schemes, such as the conversion rate of cloud water to rainwater.

This thesis deals with problems such as the following:

(1) How does the amount of the total emitted energy affect the life cycle of convective clouds and associated rain showers?

(2) For a fixed amount of total waste energy released, how does the relative contribution of sensible heat affect the rain showers?

(3) How does the size of the heat source affect the growth rate and intensity of the convection?

(4) Does the distribution of perturbation temperature and moisture within the source region affect the triggering of clouds?

(5) How much does the pollution rising from a large industrial facility affect the timing of the rainfall, the magnitude of the rainfall rate, or the total accumulated rainfall?

(6) What is the relative importance of waste sensible heat, vapour fluxes and pollution on changing convective rainfall? And how important is the mutual interaction among these three forcing factors?

1.6 Organization of thesis

This thesis consists of six chapters. Chapter 2 gives a detailed description of the model equations, numerical methods, and parameterization schemes. The means of including the sensible and heat release from an industrial facility is also discussed in the chapter. Chapter 3 describes model results that clarify the role of sensible heat and latent heat ejected by industrial complexes on convective clouds and rainfall. Sensitivity experiments are run for two different soundings. This chapter also deals with the evolution of the convection consisting of several life-cycles of individual cells. Chapter 4 introduces the treatment of pollution.

Sensitivity experiments are presented that allow an interpretation of how pollution affects convective rainfall. Chapter 5 combines the effects of waste energy and pollutants emitted from an industrial facility. A recently developed Factor Separation Method is utilized to quantify the individual as well as the mutual interactive effects of the three factors (sensible heat, vapour and pollution). The final chapter of this thesis summarizes the major findings and offers some suggestions for further research.

This thesis is written in paper format. Thus each chapter can be read independently as it has its own introduction, main section, conclusion, and references. The numbers assigned to tables, figures and equations refer to the current chapter. Chapter 3 has been accepted for publication by the Journal of Applied Meteorology and it will appear in the January 1995 issue. Chapter 4 is under review for possible publication in Atmospheric Environment.

References

Auer, A. H., Jr., 1976: Observations of an industrial cumulus. J. Appl. Meteor., 15, 406-413.

Berry, E. X., 1968: Modifications of the warm rain process. Proc. Nat. Conf. Weather Modif., 1st, Albany, N.Y. pp. 81-88.

Campistron, B., 1987: Interaction between a natural snowfall

and a cooling tower plume: An experimental study with a millimetric Doppler radar. Atmos. Environ., 21, 1375-1383.

Changnon, S.A. (Editor), 1981: METROMEX: A Review and Summary, Meteor. Monographs, **40**, Americ. Meteor. Soc., Boston, 181pp.

___, R.T. Shealy and R.W. Scott, 1991: Precipitation changes in fall, winter and spring caused by St. Louis. J. Appl. Meteor., 30, 126-134.

Clark, T. L., 1973: Numerical modelling of the dynamics and microphysics of warm cumulus convection. J. Atmos. Sci., 30, 857-878.

___, T. Hauf, and J. Kuettner, 1986: Convectively forced internal gravity waves: Results from two-dimensional numerical experiment. Q. J. R. Meteorol. Soc., 112, 899-925.

Coakley, J. A. Jr., R. L. Bernstein, and P. A. Durkee, 1987: Effect of ship-stack effluents on cloud reflectivity. Science 237, 1020-1022.

Cotton, W. R., and G. J. Tripoli, 1978: Cumulus convection in shear flow--three-dimensional numerical experiment. J. Atmos. Sci., 35, 1503-1521.

Dudhia, J., and M. W. Moncrieff, 1989: A three-dimensional numerical study of an Oklahoma squall line containing right-flank supercells. J. Atmos. Sci., 46, 3077-3107.

Eagan, R. C., P. V. Hobbs, and L. F. Radke, 1974: Particle

emissions from a large Kraft paper mill and their effects on the microstructure of warm clouds. J. Appl. Meteor. 13, 535-552.

Fovell, R. G., and Y. Ogura, 1988: Numerical simulation of a midlatitude squall line in two dimensions. J. Atmos. Sci., 45, 3846-3879.

___, and ___, 1989: Effect of vertical wind shear on numerically simulated multicell storm structure. J. Atmos. Sci., 46, 3144-3176.

Hane, E., 1978: The application of a two-dimensional convective cloud model to waste heat release from proposed nuclear energy centres. Atmos. Environ., 12, 1839-1848.

Hanna, S. R., 1976: Comments on "Observations of an industrial cumulus". J. Appl. Meteor., 15, 1232-1233.

___, and F. A. Gifford, 1975: Meteorological effects of energy dissipation at large power parks. Bull. Amer. Meteor. Soc., 56, 1069-1076.

Hedley, M., and M.K. Yau, 1991: Anelastic modeling of explosive cyclogenesis. J. Atmos. Sci., 48, 711- 727.

Hindman, E. E. II, P. V. Hobbs, and L. F. Radke, 1977a: Cloud condensation nuclei from a paper mill. Part I: Measured effects on clouds. J. Appl. Meteor. 16, 745-752.

___, P. M. Tag, B. A. Silverman, and P. V. Hobbs, 1977b: Cloud condensation nuclei from a paper mill. Part II: Calculated effects on rainfall. J. Appl. Meteor. 16, 753

755.

Hjelmfelt, M.R., 1982: Numerical simulation of the effects of St. Louis on mesoscale boundary airflow and vertical air motion: Simulations of urban versus non-urban effects. J. Appl. Meteor., 21, 1239-1257.

Hobbs, P. V., 1993: Aerosol-cloud-climate interactions. Academic press, Inc., San Diego, 233pp.

___, L. F. Radke, and S. E. Shumway, 1970: Cloud condensation nuclei from industrial sources and their apparent influence on precipitation in Washington State. J. Atmos. Sci. 27, 81-89.

Huff, F.A., and J.L. Vogel, 1978: Urban, topographic and diurnal effects on rainfall in the St. Louis region. J. Appl. Meteor., 17, 565-577.

Kessler, E. E., 1969: On the distribution and continuity of water substance in atmospheric circulations. Meteor. Monogr., No.32, Amer. Meteor. Soc., Boston, 84pp.

Klemp, J. B., and R. B. Wilhelmson, 1978: The simulation of three-dimensional convective storm dynamics. J. Atmos. Sci., 35, 1070-1096.

___, ___, and P. S. Ray, 1978: Observed and numerically simulated structure of a mature supercell thunderstorm. J. Atmos. Sci., 38, 1558-1580.

Koenig, L. R., F. W. Murray, and P. M. Tag, 1978: Differences in atmospheric convection caused by waste energy rejected in the forms of sensible and latent heats. Atmos.

Environ., 12, 1013-1019.

Kramer, M. L., D. E. Seymour, M. E. Smith, R. W. Reeves, and T. T. Frankenberg, 1976: Snowfall observations from natural-draft cooling tower plumes. Science, 193, 1239-1241.

Liu, J. V., and H. D. Orville, 1969: Numerical modelling of precipitation and cloud shadow effects on mountain-induced cumuli. J. Atmos. Sci., 26, 1283-1298.

Marshall, J. S., and W. M. Palmer, 1948: The distribution of raindrops with size. J. Meteorol., 5, 165-166.

Murray, F. W., and L. R. Koenig, 1972: Numerical experiments on the relation between microphysics and dynamics in cumulus convection. Mon. Wea. Rev., 100, 717-732.

___, ___, and P. M. Tag, 1978: Numerical simulation of an industrial cumulus and comparison with observations. J. Appl. Meteor., 17, 655-668.

Ogura, Y., and N. A. Phillips, 1962: Scale analysis of deep and shallow convection in the atmosphere. J. Atmos. Sci., 19, 173-179.

Oke, T.R., 1973: City size and the urban heat island. Atmos. Environ., 7, 769-779.

Orville, H. D., P. A. Eckhoff, J. E. Peak, J. H. Hirsch, and F. J. Kopp, 1981: Numerical simulation of the effects of cooling tower complexes on clouds and severe storms. Atmos. Environ., 15, 823-836.

___, and F. J. Kopp, 1977: Numerical simulation of life

history of a hailstorm. J. Atmos. Sci., 34, 1596-1618.

___, Y.-H. Kuo, R. D. Farley, and C. S. Hwang: 1980: Numerical simulation of cloud interactions. J. Rech. Atmos., 14, 499-516.

Radke, L. F., J. A. Jr. Coakley, and M. D. King, 1990: Direct and remote sensing observations of the effects of ships on clouds. Science 246, 1146-1149.

Reuter, G. W., and O. Jacobsen, 1993: Effects of variable wind shear on the mesoscale circulation forced by slab-symmetric diabatic heating. Atmos.-Ocean 32, 451-469.

Rotunno, R., and K. A. Emanuel, 1987: An air-sea interaction theory for tropical cyclones. J. Atmos. Sci., 44, 542-561.

Schlesinger, R. E., 1975: A three-dimensional numerical model of an isolated deep convective clouds: Preliminary results. J. Atmos. Sci., 32, 934-957.

___, 1982: Effects of mesoscale lifting, precipitation and boundary layer shear on severe storm dynamics in a three-dimensional numerical modeling study. Preprint, 12th Conference on Severe Local Storms. pp. 536-541. American Meteorological Society, Boston.

___, 1984: Effects of the pressure perturbation field in numerical models of unidirectionally sheared thunderstorm convection: two versus three dimensions. J. Atmos. Sci., 41, 1571-1587.

Skamarock, W. C., M. L. Weisman, and J. B. Klemp, 1994: Three-

dimensional evolution of simulated long-lived squall lines. J. Atmos. Sci., 51, 2563-2584.

Smolarkiewicz, P. K., and T. L. Clark, 1985: Numerical simulation of the evolution of a three dimensional field of cumulus clouds. Part I: Model description, comparison with observations and sensitivity studies. J. Atmos. Sci., 42, 502-522.

Srivastava, R. C., 1967: A study on the effects of precipitation on cumulus dynamics. J. Atmos. Sci., 24, 36-45.

Steiner, J. T., 1973: A three-dimensional model of cumulus cloud development. J. Atmos. Sci., 30, 414-435.

Stout, G. E., 1962: Cloud initiation in industrial areas. Proc. Symposium of Air Over Cities, Public Health Service, Sanitary Engineering Centre, Cincinnati, Ohio, SEC Tech. Rept. A62-5, 147-153.

Tremblay, A, and H. Leighton, 1986: A three-dimensional cloud chemistry model. J. Appl. Meteor., 25, 652-671.

Turpeinen, O., 1982: Cloud interactions and merging on Day 261 of GATE. Mon. Wea. Rev., 110, 1238-1254.

___, and M. K. Yau, 1981: Comparison of results from a three-dimensional cloud model with statistics of radar echoes on day 261 GATE. Mon. Wea. Rev., 109, 1495-1511.

Weisman, M. L., 1992: The role of convectively generated rear-inflow jets in the evolution of long-lived mesoconvective systems. J. Atmos. Sci., 49, 1826-1847.

Wilhelmson, R. B., and C. S. Chen, 1982: A simulation of the development of successive cells along a cold outflow boundary. J. Atmos. Sci., 39, 1466-1483.

___, and J. B. Klemp, 1981: A three-dimensional numerical simulation of splitting severe storms on 3 April 1964. J. Atmos. Sci., 38, 1581-1600.

Yau, M. K., and R. Michaud, 1982: Numerical simulation of a cumulus ensemble in three dimensions. J. Atmos. Sci., 39, 1062-1079.

Chapter 2

Numerical Cloud Model

2.1 Overview of model geometries

Traditionally, time-dependent cumulus cloud models have been categorized by their number of spatial dimensions: one-dimensional models, two-dimensional slab-symmetric models, axisymmetric models (sometimes also referred to as one-and-one half-dimensional models), and three-dimensional models.

In one-dimensional models the cloud is represented by a single (vertical) array of points. Hanna (1976) first used this type of model to study an "industrial cumulus". This approach has the advantages of simplicity and computing economy, but cannot adequately predict convective circulation as it does not allow for horizontal variation in cloud conditions.

Two-dimensional slab-symmetric models simulate conditions at grid points in a single vertical plane. It is assumed that in the orthogonal direction there is no variation of computed quantities with distance. These models cannot therefore be expected to represent simultaneously the ratios of the lengths, areas and magnitudes of the upward and downward motion of real clouds. Moreover, a finite heat source region is treated as an infinite band of heat in those models. Nevertheless, Murray et al. (1978) demonstrated that such models can simulate at least some of the macroscopic

properties of observed "industrial cumulus".

Ideally cloud models should be three dimensional. In such models no constraint is imposed on the flow by the geometry of the grid. They can model an environmental wind field that varies in both direction and speed with altitude. However, such models can only be run on very large computers and at considerable cost. This, coupled with the facts that we need a high spatial resolution in order to model heat and moisture sources reasonably and that many numerical experiments with different input parameters are needed, has prohibited three-dimensional simulations of industrial clouds.

Axisymmetric models can be employed to simulate convective development in the absence of wind shear. In such models the equations are developed in cylindrical polar coordinates and azimuthal variability terms are equated to zero. They thus have advantages in terms of computer storage requirements and computing time over full three-dimensional models while at the same time overcoming some of the principal limitations of the slab-symmetric assumption. In this thesis an axisymmetric model is used to study industrial cumulus clouds.

2.2 Basic model assumptions

The axisymmetric cumulus model of Steiner (1982) was suitable to study non-precipitating warm cumulus in an axially symmetric framework. Reuter and Yau (1987) have successfully

applied the model to study mixing mechanisms in cumulus congestus clouds. As part of my thesis I have extended the model code to include warm rain processes, sources of external heat and humidity, and a simple treatment of air pollution.

The model makes the following assumptions:

(1) The axisymmetric model is two dimensional. In cylindrical coordinates all azimuthal derivatives are set to zero. This assumption requires far less computing resources than fully three-dimensional models. The disadvantage of this assumption is that it does not allow wind shear; therefore, it only permits to simulate convective development in the absence of wind shear.

(2) The deep anelastic set of equations are used to filter out acoustic waves in the numerical solution. Therefore, we can use a large time step (1 s) for the numerical integration.

(3) The effect of the earth's rotation is neglected. This assumption is satisfactory even if the cloud is considered to be outside the tropical regions, since in the short lifespan of a cumulus the effect of the Coriolis force on the motion will be small.

(4) The effects of radiation are neglected.

(5) Friction at the earth's surface is neglected.

(6) Water occurs only in the vapour and liquid phases; freezing, melting, deposition and sublimation are not considered.

(7) A bulk parameterization of precipitation is used. The liquid water is divided into cloud water and rainwater. Cloud water consists of small droplets moving with the air, whereas rainwater consists of the larger drops having a finite terminal fall speed.

(8) Condensation occurs whenever the water vapour mixing ratio exceeds the saturation value. Any cloud water in an unsaturated region evaporates until saturation is achieved.

2.3 Model equations

a. Dynamics

The model equations are developed in cylindrical coordinates (r,θ,z), and the azimuthal gradients of all quantities are equated to zero. The continuity equation and the momentum equations (in flux form) are

$$0 = \frac{1}{r}\frac{\partial (ru)}{\partial r} + \frac{1}{\rho_0}\frac{\partial (\rho_0 w)}{\partial z} \tag{1}$$

$$\frac{\partial u}{\partial t} + \frac{1}{r}\frac{\partial (ru^2)}{\partial r} + \frac{1}{\rho_0}\frac{\partial (\rho_0 wu)}{\partial z} = -\frac{1}{\rho_0}\frac{\partial p'}{\partial r} \tag{2}$$

$$\frac{\partial w}{\partial t} + \frac{1}{r}\frac{\partial (ruw)}{\partial r} + \frac{1}{\rho_0}\frac{\partial (\rho_0 w^2)}{\partial z} = -\frac{1}{\rho_0}\frac{\partial p'}{\partial z} + B \tag{3}$$

where B denotes the total buoyancy:

$$B = g\left\{\frac{T'}{T_0} + 0.61 q_v' - q_c - q_r - \frac{p'}{p_0}\right\} \tag{4}$$

In the above equations u and w denote radial and vertical velocity components, p pressure, T temperature, and ρ air density. q_v, q_c and q_r denote the mixing ratios of vapour, cloud water and rainwater, g is the gravitational acceleration. All primed quantities indicate departures from a hydrostatic reference state given by $p_0(z)$, $\rho_0(z)$ and $T_0(z)$.

b. Microphysics

We use the bulk water parameterization for warm rain processes. Ice phase processes are neglected, in view of the warm cloud base temperatures. Conservation of water substance and heat can then be described by

$$\frac{\partial Q}{\partial t} = -\frac{1}{r}\frac{\partial (ruQ)}{\partial r} - \frac{1}{\rho_0}\frac{\partial (\rho_0 wQ)}{\partial z} - C_r + E_r + S_Q \qquad (5)$$

$$\frac{\partial q_r}{\partial t} = -\frac{1}{r}\frac{\partial (ruq_r)}{\partial r} - \frac{1}{\rho_0}\frac{\partial (\rho_0 q_r w)}{\partial z} - E_r + C_r + \frac{1}{\rho_0}\frac{\partial (\rho_0 q_r V_r)}{\partial z} \qquad (6)$$

$$\frac{\partial \varphi}{\partial t} = -\frac{1}{r}\frac{\partial (ru\varphi)}{\partial r} - \frac{1}{\rho_0}\frac{\partial (\rho_0 w\varphi)}{\partial z} + \frac{LE_r}{T} + S_\varphi \qquad (7)$$

where $Q = q_v + q_c$. φ is the total entropy per unit mass given by

$$\varphi = C_{pd}\ln T - R_d \ln p + Lq_v T^{-1} + const. \qquad (8)$$

where L is the latent heat of vaporization, R_d the gas constant for dry air, C_{pd} the specific heat capacity at constant pressure.

The external sources S_Q and S_φ, arising from the heat and

moisture emission of the industrial facility, are specified in section g). The mass-weighted terminal fall speed of the rain (V_r in m s^{-1}), the evaporation rate of rain (E_r in s^{-1}), and the rate of conversion of cloud to rain ($C_r = C_{auto} + C_{col}$ in s^{-1}) were adopted from Innocentini and Caetano (1992):

$$V_r = 21.18\, q_r^{0.2} \tag{9}$$

$$E_r = 0.2\, q_r^{0.675}\ (q_{vs} - q_v)\, \boldsymbol{H}(q_{vs} - q_v) \tag{10}$$

$$C_{auto} = 10^{-3}\,(q_c - \beta)\, \boldsymbol{H}(q_c - \beta) \tag{11}$$

$$C_{col} = 2.2\, q_c\, q_r^{0.875} \tag{12}$$

where **H** denotes the Heaviside step function defined by **H**(x) = 1 for $x \geq 0$ and **H**(x) = 0 for $x < 0$. Eq.(11) models the autoconversion of cloud water once its mixing ratio exceeds the threshold value of β. Eq.(12) models the collection of cloud water by falling rain, assumed to have an exponential size distribution.

c. Thermodynamics

The thermodynamic analysis employed here is essentially a development, suitable for deep convection, of the technique used for shallow convection by Ogura (1963) and Orville (1965).

In the basic state, Eq.(8) becomes

$$\varphi_0(z) = C_{pd} \ln T_0 - R_d \ln p_0 + L q_{v0} T_0^{-1} + const. \tag{13}$$

Thus

$$\varphi' = \varphi(r,z,t) - \varphi_0(z)$$

$$= C_{pd}\ln\left(1+\frac{T'}{T_0}\right) - R_d\ln\left(1+\frac{p'}{p_0}\right) + \frac{L\left(q_v' T_0 - q_{v0} T'\right)}{T_0\left(T_0+T'\right)} \qquad (14)$$

Considering that $T'/T_0 - R_d\, p'/(C_{pd}\, p_0) \sim 10^{-2}$, $q_{v0} \sim 10^{-2}$, $q_v' \sim 10^{-3}$ it follows that if all terms at least two orders of magnitude less than the largest are omitted

$$\varphi' = \left(C_{pd} - \frac{L q_{v0}}{T_0}\right)\frac{T'}{T_0} - R_d\frac{p'}{p_0} + \frac{L q_v'}{T_0} \qquad (15)$$

Once new values of φ and Q are obtained by integration of equations (5) and (7) it is necessary to determine if the air is saturated. The empirical formula for saturation vapour pressure (Rogers and Yau, 1989) is

$$e_s(T) = a\exp\left[b(T-c)/(T-d)\right] \qquad (16)$$

where a = 611.2 N m^{-2}, b = 17.67, c = 273.15 K, d = 29.65 K. Assuming that T' ~ 3 K, T_0 - d ~ 200 K and expanding the above exponentials neglecting terms at least two orders of magnitude less than the largest yields

$$e_s(T) = e_s(T_0)\left(1 + H_1(z)\,T' + H_2(z)\,T'^2\right) \qquad (17)$$

where $H_1(z) = b(c-d)/(T_0-d)^2$ and $H_2(z) = b^2(2c-d-T_0)/2(T_0-d)^2$.

The saturation mixing ratio $q_{vs} = 0.622\, e_s/(p - e_s)$ can thus be approximated by

$$q_{vs} = \frac{0.622\, e_s(T_0)}{p_0}\left(1 + H_1(z)\,T' + H_2(z)\,T'^2\right)\left[1 + \frac{e_s(T_0)}{p_0}\right] \qquad (18)$$

The approximation uses the same argument as earlier, terms at

least two orders of magnitude less than the largest term are omitted except that the whole of the term in square brackets is retained as it is of constant sign (otherwise q_{vs} as computed above would always be an underestimate).

Once φ and Q are known at a time step, the following steps are used to obtain q_v, q_c. (see Fig. 2.1)

1) Eliminating negative q_r. If $q_r < 0$, we adjust Q to $Q + q_r$ and let $q_r = 0$. Otherwise go to the second step.

2) Subtracting φ_0 and Q_0 from φ and Q to obtain φ' and Q'. On the assumption that the air is unsaturated, we use (15) to compute T' assuming that p' is known from a previous time step. Using this value of T', a value of q_{vs} is computed from (18).

3) Considering evaporation of rain. If φ and Q have been adjusted by evaporating rain, or $q_r = 0$, or q_{vs} computed in the second step is less than Q, we go to the fourth step. Otherwise, we need consider evaporation of rain. The evaporated liquid water must be subtracted from q_r and both φ and Q must be adjusted to new values due to the evaporation. After that we go to the second step.

4) If the value of q_{vs} computed in the second step exceeds Q the air must be unsaturated and hence $q_v' = Q'$, $q_c = 0$ while the value of T' is indeed that obtained from (15). On the other hand, if the value of q_{vs} so computed is less than Q the assumption of sub-saturation is clearly false. Hence q_v ($= q_{v0} + q_v'$) $= q_{vs}$, making the same assumption about p' as above and

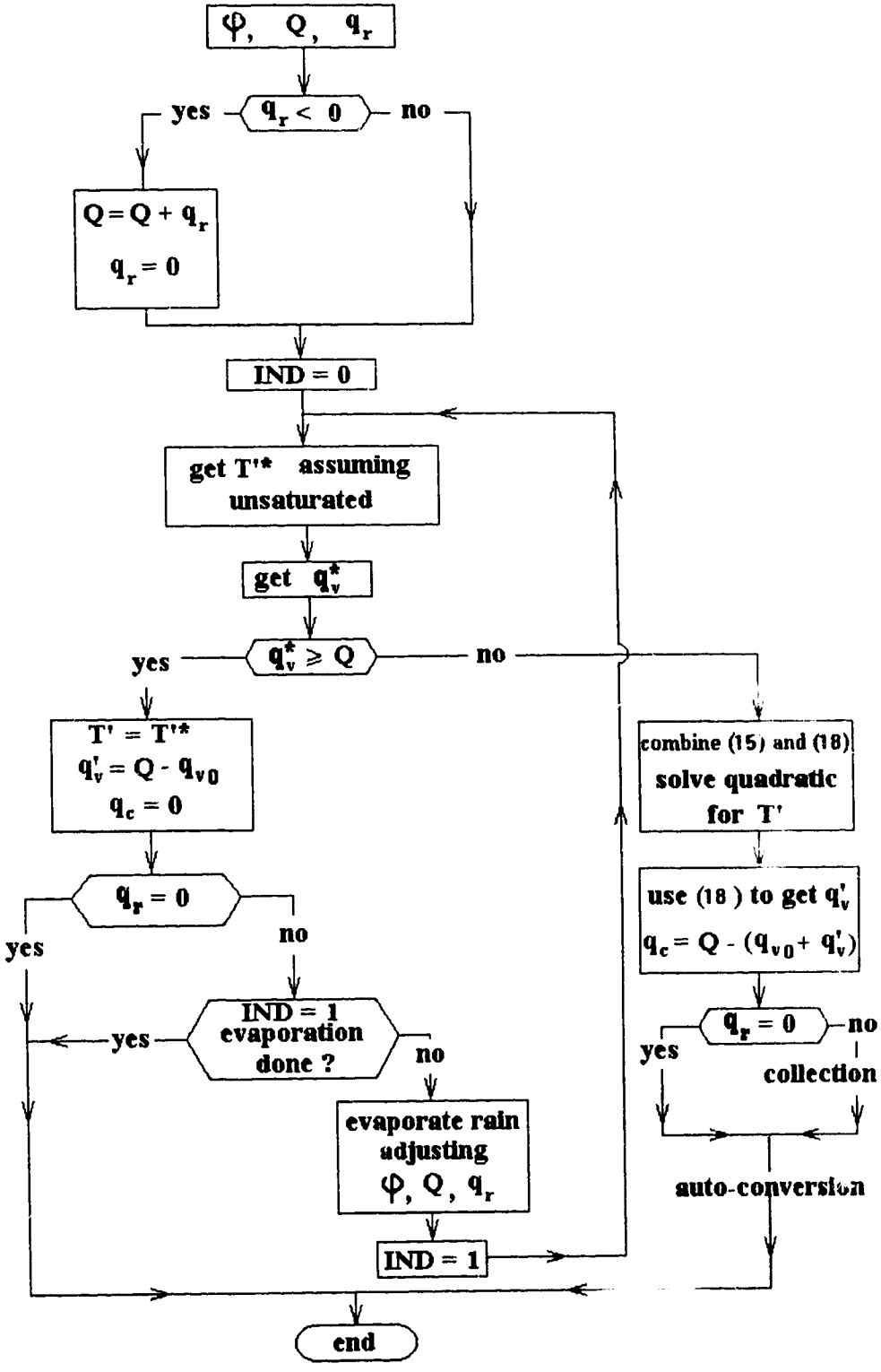

Fig. 1 Flowchart for obtaining q_v and q_c.

combining (15) and (18) one can solve the quadratic equation for T'. We also obtain $q_c = Q - q_v$.

d. Subgrid scale turbulence parameterization

The turbulence terms in (2), (3), (5) and (7) can be derived as subgrid-scale processes by averaging the original inviscid governing equations. Decompose variables (for example u) into a grid volume average (denoted by $\bar{}$) and a deviation (denoted by *)

$$u(r,z) = \bar{u} + u^* \tag{19}$$

where the averaging operator is

$$\bar{u} = \frac{1}{\Delta r \Delta z} \int_{r-\Delta r/2}^{r+\Delta r/2} \int_{z-\Delta z/2}^{z+\Delta z/2} u \, dr \, dz \tag{20}$$

By applying (19) and (20) to a typical nonlinear term such as $\partial(uw)/\partial r$ and assuming that $\overline{u^*} = 0$ and $\overline{w^*} = 0$, we get

$$\begin{aligned} \overline{\frac{\partial}{\partial r}(uw)} &= \overline{\frac{\partial}{\partial r}\bar{u}\bar{w} + \frac{\partial}{\partial r}\bar{u}w^* + \frac{\partial}{\partial r}u^*\bar{w} + \frac{\partial}{\partial r}u^*w^*} \\ &= \frac{\partial}{\partial r}\bar{u}\bar{w} + \frac{\partial}{\partial r}\overline{u^*w^*} \end{aligned} \tag{21}$$

where $\overline{u^*w^*}$ represents the horizontal and vertical transport of momentum by turbulent velocity fluctuations. This quantity is by definition unknown and we must use a closure scheme to estimate its value. We adopt the common approach that the subgrid transport terms are proportional to the gradients of the mean variables.

$$\overline{u^* w^*} = -\nu\left(\frac{\partial \bar{u}}{\partial z} + \frac{\partial \bar{w}}{\partial r}\right) \tag{22}$$

where ν is the eddy diffusion coefficient of momentum.

Applying the above averaging operator to (2), (3), (5) and (7), we get

$$\frac{d\bar{u}}{dt} = -\frac{1}{\rho_0}\frac{\partial \bar{p}}{\partial r} - \frac{1}{r}\frac{\partial}{\partial r}(r\overline{u^* u^*}) + \frac{\overline{v^* v^*}}{r} - \frac{1}{\rho_0}\frac{\partial}{\partial z}(\rho_0 \overline{u^* w^*}) \tag{23}$$

$$\frac{d\bar{w}}{dt} = -\frac{1}{\rho_0}\frac{\partial \bar{p}}{\partial z} + B - \frac{1}{r}\frac{\partial}{\partial r}(r\overline{u^* w^*}) - \frac{1}{\rho_0}\frac{\partial}{\partial z}(\rho_0 \overline{w^* w^*}) \tag{24}$$

$$\frac{d\bar{Q}}{dt} = -\frac{1}{r}\frac{\partial}{\partial r}(r\overline{u^* Q^*}) - \frac{1}{\rho_0}\frac{\partial}{\partial z}(\rho_0 \overline{w^* Q^*}) - C_r + E_r + S_Q \tag{25}$$

$$\frac{d\bar{\varphi}}{dt} = -\frac{1}{r}\frac{\partial}{\partial r}(r\overline{u^* \varphi^*}) - \frac{1}{\rho_0}\frac{\partial}{\partial z}(\rho_0 \overline{w^* \varphi^*}) + \frac{LE_r}{T} + S_\varphi \tag{26}$$

Had we not commenced our averaging with the equations of motion linearized with the thermodynamic variables, triple correlations among density and velocity fluctuations would resulted. The operator d/dt is the substantial derivative.

$$\frac{d}{dt} = \frac{\partial}{\partial t} + \bar{u}\frac{\partial}{\partial r} + \bar{w}\frac{\partial}{\partial z} \tag{27}$$

Applying the conventional stress or strain relationship:

$$\begin{aligned}
&\overline{u^* u^*} = -2\nu\frac{\partial \bar{u}}{\partial r}, && \overline{u^* w^*} = -\nu\left(\frac{\partial \bar{u}}{\partial z} + \frac{\partial \bar{w}}{\partial r}\right),\\
&\overline{v^* v^*} = -2\nu\frac{\bar{u}}{r}, && \overline{w^* w^*} = -2\nu\frac{\partial \bar{w}}{\partial z},\\
&\overline{u^* Q^*} = -\nu_s\frac{\partial \bar{Q}}{\partial r}, && \overline{w^* Q^*} = -\nu_s\frac{\partial \bar{Q}}{\partial z},\\
&\overline{u^* \varphi^*} = -\nu_s\frac{\partial \bar{\varphi}}{\partial r}, && \overline{w^* \varphi^*} = -\nu_s\frac{\partial \bar{\varphi}}{\partial z}
\end{aligned} \tag{28}$$

and dropping the overbar sign the turbulence terms take the final form

$$F_u = \frac{1}{r}\frac{\partial}{\partial r}\left(2r\nu\frac{\partial u}{\partial r}\right) - \frac{2\nu u}{r^2} + \frac{1}{\rho_0}\frac{\partial}{\partial z}\left\{\rho_0\nu\left(\frac{\partial u}{\partial z} + \frac{\partial w}{\partial r}\right)\right\} \tag{29}$$

$$F_w = \frac{1}{r}\frac{\partial}{\partial r}\left\{r\nu\left(\frac{\partial u}{\partial z} + \frac{\partial w}{\partial r}\right)\right\} + \frac{1}{\rho_0}\frac{\partial}{\partial z}\left(2\nu\rho_0\frac{\partial w}{\partial z}\right) \tag{30}$$

$$F_Q = \frac{1}{r}\frac{\partial}{\partial r}\left[\nu_s r\frac{\partial Q}{\partial r}\right] + \frac{1}{\rho_0}\frac{\partial}{\partial z}\left[\nu_s\rho_0\frac{\partial Q}{\partial z}\right] \tag{31}$$

$$F_\varphi = \frac{1}{r}\frac{\partial}{\partial r}\left[\nu_s r\frac{\partial \varphi}{\partial r}\right] + \frac{1}{\rho_0}\frac{\partial}{\partial z}\left[\nu_s\rho_0\frac{\partial \varphi}{\partial z}\right] \tag{32}$$

where $\nu_s = 3\nu$ (suggested by Deardorff, 1971; used by Cotton and Tripoli, 1978) is the eddy mixing coefficient for scalar quantities. F_u and F_w are the subgrid scale friction due to eddy momentum exchange. F_Q and F_φ represent the divergence of unresolved fluxes of Q and φ carried by the subgrid scales. Following Soong and Ogura (1973), we neglect the eddy mixing of rainwater.

Since the eddy diffusion coefficient of momentum ν (i.e., eddy viscosity) has dimensions of length squared divided by time, it can be expressed as the product of a nondimensional constant, the square of an appropriate length scale and a frequency. We adopt the scheme of Hill (1974) in which the frequency is the sum of two terms, one related to general shear and one to the buoyancy. Following Miles (1961), it is further assumed that there is no shear generated turbulence when the local Richardson number, Ri, is greater than 0.25. Ri

is given by

$$Ri = g\frac{\gamma_{vad} - \gamma_{venv}}{\left(\frac{\partial u}{\partial z}\right)^2 T} \tag{33}$$

where the difference between the (moist) adiabatic and the environmental virtual temperature lapse rates is approximated by

$$\gamma_{vad} - \gamma_{venv} = \frac{g\alpha}{C_{pd}} + \frac{\partial T}{\partial z} + 0.61\frac{\partial q_v}{\partial z} T \tag{34}$$

For unsaturated air α = 1, while for saturated air

$$\alpha = \left(1 + \frac{L q_{vs}}{R_d T}\right)\left[1 + \frac{0.622 L^2 q_{vs}}{C_{pd} R_d T^2}\right]^{-1} \tag{35}$$

The scheme for ν can now be written as

$$\begin{aligned} \nu &= 0 && for\ Ri > 0.25 \\ \nu &= c l^2 (f_s + f_b) && for\ Ri < 0.25 \end{aligned} \tag{36}$$

The nondimensional constant c = 0.4, l = $(\Delta r\ \Delta z)^{1/2}$ is the scale of the grid spacing, and f_s and f_b are the shear and buoyancy frequencies. The buoyancy term is zero if Ri > 0. Otherwise it is the frequency scale of atmospheric oscillations:

$$f_b = \left[-g\frac{\gamma_{vad} - \gamma_{venv}}{T}\right]^{1/2} \tag{37}$$

The shear term has the magnitude of the deformation tensor:

$$f_s=\left[2\left(\frac{\partial w}{\partial z}\right)^2+2\left(\frac{\partial u}{\partial r}\right)^2+2\left(\frac{u}{r}\right)^2+\left(\frac{\partial u}{\partial z}+\frac{\partial w}{\partial r}\right)^2\right]^{1/2} \tag{9}$$

e. Perturbation pressure

A diagnostic equation for the perturbation pressure p' can be obtained by combining $\partial/(r\partial r)$ [r (23)] and $\partial/(\rho_0\partial z)$ [ρ_0 (24)]

$$\frac{1}{r}\frac{\partial}{\partial r}\left[r\frac{\partial p'}{\partial r}\right]+\frac{\partial}{\partial z}\left[\frac{\partial p'}{\partial z}\right]=\frac{1}{r}\frac{\partial}{\partial r}[\rho_0 r A_u+\rho_0 r F_u] \tag{10}$$

$$+\frac{\partial}{\partial z}[\rho_0 A_w+\rho_0 F_w+\rho_0 B]+G$$

where A_u and A_w are the advective terms, and G is the rate of change of the convergence of the mass flux:

$$G=-\frac{\partial}{\partial t}\left[\rho_o\frac{1}{r}\frac{\partial(ru)}{\partial r}+\frac{\partial(\rho_0 w)}{\partial z}\right] \tag{11}$$

The term G, which is theoretically 0, is kept here to provide a negative feedback as explained later.

Strictly speaking, p' must be known before the buoyancy term in (39), $\partial/\partial z$ (ρ_0 B), can be evaluated. However, Ogura and Wilhelmson (1972) showed that the contribution of p' in determining the buoyancy is small and can be replaced by its value at the previous time step. Therefore, we use the p' calculated at the previous time step to determine the buoyancy term in (39).

f. Boundary and initial conditions

The top and bottom boundaries of the model domain are assumed to be flat, rigid and smooth. There is no transport of heat and moisture through these boundaries with the exception of rain leaving the domain at the bottom, that is

$$w = \frac{\partial u}{\partial z} = \frac{\partial Q}{\partial z} = \frac{\partial \varphi}{\partial z} = 0 \qquad at\ z = 0\ \ or\ \ z = H_z \tag{41}$$

and $\partial q_r/\partial z=0$ at $z=H_z$. (H_z is the height of the domain.) Substituting (41) into the equation of vertical motion (3) yields a boundary condition for the pressure

$$-\frac{1}{\rho_0}\frac{\partial p'}{\partial z} + B = 0 \qquad at\ z = 0\ \ or\ z = H_z \tag{42}$$

Since the air far away from the convection remains at rest, closed conditions are appropriate at the horizontal boundaries of the domain, that is

$$u = \frac{\partial w}{\partial r} = \frac{\partial Q}{\partial r} = \frac{\partial q_r}{\partial r} = \frac{\partial \varphi}{\partial r} = 0 \qquad at\ r = 0\ \ or\ \ r = r_b \tag{43}$$

where r_b is the distance between the axis to the lateral boundary (i.e., the half-width of the domain). Substituting (43) into the equation of horizontal motion (2) yields a boundary condition for the pressure

$$\frac{\partial p'}{\partial r} = 0 \qquad at\ r = 0\ \ or\ \ r = r_b \tag{44}$$

The basic state variables of the model are determined from the data of the sounding specified by surface data (temperature, pressure, and dew point) and values of the

temperature and dew point at any number of heights above the surface. Values of the thermodynamic variables at grid points are computed by linear interpolation in the vertical. The initial atmosphere is assumed horizontally uniform and at rest.

g. Emission of sensible and latent heat

Our means of including the sensible and latent heat release from an industrial facility follows closely that of Murray et al. (1978) and Orville et al. (1981). It is assumed that the total sensible and latent heat emission rates, H_s and H_l, are distributed uniformly within a cylinder with base height D_0, depth D and radius b. This cylinder, centred on the vertical z-axis, constitutes the "effective volume" of the heat release resulting from the interaction of the heat plume with the boundary layer air near the surface. The sources of vapour S_Q and total specific entropy S_φ are given by

$$S_Q = \frac{\boldsymbol{H}(b-r)\,\boldsymbol{H}(D+D_0-z)\,\boldsymbol{H}(z-D_0)}{\pi b^2 D \rho_0}\left[\frac{H_l}{L}\right] \qquad (45)$$

$$S_\varphi = \frac{\boldsymbol{H}(b-r)\,\boldsymbol{H}(D+D_0-z)\,\boldsymbol{H}(z-D_0)}{\pi b^2 D \rho_0}\left[\left(\frac{1}{T_0} - \frac{L q_{v0}}{C_{pd} T_0^2}\right) H_s + \frac{H_l}{T_0}\right] \qquad (46)$$

The increase in total specific entropy S_φ comes from an increase in temperature (first term involving H_s) and an increase in water vapour (second term involving H_l).

2.4 Numerical approximation of model equations

a. Grid stretching

In order to solve the equations on a finite difference grid with higher resolution in the horizontal near the axis (the heat source) than elsewhere, a stretched coordinate is used. The horizontal coordinate r is transformed to a coordinate s with equally space intervals Δs (=1). The transformation is described by

$$s = A \tanh (C\, r/r_b) \tag{47}$$

or

$$r = \frac{r_b}{2C} \ln\left(\frac{A+s}{A-s}\right) \tag{48}$$

where A and C are constants to be determined. The values of A and C are determined at the beginning of every simulation with the specifications of the total number of grid points in the horizontal, n, and the number of grid points, m, within a distance $k\, r_b$ from the axis (that is the number of grid points occupying portion k of the total radial distance modelled). The value of m, n and k determine A and C uniquely since

$$\begin{aligned} n \Delta s &= A \tanh C \\ m \Delta s &= A \tanh Ck \end{aligned} \tag{49}$$

Hence

$$\frac{\tanh Ck}{\tanh C} - \frac{m}{n} = 0 \tag{50}$$

This equation is solved by an iterative method. The domain,

total grid points, sounding, and constants A, C will be specified in Chapter 3, 4 and 5.

From (48), we have

$$r' = \frac{dr}{ds} = \frac{r_b}{AC}\cosh^2\left(\frac{Cr}{r_b}\right) \tag{51}$$

The horizontal velocity u and $\partial/\partial r$ can be written as

$$u = \frac{dr}{dt} = \frac{dr}{ds} \times \frac{ds}{dt} = r'\dot{s}$$

$$\frac{\partial}{\partial r} = \frac{1}{r'}\frac{\partial}{\partial s} \tag{52}$$

With the use of (52) the marching equations of the model become

$$\frac{\partial \dot{s}}{\partial t} = -\frac{1}{r r'^2}\frac{\partial}{\partial s}(r r'^2 \dot{s}^2) - \frac{1}{\rho_0}\frac{\partial}{\partial z}(\rho_0 \dot{s} w) - \frac{1}{\rho_0 r'^2}\frac{\partial p'}{\partial s} - \frac{2\nu \dot{s}}{r^2} + \frac{1}{r r'^2}\frac{\partial}{\partial s}\left[\frac{2r\nu}{r}, \frac{\partial}{\partial s}(r'\dot{s})\right] + \frac{1}{\rho_0 r'}\frac{\partial}{\partial z}\left[\rho_0 \nu\left(\frac{r'\partial \dot{s}}{\partial z} + \frac{1}{r}, \frac{\partial w}{\partial s}\right)\right] \tag{53}$$

$$\frac{\partial w}{\partial t} = -\frac{1}{r r'}\frac{\partial}{\partial s}(r r' \dot{s} w) - \frac{1}{\rho_0}\frac{\partial}{\partial z}(\rho_0 w^2) + B - \frac{1}{\rho_0}\frac{\partial p'}{\partial z} + \frac{1}{r r'}\frac{\partial}{\partial s}\left[r\nu\left(\frac{r'\partial \dot{s}}{\partial z} + \frac{\partial w}{r'\partial s}\right)\right] + \frac{1}{\rho_0}\frac{\partial}{\partial z}\left(2\rho_0 \nu \frac{\partial w}{\partial z}\right) \tag{54}$$

$$\frac{\partial Q}{\partial t} = -\frac{1}{r r'}\frac{\partial}{\partial s}(r r' \dot{s} Q) - \frac{1}{\rho_0}\frac{\partial}{\partial z}(\rho_0 w Q) + \frac{1}{r r'}\frac{\partial}{\partial s}\frac{r\nu_s}{r'}\frac{\partial Q}{\partial s} + \frac{1}{\rho_0}\frac{\partial}{\partial z}\left(\rho_0 \nu_s \frac{\partial Q}{\partial z}\right) - C_r + E_r + S_Q \tag{55}$$

$$\frac{\partial q_r}{\partial t} = -\frac{1}{r r'}\frac{\partial}{\partial s}(r r' \dot{s} q_r) - \frac{1}{\rho_0}\frac{\partial}{\partial z}(\rho_0 w q_r) + \frac{1}{\rho_0}\frac{\partial}{\partial z}(\rho_0 V_r q_r) + C_r - E_r \tag{56}$$

$$\frac{\partial \varphi}{\partial t} = -\frac{1}{rr'}\frac{\partial}{\partial s}(rr'\dot{s}\varphi) - \frac{1}{\rho_0}\frac{\partial}{\partial z}(\rho_0 w\varphi) + \frac{1}{rr'}\frac{\partial}{\partial s}\frac{r\nu_s}{r'}\frac{\partial \varphi}{\partial s} + \frac{1}{\rho_0}\frac{\partial}{\partial z}\left(\rho_0 \nu_s \frac{\partial \varphi}{\partial z}\right) + \frac{LE_r}{T} + S_\varphi \qquad (57)$$

b. Finite difference scheme

The partial differential equations are solved by numerical approximation based on a finite difference scheme on a staggered grid. Variables other than velocity components are computed at the centres of grid boxes, $\dot{s}$ is computed at the mid-points of the vertical sides of these boxes and w at the mid-points of the horizontal sides of the boxes (see Fig.2).

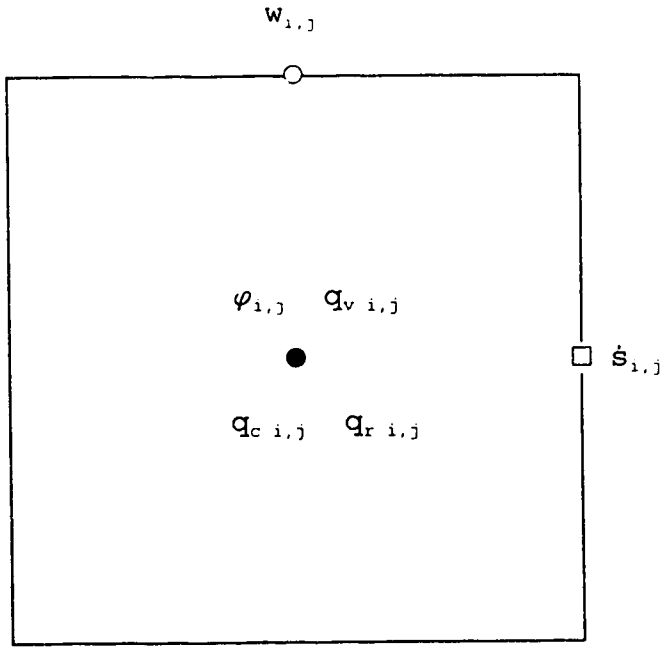

Fig. 2. A staggered grid box.

Thus all variables except $\dot{s}$ and w are computed at $(i-\frac{1}{2})\Delta s$, $(j-\frac{1}{2})\Delta z$, $i=1, 2, \cdots, NH$, $j=1, 2, \cdots, NV$ where NH and NV are the total number of grid points in the horizontal and vertical respectively; w is computed at $(i-\frac{1}{2})\Delta s$, $j\Delta z$; and $\dot{s}$ at $i\Delta s$, $(j-\frac{1}{2})\Delta z$ for the same values of i and j.

A second-order non-diffusive leapfrog method is used to solve the prognostic equations. All the terms involving the eddy turbulent exchange are lagged in time. Spatial differentiation is done using the centred difference method. Using the notation

$$\delta_s x = \frac{x_{i+1/2} - x_{i-1/2}}{\Delta s}$$

$$\delta_z x = \frac{x_{j+1/2} - x_{j-1/2}}{\Delta z}$$

$$\overline{x}^s = \frac{x_{i+1/2} + x_{i-1/2}}{2} \qquad (58)$$

$$\overline{x}^z = \frac{x_{j+1/2} + x_{j-1/2}}{2}$$

$$\delta_{2t} x = \frac{x^{\tau+1} - x^{\tau-1}}{2\Delta t}$$

the finite difference equations become:

$$\delta_{2t}\dot{s} = A_{\dot{s}}^{\tau} - \frac{1}{\rho_0 r_s'^2}\delta_s (p')^{\tau} + F_{\dot{s}}^{\tau-1} \qquad (59)$$

$$\delta_{2t} w = A_w^{\tau} - \frac{1}{\rho_0}\delta_z (p')^{\tau} + (\overline{B}^z)^{\tau} + F_w^{\tau-1} \qquad (60)$$

$$\delta_{2t} Q = A_Q^{\tau} - C_r^{\tau} + E_r^{\tau} + S_Q^{\tau} + F_w^{\tau-1} \qquad (61)$$

$$\delta_{2t} q_r = A^{\tau}_{q_r} - \frac{1}{\rho_0}\delta_z(\rho_0 q_r V_r)^{\tau} + C^{\tau}_r - E^{\tau}_r \qquad (62)$$

$$\delta_{2t}\varphi = A^{\tau}_{\dot{s}} + L\left(\frac{E_r}{T}\right)^{\tau} + S^{\tau}_{\varphi} + F^{\tau-1}_{\varphi} \qquad (63)$$

Note that r_s and r_s' refer to values at the points where $\dot{s}$ is computed. Unsubscripted r and r' are values at the centres of grid boxes. A and F denote advective and turbulent terms.

$$A_{\dot{s}} = -\frac{1}{r_s r_s'^2}\delta_s(r r'^2 \dot{s}^s \overline{\dot{s}^s}) - \frac{1}{\rho_0 r_s'}\delta_z(\rho_0 r_s' \dot{s}^z \overline{w}^s) \qquad (64)$$

$$A_w = -\frac{1}{r r'}\delta_s(r_s r_s' \dot{s}^z \overline{w}^s) - \frac{1}{\rho_0}\delta_z(\rho_0 \overline{w}^z \overline{w}^z) \qquad (65)$$

$$A_Q = -\frac{1}{r r'}\delta_s(r_s r_s' \dot{s} \overline{Q}^s) - \frac{1}{\rho_0}\delta_z(\rho_0 w \overline{Q}^z) \qquad (66)$$

$$A_{q_r} = -\frac{1}{r r'}\delta_s(r_s r_s' \dot{s} q_r{}^s) - \frac{1}{\rho_0}\delta_z(\rho_0 w q_r{}^z) \qquad (67)$$

$$A_{\varphi} = -\frac{1}{r r'}\delta_s(r_s r_s' \dot{s} \overline{\varphi}^s) - \frac{1}{\rho_0}\delta_z(\rho_0 w \overline{\varphi}^z) \qquad (68)$$

$$F_{\dot{s}} = \frac{1}{r r'^2}\frac{\partial}{\partial s}\left[\frac{2 r \nu}{r}\cdot\frac{\partial}{\partial s}(r'\dot{s})\right] - \frac{2\nu\dot{s}}{r^2} + \frac{1}{\rho_0 r'}\frac{\partial}{\partial z}\left[\rho_0 \nu\left(\frac{r}{\partial z}\frac{\partial \dot{s}}{\partial z} + \frac{1}{r}\cdot\frac{\partial w}{\partial s}\right)\right] \qquad (69)$$

$$F_w = \frac{1}{r r'}\delta_s\left[r_s \nu\left(r_s'\delta_z\dot{s} + \frac{1}{r_s'}\delta_s w\right)\right] + \frac{1}{\rho_0}\delta_z(2\rho_0\nu\delta_w) \qquad (70)$$

$$F_Q = \frac{1}{r r'}\delta_s\left(\overline{\nu_s}^s \frac{r_s}{r_s'}\delta_s Q\right) + \frac{1}{\rho_0}\delta_z\left(\overline{\nu_s}^z \rho_0 \delta_z Q\right) \qquad (71)$$

$$F_\varphi = \frac{1}{r r'} \delta_s \left(\overline{\nu_s^s} \frac{r_s}{r_s'} \delta_s \varphi \right) + \frac{1}{\rho_0} \delta_z \left(\overline{\nu_s^z} \rho_0 \delta_z \varphi \right) \tag{72}$$

The pressure equation (39) becomes

$$\delta_z \delta_z (p')^\tau + \frac{1}{r r'} \delta_s \left(\frac{r_s}{r_s'} \delta_s (p')^\tau \right) = \frac{\rho_0}{r r'} \delta_s [r r_s' (A_s^\tau + F_s^{\tau-1})] + \delta_z [\rho_0 (A_w^\tau + F_w^{\tau-1} + \bar{B}^z)] - \left[\frac{\check{D}^{\tau+1} - \check{D}^{\tau-1}}{2 r r' \Delta t} \right] \tag{73}$$

where

$$\check{D} = \frac{\rho_0}{r r'} \delta_s (r_s r_s' \dot{s}) + \delta_z (\rho_0 w) \tag{74}$$

Although the right-hand side of (40) is theoretically zero, it is likely to be nonzero in the numerical integration due to computer round-off errors. Following the method of Harlow and Welch (1965), we have retained G in the perturbation pressure equation to act as a negative feedback which prevents the divergence of mass flux increasing with time. Specifically we write G as $(\check{D}^{\tau+1}-\check{D}^{\tau-1})/(2\Delta t)$ and assume $\check{D}^{-1}=0$ while the actual value of $\check{D}^{\tau}$ is retained to ensure that the divergence of the mass flux remains small and does not increase with time.

In all the numerical experiments, the time step Δt = 1 second. A mixing procedure based on Gordon (1978) is invoked every 20 time steps to prevent the possible splitting of solutions at odd and even time steps. This involves a restart by a forward difference over ⅛ of the usual time step, followed by centred differences over ⅛, ¼, and ½ of the usual

time step before employing the regular centred time difference procedure.

2.5 Modifications of cloud model for pollution experiments

In the previous sections, the cumulus model was described as it will be used in the Chapter 3 focusing on the heat and vapour sources. The pollution effects, investigated in Chapters 4 and 5, require some minor extensions to the model. These extensions will be presented in this section.

The pollutants emitted by an industrial complex have two major effects on the cloud microphysics. Firstly, the pollutants can serve as large or giant cloud condensation nuclei (CCN) on which cloud droplets form; therefore, they increase the initial concentration of cloud droplets and modify the initial distribution of cloud droplets. Secondly, the equilibrium supersaturation in polluted clouds is lowered by dissolved pollutants.

To include the changes in the cloud droplet distribution the autoconversion scheme of Kessler's (1969) microphysics parameterization has been replaced by Berry and Reinhardt's (1973) scheme in which the rate of autoconversion of cloud water to rainwater is dependent upon the initial cloud droplet concentration N_c as well as the mass dispersion coefficient ν_c of the initial cloud droplet distribution.
Specifically, rather than using (11), the autoconversion rate is calculated according to

$$C_{auto} = \frac{10^3 \rho_0 q_c^2}{200 + (2.4 \times 10^8 \nu_c \frac{q_c \rho_0}{N_c})^{-1}} \qquad (75)$$

where N_c (in m^{-3}) and ν_c have features which characterize the properties of the environment.

The lowered supersaturation effect is dealt with by replacing the saturated vapour mixing ratio q_{vs} with $(1+S)q_{vs}$, where S denotes the effective supersaturation value of the polluted air. Heavily polluted air will have a smaller S value than clean, unpolluted air, because the polluted air contains more activated anthropogenic CCN.

One further addition has been included for the experiments described in Chapters 4 and 5. A bubble-like humidity impulse is superimposed on the initial vapour field. Following Steiner (1982) the humidity impulse is given by

$$q_v = \{RH_0 + h\,(1 - RH_0)\, e^{-r^2/\alpha_0^2}\} \times q_{vs0} \qquad (76)$$

where q_{vs0} is saturation mixing ratio of the basic state, RH_0 is the relative humidity in the basic state, r is the radial distance, and α_0 is the width parameter of the bell shaped profile. The variable h gives the vertical distribution defined by the following expressions:

$h = 0$ for $0 \le z < \alpha_1$

$h = 1$ for $\alpha_1 \le z \le \alpha_2$

$h = (\alpha_3 - z)/(\alpha_3 - \alpha_2)$ for $\alpha_2 < z < \alpha_3$

$h = 0$ for $z \ge \alpha_3$

where α_1 is the lowest level at which an impulse is introduced; α_2 is the highest level in which the impulse is constant with height, α_3 is the top of a higher layer in which the impulse decreases linearly with height. Within the range $\alpha_1 \leq z \leq \alpha_2$ the grid point nearest the axis is just saturated.

2.6 Summary

In this chapter, the axisymmetric cloud model used in the thesis is described in detail. The model consists of the anelastic set of dynamic equations and thermodynamics with a first-order closure scheme for the unresolved turbulent processes. The water substance is divided into three separate classes: vapour, non-precipitating cloud droplets, and rainwater.

In contrast with a slab-symmetric cloud model, an axisymmetric model can realistically simulate the emission of sensible and latent heat into an effective source region that has finite spatial dimensions. Moreover, an axisymmetric model requires far less computing resources than a fully three-dimensional model; yet it provides the same results as a three-dimensional model in a calm environment.

References

Berry, E. X., and R. L. Reinhardt, 1973: Modelling of Condensation and collection within clouds. Physical Sciences Publication No. 16, University of Nevada, 96pp.

Cotton, W.R., and G. Tripoli, 1978: Cumulus convection in shear flow - three-dimensional numerical experiments. J. Atmos.Sci., 35, 1503-1521.

Deardorff, J. W., 1971: On the magnitude of the sub-grid scale eddy coefficient. J. Comp. Phys., 7, 120-133.

Gordon, N. D., 1978: Numerical simulation of a long-lasting mesoscale squall line. Sc. D thesis, Massachusetts Institute of Technology, 219 pp.

Hanna, S, R., 1976: Comments on "observations of an industrial cumulus". J. Appl. Meteor., 15, 1232-1233.

Harlow, F. H., and J. E. Welch, 1965: Numerical calculation of time dependent viscous incompressible flow of fluid with free surface. Phys. of Fluids, 8, 2182-2189.

Hill, G. E., 1974: Factors controlling the size and spacing of cumulus clouds as revealed by numerical experiments. J. Atmos. Sci., 31, 646-673.

Innocentini, V., and E. S. Caetano, 1992: A numerical study of the role of humidity in the updraft driven by moist slantwise convection. J. Atmos. Sci., 49, 1092-1106.

Kessler, E. E., 1969: On the distribution and continuity of water substance in atmospheric circulations. Meteor. Monogr., No.32, Amer. Meteor. Soc., Boston, 84pp.

Miles, J. W., 1961: On the stability of heterogeneous shear flows. J. Fluid Mech., 10, 496-508.

Murray, F.W., L. R. Koenig, and P. M. Tag, 1978: Numerical simulation of an industrial cumulus and comparison with

observations. J. Appl. Meteor., 17, 655-668.

Ogura, Y., 1963: The evolution of a moist convective element in a shallow conditionally unstable atmosphere: a numerical calculation. J. Atmos. Sci., 20, 407-424.

Ogura, Y. and R. B. Wilhelmson, 1972: The pressure perturbation and the numerical modelling of a cloud. J. Atmos. Sci., 29, 1295-1307.

Orville, H. D., 1965: A numerical study of the initiation of cumulus convection over mountainous terrain. J. Atmos. Sci., 22, 684-699.

Orville, H. D., P. A. Eckhoff, J. E. Peak, J. H. Hirsch, and F. J. Kopp, 1981: Numerical simulation of the effects of cooling tower complexes on clouds and severe storms. Atmos. Environ., 15, 823-836.

Reuter, G. W., and M. K. Yau, 1987: Mixing mechanisms in cumulus congestus clouds. Part II: Numerical simulations. J. Atmos. Sci., 44, 798-827.

Rogers, R. R., and M. K. Yau, 1989: A short course in cloud physics. 3nd edition, Pergamon Press, Oxford, 293 pp.

Soong. S., and Y. Ogura, 1973: A comparison between axisymmetric and slab-symmetric cumulus cloud model. J. Atmos. Sci., 30, 879-893.

Steiner, J. T., 1982: An axially symmetric cloud model: Development and simulations. Stormy Weather Group, Scientific Report. MW-94, McGill University, 55pp.

Chapter 3

Numerical simulation of a rain shower affected by waste energy released from a cooling tower complex in a calm environment

3.1 Introduction

There is growing concern about the environmental impact of large industrial complexes such as clusters of electrical power stations and oil refineries. These facilities have large cooling systems that release their waste heat into the atmosphere. The waste heat released to the atmosphere is usually a combination of latent and sensible heat (through evaporative cooling towers) but can be in the form of sensible heat alone (through dry natural-draft towers). Possible atmospheric effects of large amounts of waste energy emitted over a small area are increased fogging and snowfall (Hanna and Gifford 1975; Kramer et al. 1976; Campistron 1987; Cha gnon et al. 1991). Here, the focus is on the possible triggering and enhancement of convective rain showers due to waste energy released into a conditionally unstable atmosphere. When the rising heat and vapour plume released from the cooling towers reaches the condensation level, cloud condensation will increase the upward buoyancy, resulting in cumulus convection that will "feed" from the much larger amounts of latent heat stored within the conditionally unstable atmosphere itself. Thus, the perturbation arising

from the cooling system might, in some instances, trigger large convective clouds and related events such as strong winds, heavy rain, and lightning.

It is hard to quantify the effects of waste heat emission on convective clouds because of the big expense associated with detailed cloud observations in different atmospheric conditions. In fact, only a few observational programs of "industrially spawned" cumuli have been undertaken. The alternative is to use numerical models. Comparing the results from a series of carefully selected model experiments can determine the sensitivity of the convection to the strength and size of the waste energy source. Model experimentation can also play an important role in planning the siting of new industrial facilities.

Early attempts to model "industrial cumuli" were made with a one-dimensional cloud model (Hanna 1976). This simple approach, however, cannot adequately predict the convective circulation as it does not allow for horizontal variation in cloud conditions. Three-dimensional cloud models are required in order to model an environmental wind field that varies realistically, both in direction and speed, with altitude. However, they require extensive computing resources. This, coupled with the fact that many numerical experiments with different input parameters are needed, has prohibited the use of three-dimensional simulations of industrial clouds. Instead, modellers have used two-dimensional slab-symmetric

models that simulate conditions in a vertical plane, assuming that there is no variation of quantities in the orthogonal direction. Murray et al. (1976) used a slab symmetric model to simulate Auer's (1976) observations of the "industrially spawned" cumulus that formed over the oil refinery complex of Wood River, Illinois. Model convection was enhanced when the rate of emission of waste energy was increased. Using the same model, Koenig et al. (1978) compared numerical experiments that had different ratios of sensible to latent heat release to evaluate the relative importance of temperature increase versus vapour increase. For a fixed amount of total heat emission, the convection became more intense as the sensible heat component increased. Orville et al. (1981) used a slab-symmetric cumulus model to simulate heat emission from a power park for severe storm conditions. They found that the addition of waste energy had little impact on triggering severe storms. Furthermore, if all the waste energy was emitted in the form of sensible heat, the severity of the simulated storm could be reduced. On the other hand, Hane's (1978) slab-symmetric cloud simulations indicated that the preconditioning of boundary layer air (due to the destabilization and humidity increases from the cooling tower effects) can enhance the convection.

The slab-symmetric assumption has some shortcomings as the wind cannot flow around a cloud tower, thereby forcing the air to subside or rise (Schlesinger 1984). Also, veering of the environmental wind cannot be reproduced. Heat and

moisture sources of finite dimensions cannot be treated realistically. Hane (1978) discussed in detail the shortcomings of representing a finite heat source region with an infinite band of heat. He argued that this slab-symmetric arrangement may be adequate to study the initiation of convection but would underestimate the rapidity with which clouds form and the intensity of the ensuing deep convection.

Based on linear theory, Reuter and Jacobsen (1993) showed that the contribution of diabatic heating towards the circulation is largest when the ambient wind is zero. In such a case, the heat plume remains intact and can build strong buoyancy. In the absence of wind, the three-dimensional airflow triggered by an axisymmetric heat source can be modeled using an axisymmetric cloud model in which the equations are developed in cylindrical polar coordinates and all azimuthal derivatives are set to zero. Axisymmetric models require far less computing resources than fully three-dimensional models, yet at the same time, they overcome some of the principal limitations of the slab-symmetric assumption.

The purpose of this chapter is to use an axisymmetric cumulus model to quantify the sensitivity of convection to the waste energy emitted as sensible and latent heat into a conditionally unstable resting atmosphere. A series of sensitivity experiments will be compared to address the following questions:

(1 How does the total amount of emitted energy affect the

life cycle of convective clouds and associated rain showers?

(2) For a fixed amount of total waste energy released, how does the relative contribution of sensible heat affect the rain showers?

(3) How does the size of the heat source affect the growth rate and intensity of the convection?

(4) Does the distribution of perturbation temperature and moisture within the source region affect the triggering of clouds?

3.2 Numerical cloud model

The axisymmetric cumulus model of Steiner (1982), Reuter and Yau (1987), and Reuter (1987) was extended to include warm rain processes and external sources of heat and moisture. The model equations are developed in cylindrical polar coordinates (r,θ,z), and the azimuthal gradients of all quantities are equated to zero. To filter out acoustic waves in the numerical solution, the deep anelastic set of equations was used. As the momentum and perturbation pressure equations have been presented in detail in the above references, they will not be repeated here.

a. Microphysics

The extended model includes a bulk-water parameterization for warm rain processes. Ice-phase processes were neglected,

in view of the warm cloud-base temperatures. Conservation of water substance and heat can be described by

$$\frac{\partial Q}{\partial t} = -\frac{1}{r}\frac{\partial (ruQ)}{\partial r} - \frac{1}{\rho_0}\frac{\partial (\rho_0 wQ)}{\partial z} + \frac{1}{r}\frac{\partial}{\partial r}\left[\nu_s r \frac{\partial Q}{\partial r}\right] + \frac{1}{\rho_0}\frac{\partial}{\partial z}\left[\nu_s \rho_0 \frac{\partial Q}{\partial z}\right] + E_r - C_r + S_Q \quad (1)$$

$$\frac{\partial q_r}{\partial t} = -\frac{1}{r}\frac{\partial (ruq_r)}{\partial r} - \frac{1}{\rho_0}\frac{\partial (\rho_0 q_r w)}{\partial z} - E_r + C_r + \frac{1}{\rho_0}\frac{\partial (\rho_0 q_r V_r)}{\partial z} \quad (2)$$

$$\frac{\partial \varphi}{\partial t} = -\frac{1}{r}\frac{\partial (ru\varphi)}{\partial r} - \frac{1}{\rho_0}\frac{\partial (\rho_0 w\varphi)}{\partial z} + \frac{1}{r}\frac{\partial}{\partial r}\left[\nu_s r \frac{\partial \varphi}{\partial r}\right] + \frac{1}{\rho_0}\frac{\partial}{\partial z}\left[\nu_s \rho_0 \frac{\partial \varphi}{\partial z}\right] + \frac{LE_r}{T} + S_\varphi \quad (3)$$

where $Q=q_v+q_c$ denotes the sum of the mixing ratio of vapour q_v and cloud water q_c, q_r denotes the mixing ratio of the rainwater, and φ denotes the total entropy per unit mass given by

$$\varphi = C_{pd}\ln T - R_d \ln p + Lq_v T^{-1} + const. \quad (4)$$

In the above equations, t is time, u and w are the radial and vertical velocity components, T is temperature, p is pressure, $\rho_0=\rho_0(z)$ is the air density of the hydrostatic basic state, C_{pd} is the specific heat capacity of dry air at constant pressure, L is the latent heat of vaporization, and R_d is the specific gas constant for dry air. Following Cotton and Tripoli (1978), the eddy mixing coefficient for φ and Q, denoted by ν_s, was set to three times the magnitude of the eddy mixing coefficient for momentum. The latter was specified using Hill's (1974) scheme, which depends on the local moist

buoyancy and the shear deformation time scales. Details about computing the eddy mixing coefficient in the axisymmetric framework were given by Reuter and Yau (1987, p. 826). Following Soong and Ogura (1973), there was no eddy mixing of rainwater.

The external sources S_Q and S_φ, arising from the heat and moisture emission of the industrial facility, are specified in the next section. The mass-weighted terminal fall speed of the rain V_r (m s^{-1}), the evaporation rate of rain E_r (s^{-1}), and the rate of conversion of cloud to rain C_r (s^{-1}) were adopted from Innocentini and Caetano (1992)

$$V_r = 21.18\, q_r^{0.2} \tag{5}$$

$$E_r = 0.2\, q_r^{0.675}\, (q_{vs} - q_v)\, \boldsymbol{H}(q_{vs} - q_v) \tag{6}$$

$$C_r = 10^{-3}(q_c - 0.0015)\, \boldsymbol{H}(q_c - 0.0015) + 2.2\, q_c q_r^{0.875} \tag{7}$$

In (6) q_{vs} denotes the saturation vapour mixing ratio, and **H** denotes the Heaviside step function defined by **H**(x) = 1 for x $\geq$ 0 and **H**(x) = 0 for x < 0. The first erm in (7) models the autoconversion of cloud water once its mixing ratio exceeds the threshold value of 0.0015 kg kg^{-1} (suggested by Hill, 1977). The second term models the collection of cloud by falling rain, assumed to have the Marshall-Palmer exponential size distribution (Kessler, 1969).

b. Modelling emission of sensible and latent heat

The sensible and latent heat release from an industrial

facility is included following the approach of Murray et al. (1978) and Orville et al. (1981). The rates for sensible and latent heat losses, H_s and H_l, are distributed uniformly within a cylinder with base height D_0, depth D and radius b. This cylinder, centred on the vertical z-axis, constitutes the "effective volume" of the heat release resulting from the interaction of the heat plume with the boundary layer air near the surface. The sources of vapour S_Q and total specific entropy S_φ are given by

$$S_Q = \frac{\boldsymbol{H}(b-r)\,\boldsymbol{H}(D+D_0-z)\,\boldsymbol{H}(z-D_0)}{\pi b^2 D \rho_0}\left[\frac{H_l}{L}\right] \tag{8}$$

$$S_\varphi = \frac{\boldsymbol{H}(b-r)\,\boldsymbol{H}(D+D_0-z)\,\boldsymbol{H}(z-D_0)}{\pi b^2 D \rho_0}\left[\left(\frac{1}{T_0} - \frac{L q_{v0}}{C_{pd} T_0^2}\right) H_s + \frac{H_l}{T_0}\right] \tag{9}$$

where T_0 and q_{v0} denote the hydrostatically balanced basic state values of temperature and vapour mixing ratio, respectively. The increase in total specific entropy S_φ comes from an increase in temperature (first term involving H_s) and an increase in water vapour (second term involving H_l). The rate of total heat loss is denoted by $H_t = H_s + H_l$. In the experiments presented here, we have set D_0 = 80 m and D = 40 m.

c. Numerical aspects and initialization

The top and bottom boundaries of the model domain are assumed to be flat, rigid, and smooth. There is no transport of heat and moisture through these boundaries with the

exception of rain leaving the domain at the bottom. Since the air far away from the convection remains at rest, closed conditions are appropriate at the lateral boundary of the domain.

The partial differential equations are solved by a finite-difference scheme on a staggered grid. Details of the scheme were presented in Steiner (1982). Any negative rainwater mixing ratio resulting from inaccurate numerical advection is eliminated by a technique described in chapter 2. In the radial direction, the resolution is 50 m near the central axis but widens smoothly towards the lateral boundaries. This grid stretching is computationally efficient, since coarser resolution is adequate near the lateral boundaries. A total of 125 horizontal mesh points were used to cover a radius of 25 km. Grid stretching was not invoked vertically, as fine resolution was required both near the ground and in the vicinity of the rising cloud top to capture adequately the heat source and cloud top entrainment, respectively. The vertical grid spacing was uniform at 40 m throughout the depth of 10 km for the midlatitude sounding and 12 km for the tropical sounding. Initial thermodynamic conditions were adopted from observed soundings, with all velocity components set to zero. The model convection was started entirely from the source of heat and vapour. To avoid a disruptive impulse at the initial time, all numerical experiments had a 10-min "warm-up" period, during which the

input of waste heat was increased linearly from zero to its full value of H_t. Thereafter, the sources were sustained at full strength for the remainder of the experiments, which covered a period of 3 h including the warm-up period. The numerical integration time step was 1 s in all experiments.

3.3 Model results

a. Overview

The simulation results of Hane (1978) and Orville et al. (1981) indicated that the effects of waste heat release on cloud convection depend on the specific environmental conditions. Since severe convective storms typically develop in an environment characterized by strong winds and vertical shear, we did not attempt here to model severe storm conditions using our axisymmetric model, which requires a calm environment. Instead, we experimented with two soundings that supported moderate convection yet differed in other aspects. One of the model soundings was sampled by aircraft on 10 August 1973 close to a major oil refinery complex at Wood River, Illinois (Auer 1976). This particular case was chosen because in-situ cloud measurements were available for comparison with model results. Furthermore, the observed wind profile indicated nearly calm conditions (never in excess of 4.5 m s^{-1}), which is a prerequisite for using the assumption of axisymmetry. For the tropics, however, an observational study of an "industrial cumulus" was not available. Our

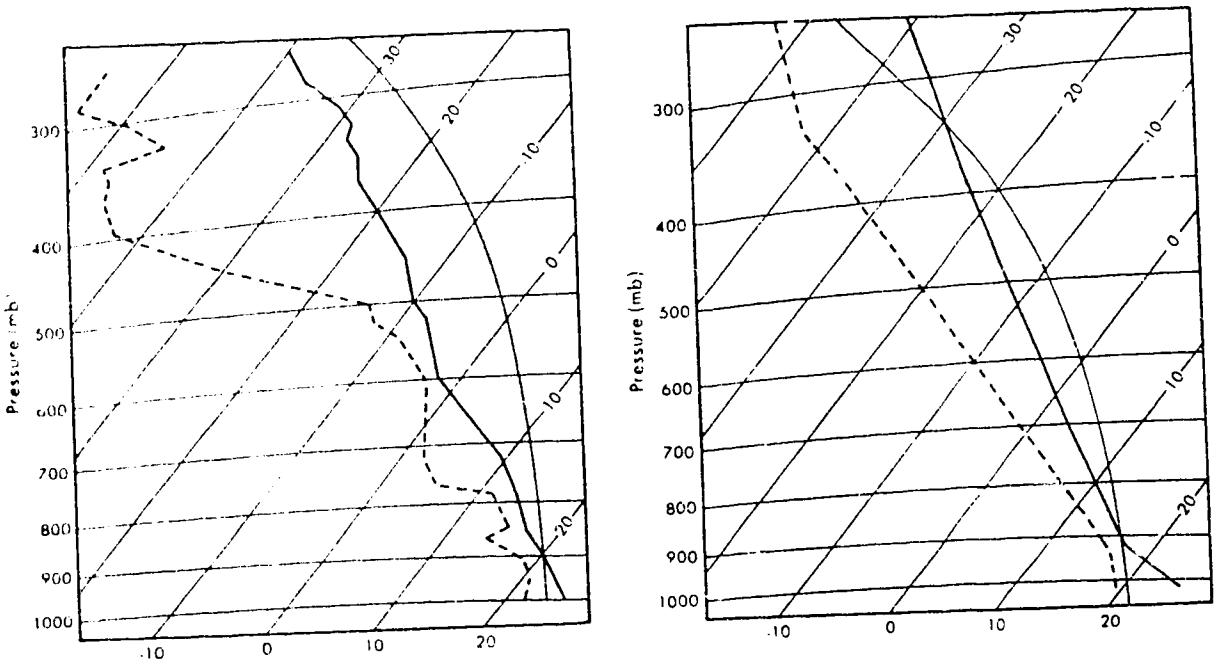

Fig. 1. Temperature (°C) (solid) and dewpoint temperature (°C) (dashed) profiles used to initialize the model: The data for the Wood River sounding (left) and the tropical sounding (right) were adopted from Murray et al. (1978) and Soong and Ogura (1973), respectively. Horizontal lines are isobars, while the skewed straight lines are isotherms. The lines curving toward the left are pseudo-adiabats.

simulation was based on Soong and Ogura's (1973) sounding, which represents a typical profile in the tropics but not any particular case.

The major difference between the soundings was that the Wood River sounding had some dry layers at low levels, whereas the tropical sounding remained humid for a great depth (Fig. 1). Table 1 compares the two soundings in terms of the positive and negative areas for an air parcel lifted adiabatically (e.g., Iribarne and Godson 1981, p. 187) and the total precipitable water of the atmosphere (e.g., Rogers 1979, p.52). The amount of potentially available energy in the Wood River sounding is about 160% of that potentially available in the tropical conditions. However, 12 J of external work are

Table 1. Comparison between Wood River sounding and tropical sounding.

	Wood River sounding	Tropical sounding
Positive Area (J kg^{-1})	1743	1097
Negative Area (J kg^{-1})	12	0
Precipitable Water (mm)	46	39

required to lift 1 kg of air from the surface to its level of free convection in the Wood River sounding, whereas no

external work is needed in the tropical case. Thus, triggering of the convection should be easier for the tropical sounding, and the effects of the heat emission should be less apparent for the tropical case.

To compare different model runs from our sensitivity tests, it was useful to introduce the following quantities: the peak updraft strength w^*, the total kinetic energy KE, the total cloud mass CM, the total rain mass RM, the total accumulated rain at the surface AR, and the total liquid water mass LM. For convenient reference, their definitions are given below:

$$w^*(t) = \max_r \max_z [w(r,z,t)] \tag{10}$$

$$KE(t) = \int_{\mathbf{V}} \frac{1}{2} \rho_0 (u^2 + w^2)\, d\mathbf{V} \tag{11}$$

$$CM(t) = \int_{\mathbf{V}} \rho_0 q_c\, d\mathbf{V} \tag{12}$$

$$RM(t) = \int_{\mathbf{V}} \rho_0 q_r\, d\mathbf{V} \tag{13}$$

$$AR(t) = \int_0^t \iint_{\mathbf{A}} (\rho_0 V_r q_r)\, d\mathbf{A}\, dt \tag{14}$$

$$LM(t) = CM + RM + AR \tag{15}$$

where **A** and **V** denote the area and volume of the numerical domain. In (14), $\rho_0 V_r q_r$ values are taken at grid points of the

lowest interior level, that is, at $z = \frac{1}{2}\Delta z$.

The organization of the remainder of this section is as follows: The control case simulation for the Wood River sounding is presented in section 3b, followed by a comparison with the observations in section 3c. Discussion of sensitivity experiments to quantify the emission effects of the industrial facility is presented in section 3d, while the results for the tropical sounding are summarized in section 3e.

b. Control case simulation for the Wood River sounding

For the control case simulation, all model input parameters were closely matched to actual conditions reported for the Wood River refinery. Murray et al. (1978) estimated that the oil refinery released sensible heat to the atmosphere at the rate of $H_s = 0.4$ GW and latent heat at the rate of $H_l = 0.6$ GW (1 GW=1 GigaWatt=10^9 Watt). The total heat loss was $H_t = 1.0$ GW. The effective area of the waste heat source was 196,000 m^2, yielding a source radius of $b = 250$ m. The effective depth of the source was 40 m.

Fig. 2 shows the time evolution of the control case simulation. In the first 10 minutes of the simulation the peak updraft grows rapidly to about 5 m s^{-1}. Thereafter, the core updraft intensifies only slightly reaching a local maximum at 60 min. Between 60 to 180 min, the peak updraft undergoes almost four complete cycles, each of which consists of a "valley" where w^* dips down to about 3 m s^{-1} and a "plateau"

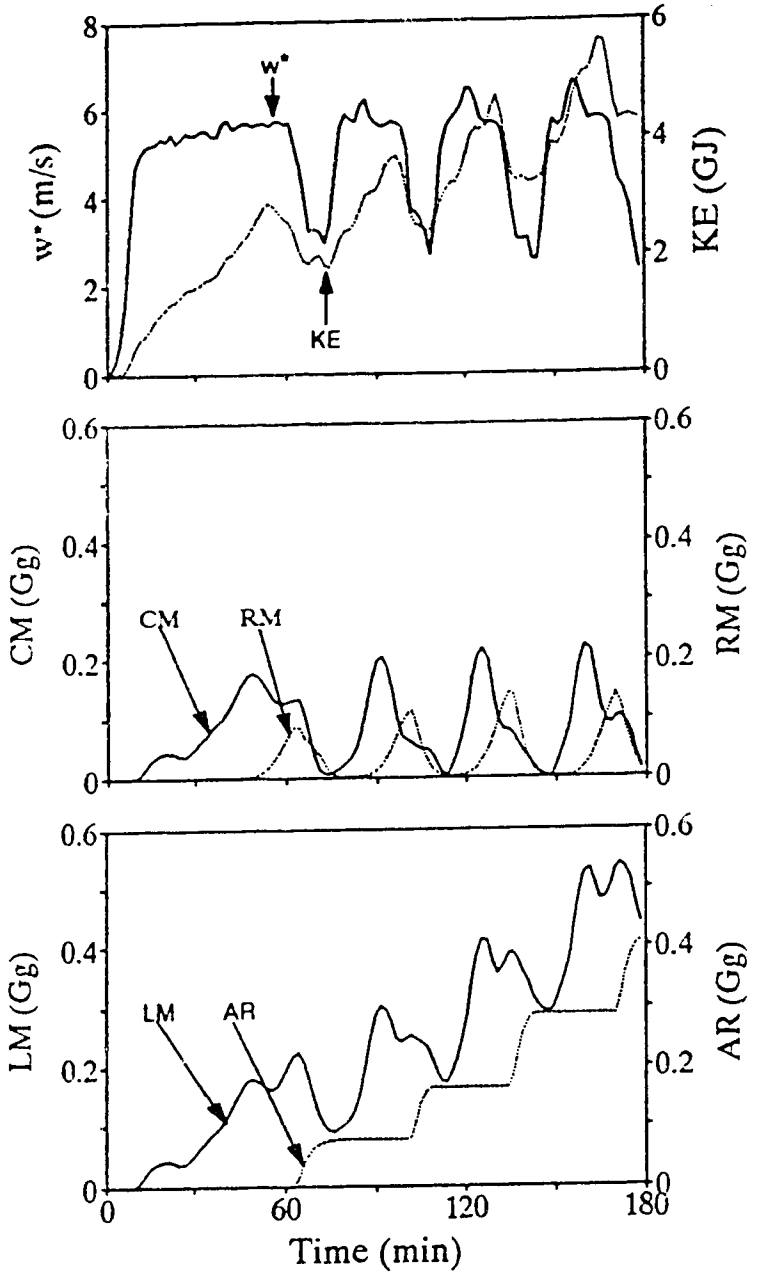

Fig. 2. Time evolution of the control run depicting peak updraft and total kinetic energy, total mass of cloud and rain, and total mass of liquid water and accumulated rain at the surface.

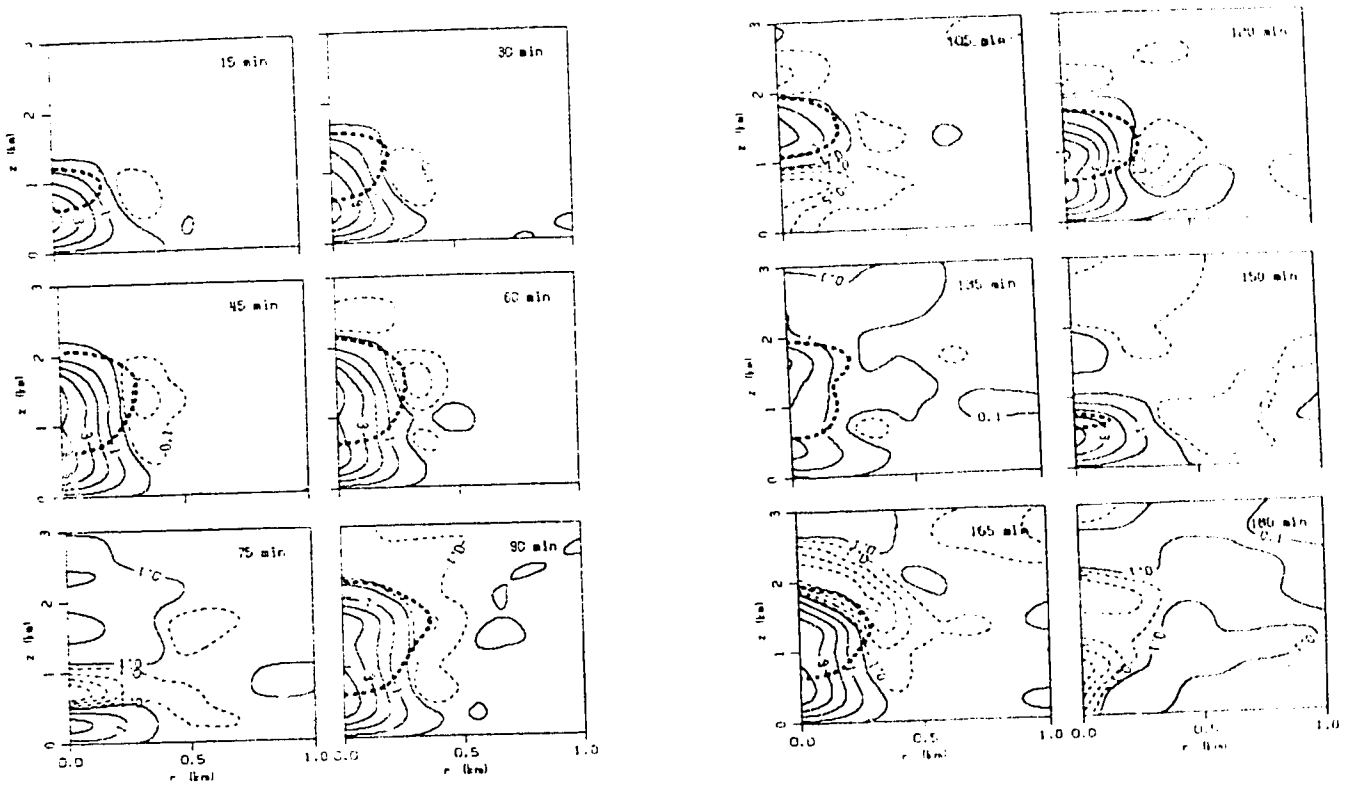

Fig. 3. Vertical velocity structure of the control run contoured every 15 min until 180 min. Upward motion is depicted in solid lines contoured every 1 m s^{-1} while downward motion is shown by dashed lines contoured every 0.5 m s^{-1}. In addition, the -0.1 and 0.1 m s^{-1} contours are also plotted. The heavy dashed line indicates the cloud boundary with a cloud water mixing ratio of 0.2 g kg^{-1}.

where w^* is about 6 m s^{-1}. The distinctive cycles of a 30-40 min period are also evident in the evolution of KE. Here, however, there is a general trend of growth as each successive local maximum exceeds the previous one. The evolution of total cloud and rainwater masses (CM and RM) indicates that weakening of the cloud circulation is preceded by the formation of large amounts of both. Apparently, the loading effect of the condensed water is responsible for the drastic weakening of the cloud updraft. In the absence of ambient wind shear in the model simulation, the downward drag of the water loading induces downdrafts that diminish the cloud development and start the dissipation of the cloud. When the rain has fallen beneath the cloud, a "new" cumulus cloud develops and the whole cumulus life cycle repeats itself. The continuous influx of heat and moisture from the waste energy source region provides the "fuel" for the regeneration of the convective cells. The surface rainfall (AR) was highly intermittent: 5-10 min bursts of rain are separated by "dry spells" lasting for 30-35 min.

The evolution of the vertical velocity structure is depicted in Fig. 3. During the developing stage of the cumulus cloud (15 and 30 min) the maximum updraft is located just below the cloud base. As the cell matures at about 45 min a second updraft maximum has developed far above the cloud base level. At this stage, strong downdrafts have formed near the cloud edges. At 60 min the cloud begins to dissipate, and 15

min later the cloud has disappeared altogether. A second, third, and fourth generation of cumulus cloud is evident at 90, 120, and 165 min, respectively. In each case, the cumulus cloud lasts for about 25 minutes, while each separate cycle has a period of about 35 min. A similar oscillatory behaviour has been found in simulations of one-dimensional cloud models (Srivastava 1967, Ćurić and Janc 1991).

c. Comparison of model results with observations

The control case simulation of the Wood River sounding will be compared with aircraft observations to assess whether the model can realistically simulate cloud convection. A major difficulty in comparing aircraft measurements with model results is the temporal variability of convective clouds. Thus, a crucial factor in the comparison is to choose the model time when the simulated cloud is at the same stage of development as the observed one. Indeed, our simulation indicates that cloud variables (such as peak updraft) change significantly in only a few minutes. The inaccuracy of the sensors is another factor that must be accounted for.

Bearing in mind these limitations, the numerical results will be compared with Auer's (1976) observations. Both observations and model results indicate that the cloud base height remained at 700 m above ground. The observed cloud top height was reported to be at 2.1 km, while the model cloud-top height varied with time from 1.5 to 2.4 km, depending on the

cloud life cycle. We chose 45 min as the time for the

Table 2. Comparison of observations and model results in terms of vertical velocity (w) and perturbation temperature (T') at three different heights above ground level.

	Aircraft Observations[a]			Model simulations[b]		
Height (km)	w_{max} (m s^{-1})	w_{avg} (m s^{-1})	T'_{avg} (^{0}C)	w_{max} (m s^{-1})	w_{avg} (m s^{-1})	T'_{avg} (^{0}C)
0.5	4.5	2.9	+0.2	5.7	3.5	-0.1
1.5	3.5	2.6	-0.5	5.3	1.8	-0.0
2.0	3.1	1.0	-0.2	0.8	0.2	-0.3

[a] As reported by Auer (1976).

[b] For control case after 45 min of simulation time.

comparison, since the simulated cloud did not yet have significant rainfall and the simulated cloud top agreed well with reported observations. Table 2 lists observed and simulated updraft and temperature values for three different altitudes. The simulated updraft values were slightly stronger than the observed ones near the cloud base but were weaker near the cloud top. Both observations and simulations had weak downward buoyancy at 1.5 and 2 km but differed at 0.5 km.

Still, the 0.3°C difference at 0.5 km was within the expected accuracy of the temperature sensor for in-cloud conditions. We abstained from comparing the liquid water contents because of the great uncertainty arising from the integration of the water content from the observed cloud droplet spectra due to sampling problems of the larger drop sizes (Auer 1976).

As the time evolution of the observed rainfall was not presented by Auer (1976), we could not verify the oscillatory nature of the simulation results. However, such intermittent rain showers are commonly observed for convectively unstable environments with no wind shear (e.g., Reuter 1990). It is likely that the presence of ambient wind shear would decrease the oscillatory tendency in the model simulation. Keeping in mind the limitations of comparing the model with observations, a realistic simulation of the industrial cumulus seems possible.

d. Sensitivity experiments for the Wood River sounding

1) Total heat (H_t)

Fig. 4 compares the evolution of peak updraft w^* and total liquid water mass LM for five numerical experiments (E0 to E4) that had H_t values of 0.0, 0.8, 1.0, 1.2, and 2.0 GW. During the 10 min "warm-up period" experiment E0 received a gradual total heat flux identical to experiment E1 to trigger

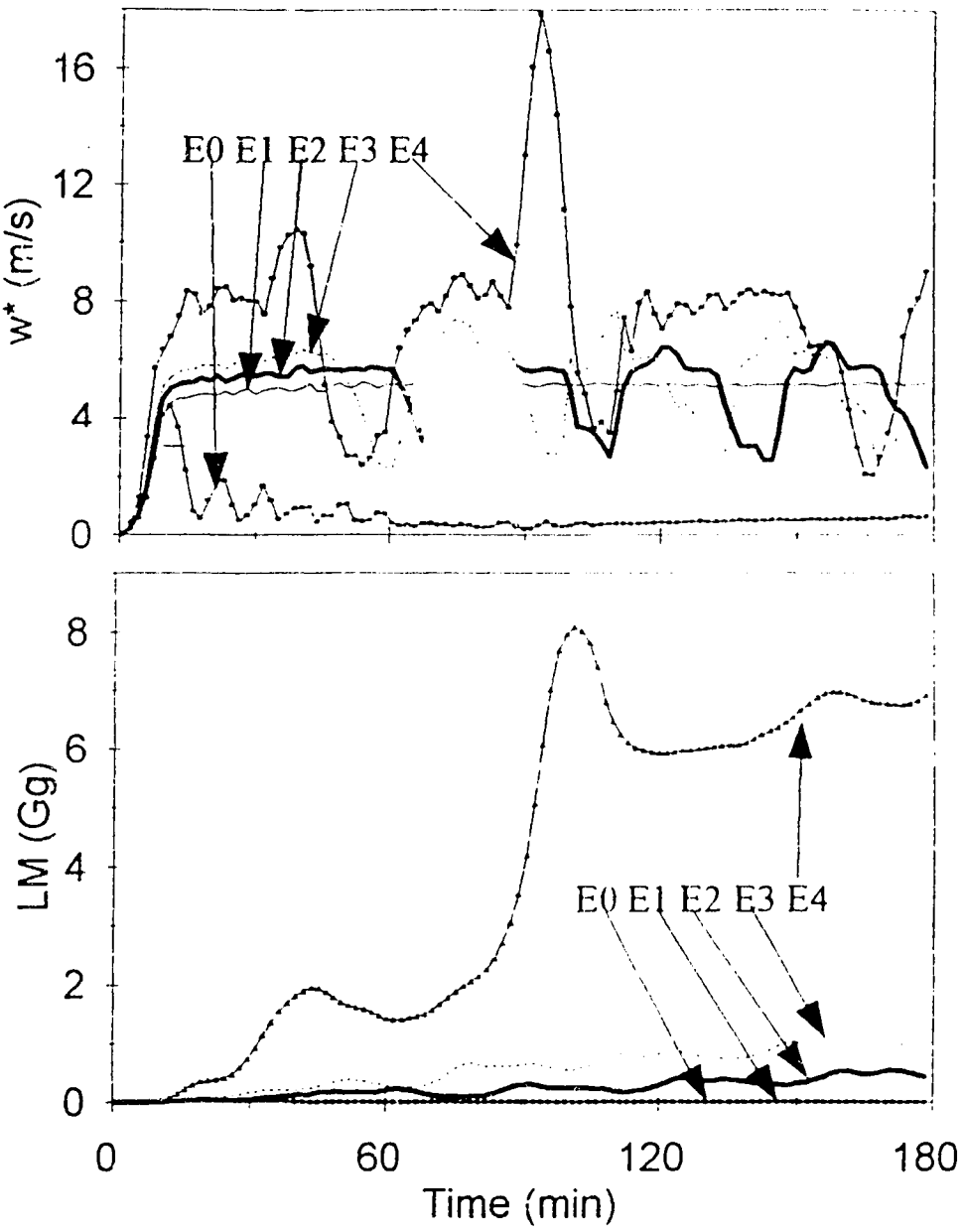

Fig. 4. Peak vertical updraft, w*, and total liquid water mass, LM, plotted versus time for experiments E0 to E4. The H. values were 0.0 (E0), 0.8 (E1), 1.0 (E2), 1.2 (E3), and 2.0 GW (E4).

convection. When after these 10 min the heating was terminated, the updraft ceased and the model cloud evaporated. An experiment was also made in which the total heating rate was identical to the control case but was terminated after 30 min. Again, the convection rapidly decayed once the industrial heating source was terminated. The model simulations suggest that for this particular sounding, sustained heating is mandatory for cloud convection.

The graph shows the sensitivity of convection to the magnitude of the total heating rate. As H_t increases, w^* and LM are also increased. A larger H_t value also speeds up the cloud formation initially. By comparing E3 to E2, it is evident that by increasing the value of H_t by 20% over its control case value, the amount of cloud condensate can be doubled. Even more striking, a reduction in H_t to 80% of its control case value terminates the formation of precipitation altogether (E1). In this case, after its initial growth, w^* remains near 4 m s^{-1} as there is no precipitation-induced downdraft and associated cumulus decay. In the extreme case E4, where H_t is twice its control case value, the convection develops dramatically at about 100 min, with a w^* "spike" of almost 18 m s^{-1}. A closer inspection of E4 reveals that in this case the simulated cloud penetrated through the dry layer located between 2.0 and 4.0 km, and the cloud tower rose up to 7.8 km. The comparison of maximum kinetic energy values (KE_{max}) indicated that KE_{max} increased monotonically as H_t was

increased (Table 3). This may have an interesting implication for the control of operating an industrial facility under pre-storm conditions: A small reduction of waste energy may result in a substantial reduction in the severity of a convective outburst for some environmental conditions such as the Wood River sounding.

2) Ratio of sensible to total heat (H_s/H_t)

Waste energy released from an industrial complex into the atmosphere is usually in the form of both sensible heat (H_s) and latent heat (H_l). The exact ratio of the two depends on the combination of dry and evaporative cooling towers in operation. A cooling system emitting solely latent heat is not available for large industries, but a ratio of sensible heat over total heat (H_s/H_t) of 20% is feasible. On the other hand, there exist huge dry cooling towers without evaporation. A series of numerical experiments was run in which H_s/H_t varied from 0.2 to 1. The numerical results are summarized in Table 3 and Fig. 5. For H_s/H_t=20% (E9), the convection remained rather weak and there was no rainfall. As the relative contribution of sensible heat becomes larger, the convection becomes progressively more organized with stronger updrafts and more rain. When all of the waste energy was released in sensible heat, the cloud developed dramatically, producing much more rain than in the other cases.

Our results confirm the finding of Koenig et al. (1978) that "sensible heat is much more likely to initiate convective

Table 3. Comparison of experiments initialized with the Wood River sounding for different input parameters: Total emission rate of waste heat (H_t), ratio of sensible versus total heat (H_s/H_t) and radius of heat source region (b).

Exp	H_t GW	H_s/H_t	b m	w^*_{max} m s^{-1}	KE_{max} GJ	TOP_{max} km	CM_{max} Gg	RM_{max} Gg	AR_{max} Gg	LM_{max} Gg
E0[a]	0.0	0.4	250	4.4	0.5	1.0	0.01	0.00	0.00	0.01
E1	0.8	0.4	250	5.2	3.1	1.4	0.02	0.01	0.00	0.02
E2[b]	1.0	0.4	250	6.6	5.7	2.5	0.22	0.14	0.41	0.54
E3	1.2	0.4	250	7.7	7.6	2.9	0.35	0.30	0.97	1.09
E4	2.0	0.4	250	17.9	56.7	7.8	1.64	4.71	6.74	8.08
E5	1.0	1.0	250	15.4	28.6	6.5	0.89	1.51	2.72	4.49
E6	1.0	0.8	250	8.0	9.5	3.9	0.37	0.43	1.52	1.80
E7	1.0	0.6	250	6.8	7.3	2.5	0.26	0.23	0.83	0.93
E8[b]	1.0	0.4	250	6.6	5.7	2.5	0.22	0.14	0.41	0.54
E9	1.0	0.2	250	4.6	2.5	1.7	0.03	0.00	0.00	0.03
E10	1.0	0.4	200	7.3	6.3	2.6	0.24	0.17	0.49	0.78
E11[b]	1.0	0.4	250	6.6	5.7	2.5	0.22	0.14	0.41	0.54
E12	1.0	0.4	300	5.8	4.3	2.2	0.15	0.08	0.14	0.27
E13	1.0	0.4	350	5.2	4.2	2.1	0.14	0.05	0.05	0.17
E14	1.0	0.4	400	4.6	4.2	1.3	0.03	0.00	0.00	0.03
E15[c]	1.0	0.4	250	6.8	5.2	2.5	0.22	0.13	0.40	0.61
E16[b]	1.0	0.4	250	6.6	5.7	2.5	0.22	0.14	0.41	0.54

[a] H_t increases linearly from 0.0 to 0.8 GW in the first 10 min. Thereafter H_t = 0 GW.

[b] Control case simulation.

[c] Fluxes increase linearly with radius (see text for details).

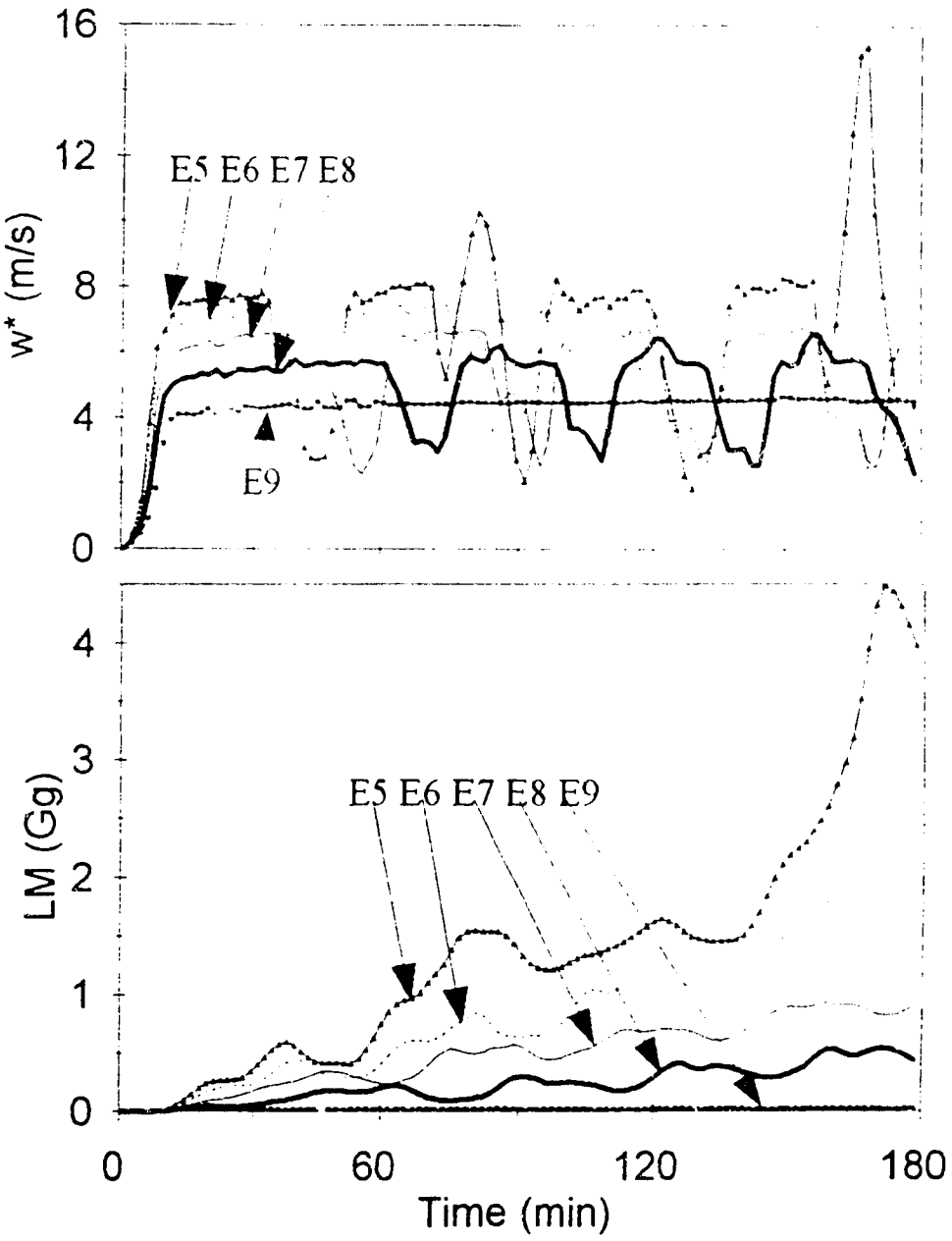

Fig. 5. Comparison of the evolution of w^* and LM for experiments E5 to E9 that differed in their H_s/H_t values being 1.0 (E5), 0.8 (E6), 0.6 (E7), 0.4 (E8) and 0.2 (E9).

circulations and anomalous cloudiness than latent heat". A plausible physical explanation of why sensible heating provides more "fuel" for convective triggering compared to latent heat is that the subcloud buoyancy is much more affected by a temperature perturbation than a vapour perturbation: For an equal increment of specific energy, sensible heat increases the buoyancy 13 times as much as latent heat (e.g., Koenig et al. 1978). However, numerical models for severe storm conditions (Orville et al. 1981) suggest that there exist cases where dry cooling towers are preferable to wet ones for the release of large quantities of heat. Effects other than buoyancy seem to dominate in these cases.

3) Radius of effective source region (b)

The next series of experiments (E10 to E14) was made to examine the role of the area of the waste heat plume. In these experiments the values for H_t and H_s/H_t were kept the same, but the radius of the heat source was increased from 200 to 400 m in steps of 50 m. The most intense convection occurred in E10, which had the smallest b value (Fig. 6). As the source region was expanded, the simulated convection became weaker. For the 400 m wide heat source (E14) the cumulus never reached its precipitation stage. Table 3 shows the relative importance of the area of the heat source versus its intensity. The changes in cloud parameters due to different b values (E10 to E14) tended to be smaller than changes due to different H_t values

(E0 to E4) or to different H_s/H_t values (E5-E9).

ial distribution of heat within the source region

A[illegible]merical experiments described so far had the waste energy flux distributed uniformly within the effective source region. In reality, however, the heat flux will likely have some spatial variability, details of which depend on the locations of the individual towers that make up the cooling complex. To test the sensitivity of the axisymmetric model to the radial variability of the heat flux within the effective source region, experiment E15 was run differing from the control case simulation only in that the latent and sensible heat were highest at the central axis and decreased linearly outward to zero at r = b. Specifically, the source of vapour was modelled by

$$S_\varrho = 3\,\frac{b-r}{b}\,\frac{\boldsymbol{H}(b-r)\,\boldsymbol{H}(D+D_0-z)\,\boldsymbol{H}(z-D_0)}{\pi b^2 D \rho_0}\left[\frac{H_1}{L}\right] \qquad (16)$$

with a similar expression for entropy. All symbols above have the same meaning as in (8). Comparison of E15 with E16 (the control case) indicated that the linear distribution of fluxes within the source region resulted in a stronger peak updraft (Fig. 7). In E15 the total rainfall after 3 h was 2% smaller, while the KE_{max} value was 8% smaller (Table 3). Clearly, the simulation results depend on the specific distribution of fluxes within the source region, but the effects were rather small. From a modelling point of view, it is encouraging that the details of the spatial distribution of the fluxes within

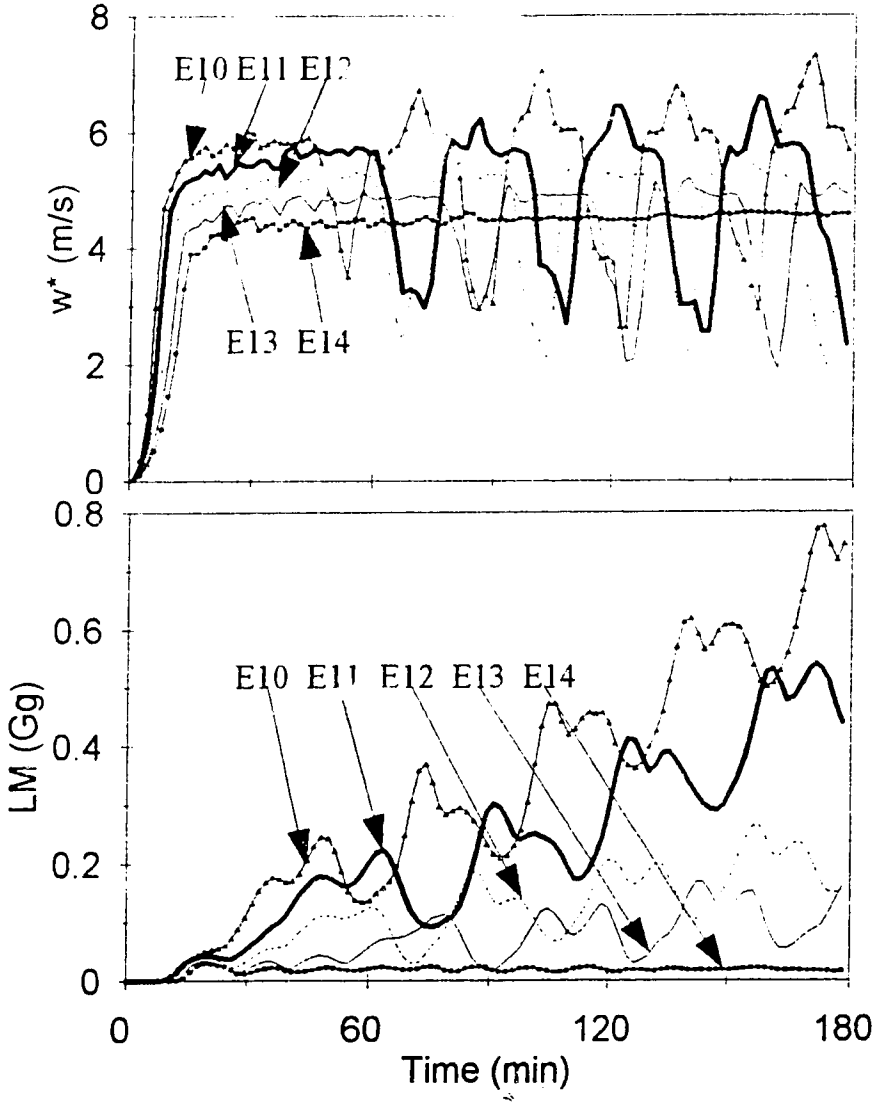

Fig. 6. Comparison of the evolution of w^* and LM for experiments E10 to E14 differing in their source radius, b: 200 (E10), 250 (E11), 300 (E12), 350 (E13), and 400 m (E14).

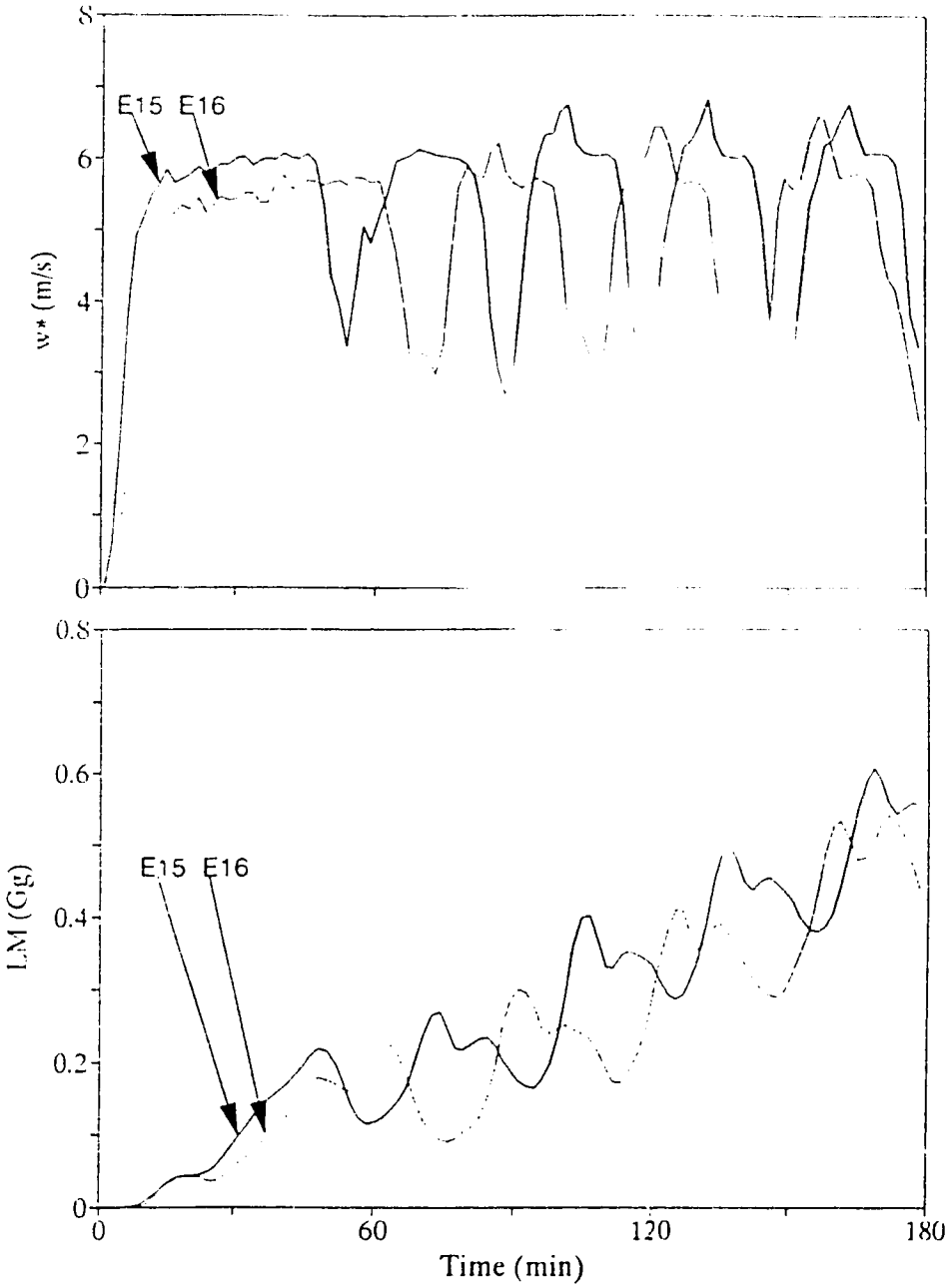

Fig. 7. Comparison of the evolution of w^* and LM for experiments E15 and E16. In E15 the sensible and latent heat fluxes were decreased linearly with increasing radius from the centre to become zero when r=b, whereas in the control case E16 the fluxes have a top-hat profile with uniform distribution for all r<b.

Table 4. Comparison of experiments initialized with the tropical sounding for different input parameters.

Exp	H_t GW	H_s/H_t	b m	w^*_{max} m s^{-1}	KE_{max} GJ	TOP_{max} km	CM_{max} Gg	RM_{max} Gg	AR_{max} Gg	LM_{max} Gg
T0[a]	0.0	0.4	250	6.4	1	2.4	0.2	0.0	0.0	0.2
T1	0.8	0.4	250	12.2	34	5.8	1.5	2.8	8.6	10.0
T2[b]	1.0	0.4	250	12.7	32	6.3	1.3	2.7	10.2	11.4
T3	1.2	0.4	250	12.6	42	6.6	1.4	3.5	13.2	14.8
T4	2.0	0.4	250	16.4	67	7.3	2.3	5.7	23.1	25.5
T5	1.0	1.0	250	14.6	53	7.0	1.9	4.2	16.2	17.4
T6	1.0	0.8	250	13.9	47	6.8	1.7	3.7	15.2	16.4
T7	1.0	0.6	250	12.8	41	6.6	1.5	3.4	14.1	15.5
T8[b]	1.0	0.4	250	12.7	32	6.3	1.3	2.7	10.2	11.4
T9	1.0	0.2	250	12.6	33	5.8	1.3	2.3	6.7	9.9
T10	1.0	0.4	200	13.1	41	6.2	1.9	4.4	12.9	14.5
T11[b]	1.0	0.4	250	12.7	32	6.3	1.3	2.7	10.2	11.4
T12	1.0	0.4	300	13.0	32	6.2	1.2	2.4	10.0	12.2
T13	1.0	0.4	350	13.4	37	5.9	1.6	2.8	10.0	10.9
T14	1.0	0.4	400	13.1	39	5.8	1.6	2.9	8.2	10.8
T15[c]	1.0	0.4	250	13.4	33	6.1	1.8	3.8	10.4	12.0
T16[b]	1.0	0.4	250	12.7	32	6.3	1.3	2.7	10.2	11.4

[a] H_t increases linearly from 0 to 0.8 GW in the first 10 min. Thereafter H_t = 0 GW.

[b] Control case simulation.

[c] Fluxes decrease linearly with radius (see text for details).

the source region seemed to be only of secondary importance and may perhaps be ignored.

5) OTHER MODEL PARAMETERS

We conducted many more sensitivity experiments on different model parameters (see appendix 1). For the sake of conciseness and focus, only a brief summary of the major results is attempted here.

a) The convection depended on the depth of the sensible and latent heat source. Increasing the depth from 40 m to 80 m weakened the simulated cloud.

b) The model results depended slightly on the constants used in the microphysical parameterization scheme.

c) The model results depended slightly on the constants of the turbulence closure scheme.

e. Model results for tropical sounding

Table 4 compares the tropical sounding experiments having different values for H_t, H_s/H_t and b, respectively. Graphs of the time evolution of selected cloud parameters are available in appendix 2. Comparison of the results for experiments T0 to T4 shows that as the total waste heat flux increases, so does the accumulated rain at the surface. The total maximum kinetic energy (KE_{max}) was 34 GJ for H_t = 0.8 GW (in T1) but only 32 GJ for H_t = 1.0 GW (in T2). Clearly, a small increase in the heat influx value does not always strengthen all integral cloud parameters, despite the fact that this seems to

be the general tendency.

The results for experiments T5 to T9 (Table 4) indicated that as the relative contribution of sensible heat waste was increased, the cloud convection became stronger and more rain was formed. However, an increase in the H_s/H_t value did not always increase KE_{max}, underscoring the fact that the intensity of the convection is not a simple monotonic function of H_s/H_t. We found that a change in source radius had only a small impact; the AR values hinted that more rain fell for smaller b values, but other cloud parameters did not show a similar trend.

Despite the fact that the tropical sounding had about 35% less available potential energy than the midlatitude sounding, the tropical sounding yielded a larger total kinetic energy and total rain accumulation. The stronger tropical convection can be attributed to the fact that the midlatitude sounding required work to lift the surface air to its level of free convection, whereas no such work was required for the tropical case. In concert with this, the simulation results indicated that the tropical convection was less sensitive to changes in the parameters of the industrial heating source than the convection based on the midlatitude sounding.

3.4 Summary and conclusions

An axisymmetric cloud model was used to simulate cumulus convection triggered by waste energy emitted from an

industrial complex into a calm environment. In contrast with the slab-symmetric geometry used in previous studies, the axisymmetric framework can realistically model the emission of sensible and latent heat into an effective source region that has finite spatial dimensions. To allow for the formation of rain, the cloud model includes a bulk water parameterization. In order to capture the convection realistically, a high spatial resolution has been adopted: 40 m vertically, and between 50 and 52 m radially in the vicinity of the cloud. Sensitivity experiments were done using two different sets of initial conditions adopted from a midlatitude sounding sampled at Wood River, Illinois and a schematic tropical sounding. Comparison of model results with aircraft observations suggests that the cloud model can realistically simulate the observed cloud depth and updraft strength. The model simulations were run for 3 h, covering multiple life cycles of cumulus cells yielding intermittent rainfall at the ground.

For the midlatitude sounding, cloud convection depended markedly on the total heat emission (H_t) and the ratio of sensible to total heat emission (H_s/H_t) (Fig. 8). The tropical convection, however, showed much smaller sensitivity to changes in the heat source parameters. A larger total heat emission rate tended to cause a stronger circulation (i.e., larger KE_{max}) and more rain accumulation (AR_{max}). While this trend is monotonic for the Wood River sounding, it is less apparent for the tropical case, where an increase in H_t from

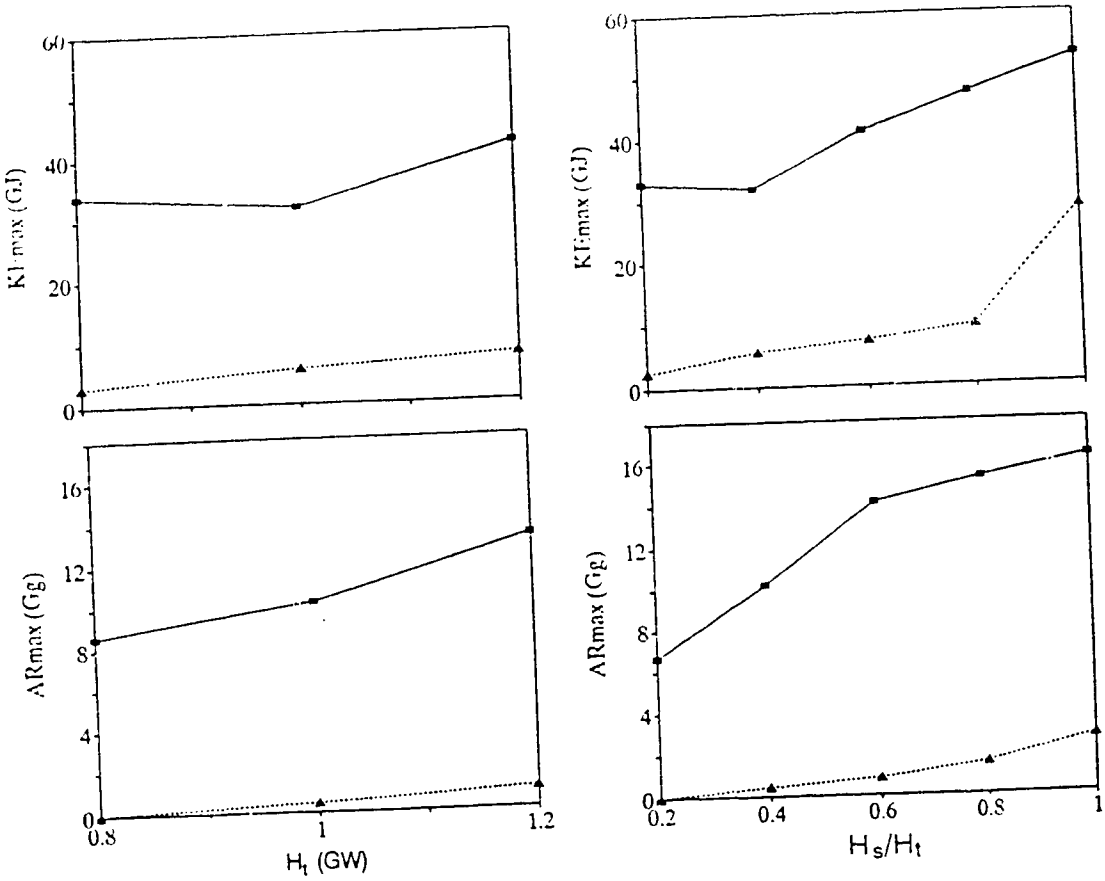

Fig. 8. Maximum total kinetic energy (KE_{max}) and maximum accumulated rain at the surface (AR_{max}) plotted versus H_t (left) and H_s/H_t (right). Results for the tropical sounding are in solid line; the dashed line shows the results for the Wood River sounding.

0.8 to 1.0 GW even resulted in a small decrease in KE_{max}. As the relative contribution of the sensible heat is increased, the circulation becomes more organized with more rain falling to the ground. A tentative conclusion, based on a limited number of experiments, is that wet cooling towers may have some environmental advantages over the more costly dry cooling towers in that they may be less likely to trigger severe convection. The same finding was evident in the slab-symmetric simulation reported by Koenig et al. (1978).

For the Wood River sounding, the radius of the effective heat source (b) was also important. If the heat source region was smaller, the convection was more intense. Numerical experiments suggested that the simulated convection was only marginally sensitive to the radial distribution of the sensible and latent heat fluxes within a fixed source region.

This chapter indicates that an axisymmetric cloud model can be a useful tool to investigate "industrially triggered" cumulus clouds and rain showers in the absence of horizontal wind. It would be of interest to determine to what extent a strongly sheared ambient flow could modify the findings presented here. A high-resolution three-dimensional cloud model will be needed for such an investigation. If computing power continues its present growth, this will soon be feasible.

References

Auer, A. H., Jr., 1976: Observations of an industrial cumulus. J. Appl. Meteor., 15, 406-413.

Campistron, B., 1987: Interaction between a natural snowfall and a cooling tower plume: An experimental study with a millimetric Doppler radar. Atmos. Environ., 21, 1375-1383.

Changnon, S.A., R.T. Shealy, and R.W. Scott, 1991: Precipitation changes in fall, winter and spring caused by St. Louis. J. Appl. Meteor., 30, 126-134.

Cotton, W.R., and G. Tripoli, 1978: Cumulus convection in shear flow - three-dimensional numerical experiments. J. Atmos.Sci., 35, 1503-1521.

Ćurić, M., and D. Janc, 1991: Graupel growth and trajectories in a shallow Cb cloud determined by a forced 1-D model. Atmos.-Ocean, 29, 462-478.

Hane, E., 1978: The application of a two-dimensional convective cloud model to waste heat release from proposed nuclear energy centres. Atmos. Environ., 12, 1839-1848.

Hanna, S. R., 1976: Comments on "observations of an industrial cumulus". J. Appl. Meteor., 15, 1232-1233.

___, and F. A. Gifford, 1975: Meteorological effects of energy dissipation at large power parks. Bull. Amer. Meteor. Soc., 56, 1069-1076.

Hill, G. E., 1974: Factors controlling the size and spacing of cumulus clouds as revealed by numerical experiments. J. Atmos. Sci., 31, 646-673.

___, 1977: Initiation mechanisms and development of cumulus convection. J. Atmos. Sci., 34, 1934-1941.

Innocentini, V., and E. S. Caetano, 1992: A numerical study of the role of humidity in the updraft driven by moist slantwise convection. J. Atmos. Sci., 49, 1092-1106.

Iribarne, J.V., and W. L. Godson, 1981: Atmospheric Thermodynamics. 2nd ed., D. Reidel Publ., Dordrecht, 259 pp.

Kessler, E. E., 1969: On the distribution and continuity of water substance in atmospheric circulations. Meteor. Monogr., No. 32, Amer. Meteor. Soc., Boston, 84 pp.

Koenig, L. R., F. W. Murray and P. M. Tag, 1978: Differences in atmospheric convection caused by waste energy rejected in the forms of sensible and latent heats. Atmos. Environ., 12, 1013-1019.

Kramer, M. L., D. E. Seymour, M. E. Smith, R. W. Reeves, and T. T. Frankenberg, 1976: Snowfall observations from natural-draft cooling tower plumes. Science, 193, 1239-1241.

Murray, F.W., L. R. Koenig, and P. M. Tag, 1978: Numerical simulation of an industrial cumulus and comparison with observations. J. Appl. Meteor., 17, 655-668.

Orville, H. D., P. A. Eckhoff, J. E. Peak, J. H. Hirsch, and

F. J. Kopp, 1981: Numerical simulation of the effects of cooling tower complexes on clouds and severe storms. Atmos. Environ., 15, 823-836.

Reuter, G. W., 1987: Penetrative downdrafts in mixed-phase clouds. S. Afr. J.Phys., 10, 139-145.

___, 1990: Radar observations of precipitation production in thunderstorms. Atmos.-Ocean, 28, 216-229.

___, and O. Jacobsen, 1993: Effects of variable wind shear on the mesoscale circulation forced by slab-symmetric diabatic heating. Atmos.-Ocean, 32, 451-469.

___, and M. K. Yau, 1987: Mixing mechanisms in cumulus congestus clouds. Part II: Numerical simulations. J. Atmos. Sci., 44, 798-827.

Rogers, R.R., 1979: A short course in cloud physics. 2nd edition, Pergamon Press, Oxford, 235 pp.

Schlesinger, R. E., 1984: Effects of the pressure perturbation field in numerical models of unidirectionally sheared thunderstorm convection: two versus three dimensions. J. Atmos. Sci., 41, 1571-1587.

Soong, S., and Y. Ogura, 1973: A comparison between axisymmetric and slab-symmetric cumulus cloud model. J. Atmos., Sci. 30, 879-893.

Srivastava, R.C., 1967: A study of the effect of precipitation on cumulus dynamics. J. Atmos. Sci, 24, 36-45.

Steiner, J. T., 1982: An axially symmetric cloud model: Development and simulations. Stormy Weather Group,

Scientific Report.MW-94, McGill University, 55 pp.

Chapter 4

Effects of industrial pollution on cumulus convection and rain showers: A numerical study

4.1 Introduction

Burning of fossil fuel in large industrial plants emits significant amounts of sulphur dioxide which are converted into sulphate aerosols in the atmosphere. Since atmospheric sulphates occur in a size of the order of a few tenths of a micrometer and are water soluble, they act as cloud condensation nuclei (CCN). Some of the CCN from industrial sources have a large affinity with water, and hence act as giant CCN that tend to broaden the initial cloud droplet spectrum of warm cumuli forming in the polluted air.

Airborne measurements indicate that industrial facilities can indeed change the drop size spectra of warm cumulus clouds developing in plumes with high CCN concentrations (Hobbs et al., 1970; Eagan et. al., 1974; Hindman et al., 1977a, b; Mather, 1991). The major impact of the higher concentrations of CCN is to increase the cloud droplet concentration N_c and the relative cloud droplet mass variance ν_m (Leaitch and Isaac, 1994). Hindman et al.'s (1977b) measurements indicated that clouds located in and out of a visible paper mill plume differed in their average N_c values by a factor of 1.3-1.8 and in their ν_m values by a factor of about 1.1. In unpolluted air, cloud droplets grow only after the vapour

pressure exceeds the saturation value. Supersaturation values in natural warm cumuli are a few tenths of one percent (Hobbs, 1993). In contrast, industrially polluted plumes with giant CCNs diminish in-cloud supersaturation values.

Hobbs et al. (1970) postulated that CCN emitted from industrial sources cause an increase in the local rainfall. Observational support for this hypothesis came from the analysis of Eagan et al. (1974) and Mather (1991). However, detailed model calculations indicated that the increase in giant CCN cannot account for the observed increase in rainfall (Hindman et al. 1977c). Instead it was speculated that the enhancement of rainfall was caused by the vapour and sensible heat emitted from the industrial plants.

The purpose of this chapter is to clarify the possible role of industrial pollution in convective rain showers using a numerical model. In contrast with Hindman et al.'s cloud model (which had a crude dynamic but detailed microphysical framework) our approach is to use a model with good dynamics and a bulk-water microphysical scheme. The environmental conditions for the model simulations were adopted from Auer's (1976) aircraft measurements sampled in polluted air in the vicinity of an oil refinery. To quantify the possible impact of the pollution on cumulus development and rainfall, model experiments with different cloud droplet spectra and different supersaturation values were run. The individual contributions caused by the supersaturation and the cloud droplet spectra

will be analyzed using the Factor Separation Method proposed by Stein and Alpert (1993).

4.2 Numerical cloud model

The numerical cloud model used in this study is an extension of the time-dependent non-hydrostatic cumulus model developed by Steiner (1982), Reuter and Yau (1987), Reuter (1987). It is very economical in terms of computing resources since it based on the assumption of axisymmetry, a stretched grid in the radial direction and an efficient thermodynamic scheme. Since the model equations are given in chapter 2, only the major features are briefly summarized here.

The dynamic equations are based on the deep anelastic approximation that filters out all spurious acoustic waves. Perturbation pressure is computed diagnostically from the Poisson equation obtained by taking the divergence of the momentum equations. The sub-grid scale turbulent processes are parameterized using a first-order closure scheme in which Reynolds stresses are proportional to the local velocity deformation. The turbulent exchange coefficient depends on the time scales of both moist buoyancy and shear deformation. In regions where the local Richardson number exceeds ¼ the shear generated turbulence is set to zero to prevent artificial mixing in the presence of marked static stability.

A bulk water parameterization scheme is used to model the microphysics for warm rain processes. Water substance is

divided into vapour, cloud water and rainwater. The cloud water consists of droplets having diameter less than about 50 μm that move with the ambient air, while the rain consists of the larger drops that have a finite terminal fall speed. The model includes conservation equations for $Q = q_v+q_c$ (the sum of mixing ratios of vapour and cloud water), q_r (mixing ratio of rainwater) and φ (total moist specific entropy). Once Q, q_r and φ are estimated from advection and diffusion at a given time step the following iterative procedure is invoked to determine q_v and q_c. On the assumption that $Q \leq (1+S)\ \epsilon\ e_s(T)/p$, we compute T from φ. Here S denotes the effective supersaturation value assumed for cloudy air, ϵ=0.622, e_s is the equilibrium saturation vapour pressure over a plane liquid water surface, T is the local temperature and p is the local pressure of dry air. Using this value of T, the value of $q_v^* = (1+S)\ \epsilon\ e_s(T)/p$ is computed. If this value q_v^* exceeds Q, the vapour mixing ratio is indeed less than its supersaturation value required for cloud condensation, and hence $q_v = Q$ and q_c=0. On the other hand, if q_v^* is less than Q, the assumption of sub-saturation is clearly false. Hence, q_v^* is substituted in the expression for φ which is solved for a more accurate T value. This new estimate for T is then used to obtain a better estimate for q_v^*, and the procedure is iterated until convergence is reached. At that stage, we set $q_v = q_v^*$ and $q_c=Q-q_v^*$. In the presence of rainwater, a similar procedure is used that accounts for evaporation of rain falling in sub-

saturated air (details given in chapter 2).

In our model the rate of autoconversion of condensed liquid water from cloud droplets to raindrops is based on Berry and Reinhardt's (1973) parameterization. In contrast to the commonly used Kessler's (1969) scheme in which the autoconversion rate C_{cr} depends only on the cloud water mixing ratio q_c, Berry and Reinhardt's approach allows also for dependence on the cloud droplet mass spectrum. The autoconversion is dependent upon q_c, the initial cloud droplet concentration N_c, and the mass dispersion ν_m of the initial droplet distribution:

$$C_{cr} = \frac{[\rho_0 q_c]^2}{[0.2\,\rho_0] + [2.4\times10^5 q_c \nu_m / N_c]^{-1}} \qquad (1)$$

where ρ_0 is the air density in kg m^{-3}, N_c in cm^{-3}, q_c in kg/kg, C_{cr} in s^{-1}. This formulation exhibits a roughly cubic dependence on q_c, a direct dependence on the initial mass cloud droplet dispersion, and an inverse dependence on the initial cloud droplet concentration.

The formulations for terminal fall speed of rainwater, evaporation of rainwater and the rate of change of rainwater mixing ratio by accretion of cloud droplets have been presented in chapter 2.

The model includes sensible heat and vapour released from a near surface source following the approach of Murray et al. (1978) and Orville et al. (1981). The emission is distributed uniformly within a specified source region at a constant rate.

A weak perturbation in humidity is used at the initial time to focus the developing cloud near the domain centre. Details about the heat and moisture sources and the initial humidity perturbation are presented in chapter 2.

Top and bottom boundaries are assumed to be rigid and free-slip. Closed conditions are used at the lateral boundary of the domain. The system of non-linear partial equations is solved using a finite difference scheme on a staggered grid. Second-order centred differences are used in space. The time integrations are calculated using a non-diffusive leapfrog scheme. The computation of sub-grid scale motion terms is lagged in time. A time filtering procedure which prevents splitting of solutions at odd and even time steps is used.

The model domain in our simulations has a depth of 10 km and a diameter of 40 km. The vertical resolution is uniform at 100 m. In the radial direction, 125 mesh points are used with stretched resolution. Near the central axis the horizontal grid spacing is 83 m and widens smoothly towards the lateral boundaries. The resolution ranges from 83 m to 100 m inside the first 5 km of the central axis, the region of primary interest.

4.3 Results

a. Heavy pollution case

The initial conditions of the control run were taken from observed conditions on 10 August 1973 sampled near an oil

refinery complex in Wood River, Illinois (Auer 1976). This case allows to verify model results as aircraft observations were taken in small cumuli developing in the plume "characterised by the strong stench of the refinery effluent". The thermodynamic conditions were taken from the sounding data collected by aircraft (Koenig et al., 1978; Murray et al., 1978). The calm wind conditions reported are consistent with the model assumption of axisymmetry. The refinery emits sensible and latent heat at rates of 400 and 600 Mega Watts within the area of 196,000 m^2 (Murray et al. 1978). The depth of the heat source is assumed to be 100 m.

Auer (1976) compared CCN measurements sampled below cloud base over the refinery with those of unpolluted air from 13 km upstream. The concentrations of CCN activated at 0.2% supersaturation were about a factor of 5 higher in the pollution plume. From the observed cloud droplet size spectra near cloud base within the core of maximum equivalent potential temperature we estimated the average cloud droplet number concentrations N_c = 620 cm^{-3} and the relative variance of cloud droplet mass as ν_m = 0.73. Considering the high CCN value, we assumed the average supersaturation value is S=0%.

Fig.1 depicts the evolution of the model cloud in terms of the peak instantaneous updraft speed (w^*), the total kinetic energy (KE), the total cloud water mass (CM), the total rainwater mass (RM), and the accumulated rainwater

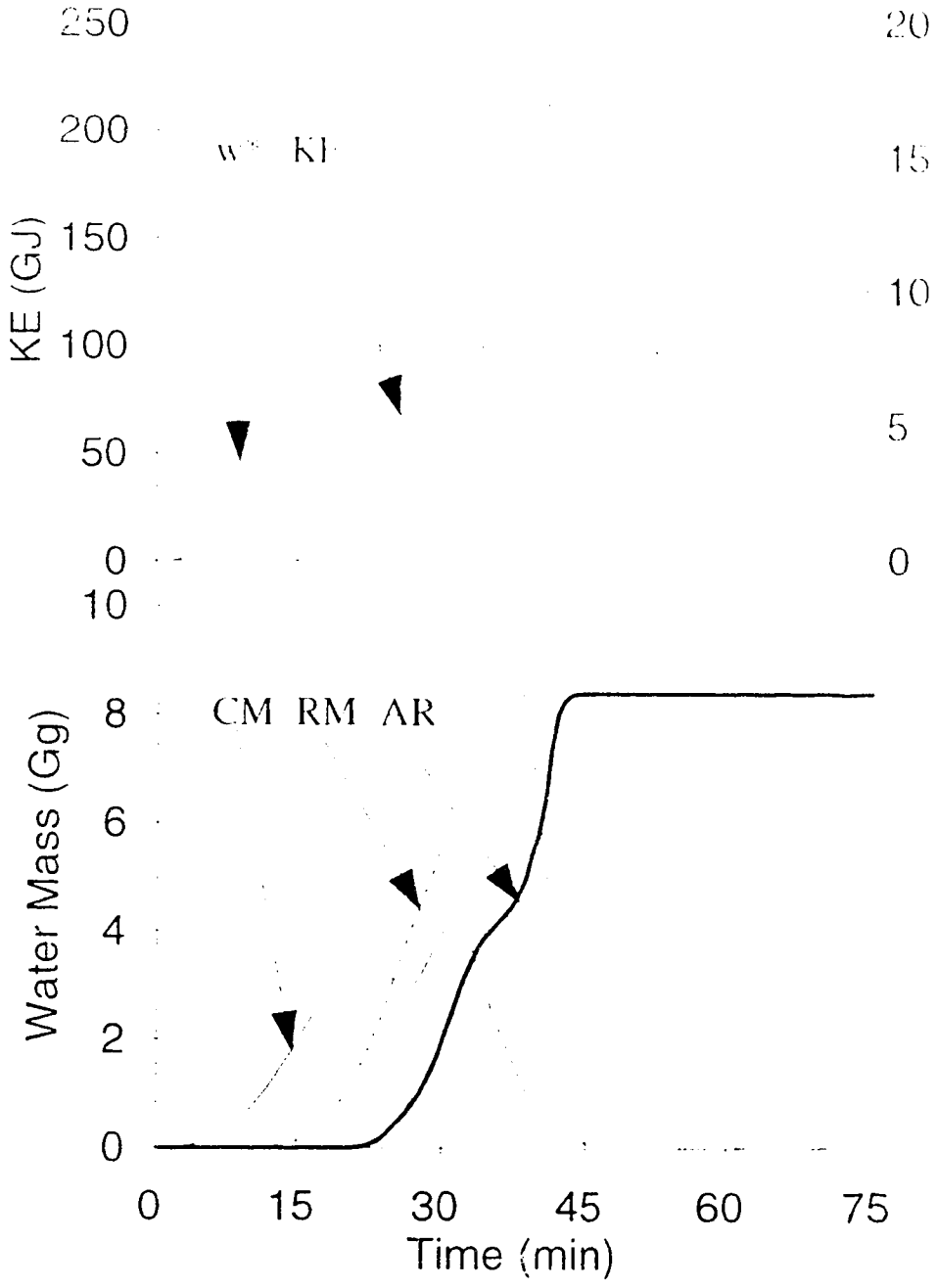

Fig. 1. Time evolution of the heavy pollution simulation run depicting peak updraft (w^*), total kinetic energy (KE), total cloud mass (CM), total rain mass (RM), and accumulated rain mass at the ground (AR).

mass at the surface (AR). The peak cloud updraft develops rapidly during the first 7 minutes; and then keeps fairly uniform at about 4.5 m s^{-1} for the next 12 minutes as the cumulus meets and penetrates a drier and stable air layer. After that w* increases very rapidly to 17.6 m s^{-1} and then decreases after about 30 min. The evolution of the total kinetic energy shows two local maxima. The first peak corresponds the maximum of w* while the second coincides with the development of a broad region of descending air motion. The total cloud mass increases steadily for the first 22 min, then decreases slightly as cloud water is converted to rain. From 27 min to 31 min CM increases again as the cloud updraft strengthened. The total life cycle of the cumulus is about an hour. The evolution of CM controls the evolution of the total rain mass. Rainwater increases and reaches its peak at 36 min. The precipitation starts at 19 min, and stops at 45 min.

Auer (1976) reported aircraft measurements sampled during the developing stage of an industrial cloud. The observed cloud extended from 700 m to 2050 m in height and was 2100 m wide. The simulated cloud structure at 15 min agrees well with these cloud dimensions (Fig.2). The simulated cloud has its base at 700 m, its top at 2100 m and a width of 2000 m. Consistent with Auer's observations, the model cloud shows a broad region of ascending motion with only weak downdrafts near the lateral cloud edges. The maximum and average vertical drafts from the model show a fair agreement with aircraft

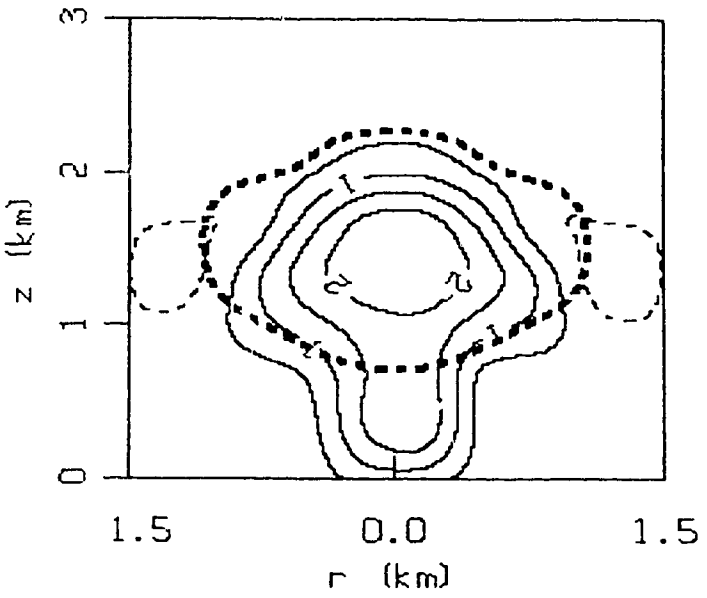

Fig. 2. Vertical cross section at 15 min depicting the updraft field of the heavily polluted cloud. Solid contours are plotted at 0.5 m s^{-1} intervals, while the dashed contour denotes the -0.1 m s^{-1} value. The heavy dashed line denotes the cloud boundary set at q_c = 0.2 g kg^{-1}.

Table 1. Comparison of observed and simulated updraft values (ms^{-1}) at three different levels above ground.

	Aircraft Observations		Model simulations	
Height (m)	Avg	Max	Avg	Max
500	2.9	4.5	2.6	3.5
1500	2.6	3.5	1.5	3.1
2000	1.0	3.1	0.73	0.97

observations sampled at three different levels (Table 1). Noting that the uncertainty in the observed updraft values is about 1 m s^{-1} (Auer 1976), we conclude that the model cloud provides a realistic portrait of the observed updraft structure.

b. Effects of pollution

To estimate the effects of pollution on rainfall, a series of numerical experiments was performed (Table 2). The

Table 2. Comparison of input data and selected results for sensitivity experiments.

Exp	N_c cm^{-3}	ν_m	S %	AR_{max} Gg	CM_{max} Gg	RM_{max} Gg	KE_{max} GJ	w^*_{max} m s^{-1}
HP	620	0.73	0.0	8.373	4.093	9.513	212.5	17.59
LP	430	0.62	0.2	8.240	3.940	9.000	179.2	17.80
NP	239	0.50	0.4	8.226	3.845	8.952	179.0	17.57
NS	620	0.73	0.4	7.785	3.870	8.711	178.4	17.94
ND	239	0.50	0.0	8.357	3.900	9.035	176.3	17.98

experiments denoted by HP, LP and NP constitute the conditions of heavy pollution, low pollution and no pollution, respectively. The choices of N_c, ν_m and S for HP have been

motivated in the previous section. For the NP case we adopted typical cloud droplet spectra for continental air mass given by N_c = 239 cm^{-3}, ν_m = 0.5 (Berry and Reinhardt 1973) and S= 0.4% (Hobbs, 1993). The parameters for the LP case constitute the means of the HP and NP parameters. Table 2 indicates that the effect of industrial pollution is rather small. In comparison to the unpolluted cloud, the heavily polluted cloud showed slightly larger values for accumulated rainfall (AR_{max}), maximum cloud water mass (CM_{max}) and rainwater mass (RM_{max}). The respective values for the LP case lie between the extreme cases but closer to the NP case. The changed cloud microphysics associated with the pollution has also some bearing on the cloud dynamics. As the level of the pollution increased so did the maximum total kinetic energy (KE_{max}).

Fig. 3 depicts the time evolution of difference curves obtained by subtracting the NP values from the HP values. The data suggest that heavily polluted cloud develops more rapidly, which results in a larger updraft, kinetic energy, and cloud water. However, rainwater and rainfall are initially less than those in unpolluted cloud because autoconversion rate in a polluted cloud is smaller than that in a natural cloud.

c. Supersaturation versus drop spectrum effects

In our model simulations the pollution can affect the cloud convection and rainfall through two different processes:

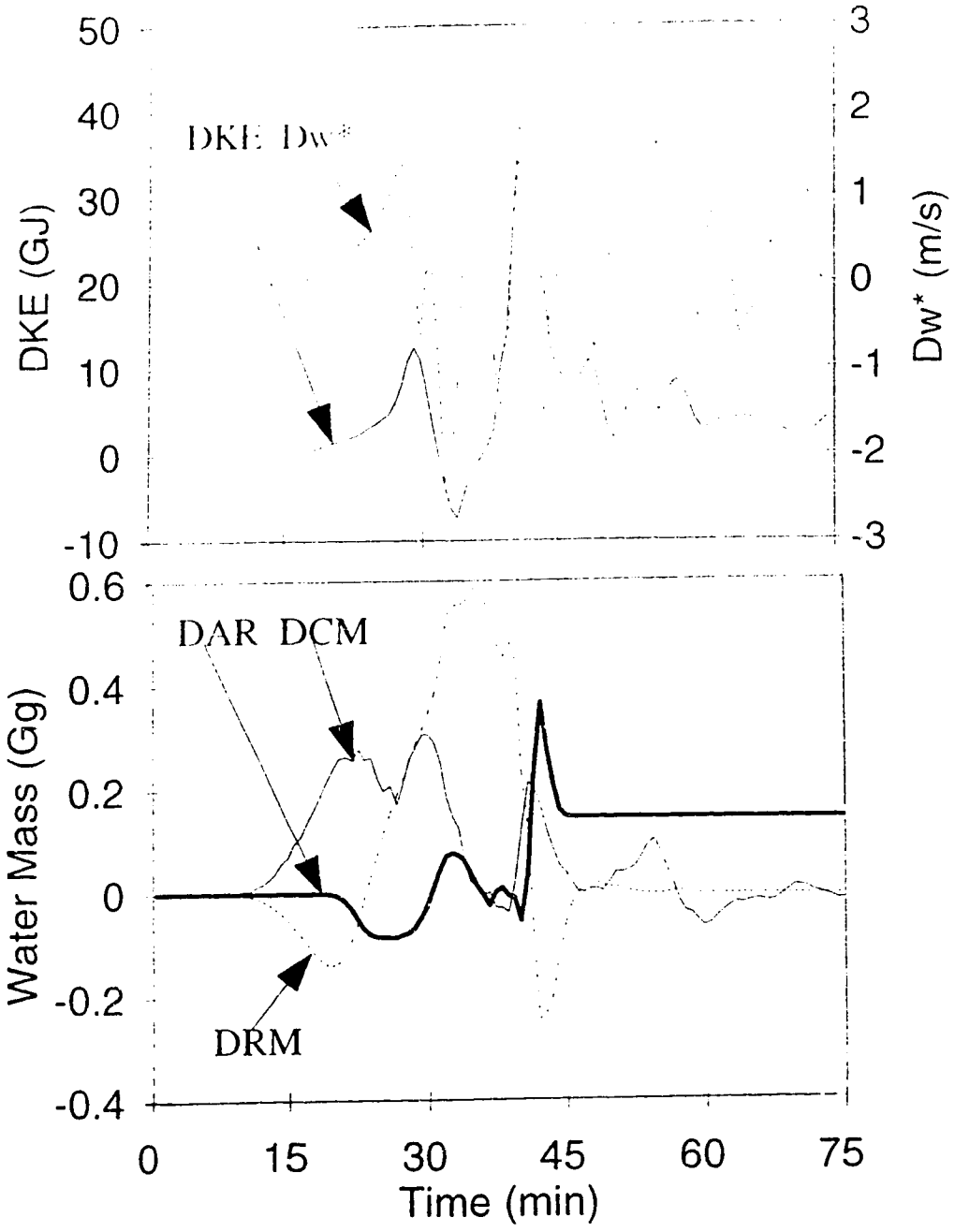

Fig.3. Time evolution of difference values of peak updraft (Dw*), total kinetic energy (DKE), cloud mass (DCM), rain mass (DRM) and accumulated rain (DAR) obtained by subtracting the no pollution case from the heavily pollution case.

the rate of cloud condensation and the rate of conversion of cloud water to rainwater, which depends on the supersaturation and drop size spectra, respectively. For convenience, we will speak here of the supersaturation and the drop spectrum effect. The issue to be dealt with is the relative contributions of the supersaturation and drop spectrum effects. The technique commonly used to evaluate the relative contribution of a specific process is to make a model run with the specific process being "switched off". For our problem this would entail to make experiment NS (no supersaturation effect) and ND (no drop spectrum effect). Table 2 lists selected results for these experiments. The common interpretation for the contribution of the supersaturation effect on a variable f is based on the difference value f(HP)-f(NS). Likewise, the drop spectrum effect is given by difference f(HP)-f(ND). Recently, Stein and Alpert (1993) severely criticized this interpretation of individual effects, based on the following consideration. The value f(HP)-f(NS) does not only include the individual effect of the supersaturation but also the mutual effect arising from the interaction of the supersaturation effect with the drop spectrum effect. Likewise, f(HP)-f(ND) includes the individual effect of the drop spectrum and the mutual interactions of supersaturation and drop spectrum effect. If the mutual interaction effect is significant the simple interpretation of comparing the switch-off run with the full-physics run is

misleading. Stein and Alpert's critique was constructive in that they described an alternative technique based on factor separation that avoids the ambiguity related to the mutual interaction effect. The mathematical framework of the factor separation technique is given in Stein and Alpert (1993) and chapter 5. Here we only summarize the results for our specific case. The total pollution effect (f_T), the supersaturation effect (f_S), the drop spectrum effect (f_D) and the mutual interaction effect (f_M) can be computed (in percentages) by the following expressions:

$$
\begin{aligned}
f_T &= \frac{f(HP) - f(NP)}{f(NP)} \times 100\% \\
f_S &= \frac{f(ND) - f(NP)}{f(NP)} \times 100\% \\
f_D &= \frac{f(NS) - f(NP)}{f(NP)} \times 100\% \\
f_M &= \frac{f(HP) + f(NP) - f(NS) - f(ND)}{f(NP)} \times 100\%
\end{aligned}
\qquad (2)
$$

The total pollution effect consists of the sum of the two individual effects plus the mutual interaction effect: $f_T = f_S+f_D+f_M$. Table 3 lists the total, individual and mutual contributions (in percentage) towards the total accumulated rainfall (AR_{max}), maximum cloud mass (CM_{max}), maximum rain mass (RM_{max}) and the maximum kinetic energy (KE_{max}), respectively. The negative values for $f_D(AR_{max})$ and $f_D(RM_{max})$ together with a positive value for $f_D(CM_{max})$ indicate that conversion of cloud water to rainwater is reduced due to the changes of the initial drop size spectrum associated with the additional CCN

Table 3. Contributions of the total effect (f_T), the drop size spectrum effect (f_D), the supersaturation effect (f_S), and the mutual interaction effect (f_M) in percentages.

	f_T	f_D	f_S	f_M
AR_{max}	1.8	-5.4	1.6	5.6
CM_{max}	6.4	0.6	1.4	4.4
RM_{max}	6.3	-2.7	0.9	8.0
KE_{max}	18.8	-0.3	-1.5	20.6

from the heavy pollution. This reduction in the conversion rate into rain can be attributed to Berry and Reinhardt's expression for the instantaneous autoconversion rate of cloud to rain C_{cr} given in (1). For a fixed amount of cloud water, the dependence of C_{cr} upon the ratio ν_m/N_c is roughly proportional. Comparing the ratio ν_m/N_c for the polluted case with the unpolluted case, we have 1.18×10^{-3} cm^3 versus 2.09×10^{-3} cm^3 causing C_{cr} for polluted cloud to be smaller than C_{cr} for the unpolluted cloud. The positive values for $f_S(AR_{max})$, $f_S(CM_{max})$ and $f_S(RM_{max})$ indicate that the reduction of the effective supersaturation value S in the polluted cloud results in slightly enhanced condensation, a larger amount rainwater and more accumulated rain at the ground. The largest impact on the rainfall, however, arises from the mutual

interaction of the supersaturation and the drop spectrum effect: $f_M(AR_{max})$ is about 3.5 times larger than $f_S(AR_{max})$. The total effect of the heavy pollution on accumulated rain remains still at only 1.8% which is completely shadowed by natural variability in convective rain showers. An interesting feature shows up in the effects of the pollution on the maximum perturbation kinetic energy. The individual contributions of the supersaturation effect and the drop size spectrum effect are very small reductions. The mutual interaction of these two effects, however, is significant increasing the KE_{max} by about 20%. This is a perfect example that a conclusion based only on the individual effects is misleading, if there is strong interaction between the individual processes.

A set of numerical experiments was also made to isolate the individual effects and the mutual interactive effects for the case of low pollution. The factor analysis shows that the relative contributions in the low pollution case are very similar to the heavy pollution case, differing mainly in that the percentage values are smaller compared to the HP case. The details of the model parameters and the data from the factor analysis are presented in appendix 3.

4.4 Summary and conclusions

A simple model approach has been adopted to determine how rainfall from an isolated convective cloud depends on the

CCN's released from a major petroleum refinery. The model employs non-hydrostatic dynamics in an axisymmetric geometry affected by the release of heat and moisture from a surface source. A bulk water scheme is used to parameterize the warm rain processes. Condensation of cloud water occurs when the local humidity value exceeds a prescribed effective supersaturation value. The autoconversion of cloud water to rainwater depends on the cloud droplet spectra following Berry and Reinhardt's (1973) approach.

Verification against aircraft observations confirmed that the model provides a realistic cloud simulation. Sensitivity experiments suggest that the total effect of the pollution is to increase the accumulated rainfall by 1.8% for heavy pollution and 0.2% for low pollution. Heavy pollution also increases the maximum perturbation kinetic energy. Using the Factor Separation Method of Stein and Alpert (1993) the individual effects of the supersaturation and the drop spectrum effect are isolated. The reduced supersaturation value in the polluted cloud caused a small increase in cloud condensation, while the drop spectrum effect tended to reduce the conversion of cloud water to rainwater. The interactive effect of these two factors is the most prominent in affecting the convection and rainfall.

Based on this case we agree with Hindman et al. (1977c) that pollution can hardly be responsible for the large increase of rainfall observed in the vicinity of some

industrial complexes. More likely it seems that the observed increase in convective rainfall is caused by the heat and moisture emitted from industrial plants (Murray et al., 1978; chapter 3).

References

Auer, A. H., Jr., 1976: Observations of an industrial cumulus. J. Appl. Meteor. 15, 406-413.

Berry, E. X., and R. L. Reinhardt, 1973: Modelling of Condensation and collection within clouds, Physical Sciences Publication No. 16, University of Nevada, Reno, 96 pp.

Eagan, R. C., P. V. Hobbs, and L. F. Radke, 1974: Particle emissions from a large Kraft paper mill and their effects on the microstructure of warm clouds. J. Appl. Meteor. 13, 535-552.

Hindman, E. E. II, P. V. Hobbs, and L. F. Radke, 1977a: Cloud condensation nucleus size distribution and their effects on cloud droplet size distribution. J. Atmos. Sci. 34, 951-956.

Hindman, E. E. II, P. V. Hobbs, and L. F. Radke, 1977b: Cloud condensation nuclei from a paper mill. Part I: Measured effects on clouds. J. Appl. Meteor. 16, 745-752.

Hindman, E. E. II, P. M. Tag, B. A. Silverman, and P. V. Hobbs, 1977c: Cloud condensation nuclei from a paper mill. Part II: Calculated effects on rainfall. J. Appl.

Meteor. 16, 753-755.

Hobbs, P. V., 1993: Aerosol-cloud-climate interactions Academic press, Inc., San Diego, 233pp.

Hobbs, P. V., L. F. Radke, and S. E. Shumway, 1970: Cloud condensation nuclei from industrial sources and their apparent influence on precipitation in Washington State. J. Atmos. Sci. 27, 81-89.

Kessler, E. E., 1969: *On the distribution and continuity of water substance in atmospheric circulations*. Meteor. Monogr., No. 32, Amer. Meteor. Soc., Boston, 84 pp.

Koenig, L. R., F. W. Murray, and P. M. Tag, 1978: Differences in atmospheric convection caused by waste energy rejected in the forms of sensible and latent heats. Atmos. Environ. 12, 1013-1019.

Leaitch, W. R., and G. A. Isaac, 1994: On the relationship between sulphate and cloud droplet number concentrations. J. Climate 7, 206-212.

Mather, G.K., 1991: Coalescence enhancement in large multicell storms caused by the emissions from a kraft paper mill. J. Appl. Meteor. 30, 1134-1146.

Murray, F.W., L. R. Koenig, and P. M. Tag, 1978: Numerical simulation of an industrial cumulus and comparison with observations. J. Appl. Meteor. 17, 655-668.

Orville, H. D., P. A. Eckhoff, J. E. Peak, J. H. Hirsch, and F. J. Kopp, 1981: Numerical simulation of the effects of cooling tower complexes on clouds and severe storms.

Atmos. Environ. 15, 823-836.

Reuter, G. W., 1987: Penetrative downdrafts in mixed-phase clouds. S. Afr. J. Phys. 10, 139-145.

Reuter, G. W., and M. K. Yau, 1987: Mixing mechanisms in cumulus congestus clouds. Part II: Numerical simulations. J. Atmos. Sci. 44, 798-827.

Stein, U. and P. Alpert, 1993: Factor separation in numerical simulations. J. Atmos. Sci. 50, 2107-2115.

Ste P., 1982: An axially symmetric cloud model: nent and simulations. Army Weather Group Sc tific Report MW-94,McGill University, Montreal, 55pp.

Chapter 5

Relative contributions of sensible heat, latent heat and pollution emitted from an industrial complex on a convective rain shower

(An extended version of this chapter will be submitted to the Journal of Applied Meteorology once the paper on modelling the pollution has been accepted. The reason for this delay is that the results of this chapter depend on the approval of how the pollution effects are included in the cloud model).

5.1 Introduction

There is considerable interest in large industrial facilities which affect meteorological phenomena (Hanna and Gifford 1975). Preferential cumulus formation has been observed above electrical power plants (Stout 1962) and oil refineries (Auer 1976). Hobbs et al. (1970) reported that in regions adjacent to or down wind of the Port Townsend paper mill the annual rainfall recorded is 30% larger than the rainfall from nearby stations. This dramatic increase in annual precipitation is likely caused by the presence of the paper mill. Hobbs et al. speculated that the enhanced rainfall might be attributed to the large and giant cloud condensation nuclei (CCN) emitted from the paper mill into the pollution plume. Support for this hypothesis came from Eagan et al.'s (1974) study. They found a much broader spectrum of cloud droplet sizes in clouds that formed in the pollution plume

over the paper mill, than in clouds that formed in the ambient air unaffected by the plume. In addition, the polluted clouds contained a significant number of droplets with diameters larger than 30 μm, which were rare in the unpolluted clouds. Thus, polluted clouds were believed to have a more efficient collision-coalescence mechanism of raindrop formation. However, Hindman et al. (1977) made calculations of the growth of droplet distributions using the observed spectrum from the paper mill as input data. The model results indicated that the higher concentrations of large droplets in the pollution plume from the paper mill did not cause a significant enhancement in rainfall. They concluded that the large and giant cloud condensation nuclei emitted by the mill cannot by themselves be responsible for the observed increase in local rainfall. Instead, they suggested that sensible heat and vapour emitted by the mill, in combination with the pollution, accounted for the observed rain stimulation.

Similar findings were reported for the effects on rainfall near a large oil refinery located at Wood River, St. Louis. Rainfall measurements taken from just upwind and downwind of the refinery indicated that the refinery caused an increase in precipitation of 38% during the three summer months. Modelling studies for a particular case showed that the waste energy in form of sensible and latent heat provided a large stimulus to the triggering and development of cumulus convection and rain showers (Murray et al. 1978, Chapter 3).

On the other hand, the impact of the pollution for this case was rather small (Chapter 4).

Large industrial complexes emit waste energy as sensible heat and vapour, as well as industrial aerosols that act as efficient cloud condensation nuclei. Experts agree that each of these three factors can contribute to cloud formation. However, the relative importance of the three factors and their possible interactions are not obvious. The purpose of this chapter attempts to clarify the role of waste heat, vapour and pollution on rain enhancement for short-lived cumuli developing in an industrial plume. As in previous chapters, we focus on calm wind conditions that permits the use of an axisymmetric cumulus model.

To quantify the relative importance of the three factors we have to isolate their individual contribution, as well as the contributions due to their mutual interactions. The Factor Separation Method suggested by Stein and Albert (1993) can isolate these individual and mutual contributions and will thus be used.

The organization of this chapter is as follows: The major features of the cumulus model are summarized in section 5.2; the Factor Separation Method for three factors is described in section 5.3; the simulation results are presented in section 5.4; and, finally, section 5.5 summarizes and discusses the major conclusions.

5.2 Cumulus cloud model

For analyzing the effects of industrial complexes on cumulus formation and convective rainfall in a calm environment, we require a numerical model that can capture the non-hydrostatic cumulus dynamics and warm rain processes. In addition, there is a need to have a realistic presentation of the input of waste heat, vapour and pollutant emitted from the industrial complex. An extended version of the axisymmetric model developed by Steiner (1982), and Reuter and Yau (1987) provided the necessary features. The version of the model is identical to that used in Chapter 4. Only the major characteristics of this model will be briefly summarized here:

1) The time-dependent non-linear equations for conservation of mass, momentum, thermal energy and water substances are written in cylindrical polar co-ordinates. Assuming axisymmetry, the azimuthal gradients of all quantities are then equated to zero.

2) To filter out acoustic waves the deep anelastic system of equations of Ogura and Phillips (1962) is used. The basic state is non-isentropic, and adopted from observed sounding data.

3) The effects of the earth's rotation and friction at the earth's surface are neglected. Also, shortwave and long wave radiation effects are omitted.

4) The subgrid-scale (turbulent) processes are modelled using a first-order closure scheme. We adopt Hill's (1974)

scheme in which the eddy exchange coefficient depends on the local deformation shear and the local moist buoyancy time scales. Shear-generated turbulence is suppressed in regions of marked static stability (Miles, 1961).

5) At each time step, the perturbation pressure deviation from its hydrostatic equilibrium value is computed from the diagnostic Poisson equation obtained by taking the divergence of the momentum equations.

6) Bulk parameterization of cloud and precipitation particles is used. The liquid water is divided into cloud water and rainwater. Cloud water consists of small droplets moving with the air, whereas rainwater consists of the larger drops having a finite terminal fall speed. Following Berry and Reinhardt (1973), the rate of autoconversion of cloud water to rainwater depends on the cloud water mixing ratio, the initial cloud droplet concentration, and the mass dispersion coefficient of the initial cloud droplet distribution. Since the cloud droplet size spectrum depends on the distribution of activated cloud condensation nuclei, the autoconversion rate into rain becomes dependent on the pollution level of the air. The supersaturation value required for cloud condensation is also related to the pollution level.

7) The partial differential equations are solved by numerical approximation based on a finite difference scheme on a staggered grid. Variables other than velocity components are computed at the centre of a grid box and wind velocities at

its sides. A second-order non-diffusive leapfrog method in time and centred difference method in space is used to solve the prognostic equations. All the terms involving the eddy turbulent exchange are lagged in time.

8) The vertical grid spacing is uniform at 100 m. In the radial direction, the resolution is 83 m near the central axis, but widens smoothly towards the lateral boundaries. This grid stretching is computationally efficient, since coarser resolution is adequate near the lateral boundaries. A total of 125 horizontal mesh points are used to cover a radius of 20 km. The depth of the domain is 10 km for the midlatitude sounding and 12 km for the tropical sounding.

9) Our approach of including sensible heat and latent heat release from industrial complexes follows closely that of Murray et al. (1978) and Orville et al. (1981). The sensible heat and latent heat emitted from the facility are distributed uniformly in a prescribed source region. The assumption seems reasonable since we have shown in chapter 3 that the details of spatial distribution of the heat fluxes within the source region are only of secondary importance.

10) Preliminary experiments indicated the need for an initial impulse in humidity to initiate cloud formation. Without the initial impulse, there is no cloud formation in the sensitivity experiments with the source of sensible and latent heat being switched off. Without these simulated clouds, comparisons among numerical experiments become

problematic. The details of the humidity impulse were given in chapter 2.

11) The top and bottom boundaries of the model domain are assumed to be flat, rigid and smooth. There is no transport of heat and moisture through these boundaries with the exception of rain leaving the domain at the bottom. Closed conditions are used at the lateral boundary of the domain.

12) The numerical integration time step is 1 second and the model simulations are run for 3 hours for all experiments. A mixing procedure is invoked every 20 time steps to prevent the possible splitting of solutions at odd and even time steps.

5.3 Factor Separation Method

Suppose the predicted field f (e.g., accumulated rainfall) depends on three factors ψ_1, ψ_2, and ψ_3 (e.g., sensible heat source, latent heat source and pollution). If a continuous change is made in any factor of these ψ_i, the resulting f will change continuously as well. This "continuity" can be expressed mathematically as follows: Each factor ψ_i can be multiplied by a changing coefficient c_i so that

$$\psi_i(c_i) = c_i \psi_i \qquad 0 \le c_i \le 1, \tag{1}$$

and the resulting f becomes a continuous function of c_1, c_2, and c_3:

$$f = f(c_1, c_2, c_3) \tag{2}$$

so that f(1,1,1) is the control simulation with all three factors included and f(0,0,0) is simulation where all three factors are omitted. The common method of evaluating the contribution of the factor ψ_1 on f is by comparing the control run and a simulation where this factor is switched off. Thus, the difference value f(1,1,1) - f(0,1,1) is interpreted in the common method to quantify the effect of the factor ψ_1. However, f(1,1,1) - f(0,1,1) does not only include the effect of factor ψ_1 but also the joint effect (interaction) of factor ψ_1 with factors ψ_2 and ψ_3. If the interactions among factors are not isolated, the difference f(1,1,1) - f(0,1,1) does not have the simple meaning as is commonly thought and in fact might be quite misleading for cases of strong interactions.

Stein and Albert (1993) presented the Factor Separation Method which isolates the resulting values due to any factor in its pure form from the possible interactions with other factors. The technique was presented in a general form for n factors (where n denotes any integer larger than one). Since a general formulation for n factors is rather complicated with a cumbersome notation, it was considered useful to summarize their technique for three factors only.

Through a Taylor series expansion, the function f can be decomposed as follows:

$$f(c_1,c_2,c_3) = \hat{f}_0 + \hat{f}_1(c_1) + \hat{f}_2(c_2) + \hat{f}_3(c_3) + \hat{f}_{12}(c_1,c_2) + \hat{f}_{13}(c_1,c_3) + \hat{f}_{23}(c_2,c_3) + \hat{f}_{123}(c_1,c_2,c_3) \quad (3)$$

The notation is as follows:

$f(c_1,c_2,c_3)$ denotes the value of the predicted field dependent on the coefficients c_1, c_2, c_3; $\hat{f}(c_1,c_2,c_3)$ denotes the factor-separated part of the predicted field which depends only on the coefficients c_1, c_2, c_3;

$\hat{f}_0=\hat{f}(0,0,0)$ is the part of the predicted field independent of the three factors;

$\hat{f}_1=\hat{f}(1,0,0)$ is the part of the predicted field when only factor ψ_1 is fully switched on;

$\hat{f}_2=\hat{f}(0,1,0)$ is the part of the predicted field when only factor ψ_2 is fully switched on;

$\hat{f}_3=\hat{f}(0,0,1)$ is the part of the predicted field when only factor ψ_3 is fully switched on;

$\hat{f}_{12}=\hat{f}(1,1,0)$ is the part of the predicted field dependen solely on combination of factors ψ_1 and ψ_2;

$\hat{f}_{13}=\hat{f}(1,0,1)$ is the part of the predicted field dependent solely on combination of factors ψ_1 and ψ_3;

$\hat{f}_{23}=\hat{f}(0,1,1)$ is the part of the predicted field dependent solely on combination of factors ψ_2 and ψ_3; and

$\hat{f}_{123}=\hat{f}(1,1,1)$ is the part of the predicted field where all three factors are on.

Here $\hat{f}_{i..}$ is a short form for $\hat{f}_{i..}(c_i,..)$. Each function $\hat{f}_{i..}(c_i,..)$ becomes identically zero if any of its variables c_i is zero. Setting c_1, c_2, and c_3 to either 1 or 0 in (3), eight independent linear equations are obtained. Using substitution

we can solve for the eight unknowns $\hat{f}_0$, $\hat{f}_1$, $\hat{f}_2$, $\hat{f}_3$, $\hat{f}_{12}$, $\hat{f}_{13}$, $\hat{f}_{23}$ and $\hat{f}_{123}$:

$$\hat{f}_0 = f(0,0,0) \tag{4}$$

$$\hat{f}_1 = f(1,0,0) - f(0,0,0) \tag{5}$$

$$\hat{f}_2 = f(0,1,0) - f(0,0,0) \tag{6}$$

$$\hat{f}_3 = f(0,0,1) - f(0,0,0) \tag{7}$$

$$\hat{f}_{12} = f(1,1,0) - [f(1,0,0) + f(0,1,0)] + f(0,0,0) \tag{8}$$

$$\hat{f}_{13} = f(1,0,1) - [f(1,0,0) + f(0,0,1)] + f(0,0,0) \tag{9}$$

$$\hat{f}_{23} = f(0,1,1) - [f(0,1,0) + f(0,0,1)] + f(0,0,0) \tag{10}$$

$$\hat{f}_{123} = f(1,1,1) - [f(1,1,0) + f(1,0,1) + f(0,1,1)] + [f(1,0,0) + f(0,1,0) + f(0,0,1)] - f(0,0,0) \tag{11}$$

5.4 Results

a. Specifications of sensitivity experiments

Our analysis of the relative importance of fluxes of sensible heat, latent heat and pollution is based on two different sets of environmental conditions, referred to here as the midlatitude and tropical conditions, respectively. Fig. 1 shows the two thermodynamic soundings adopted from Murray et al. (1978), and Soong and Ogura (1973), respectively. The characteristics of these soundings have been discussed in Chapter 3, and will not be repeated here.

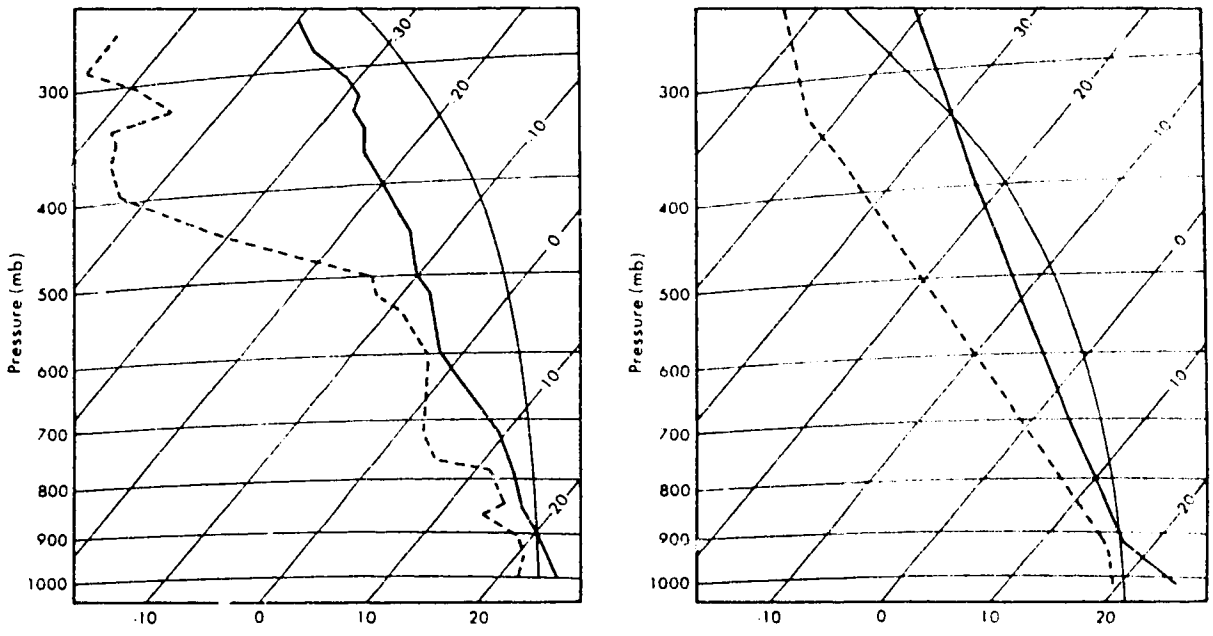

Fig. 1. Temperature (°C) and dewpoint temperature (°C) profiles used to initialize the model: The data for the Wood River sounding (left) and the tropical sounding (right).

It is assumed that heat and vapour fluxes are released uniformly from a finite source region. Specifically the source region is a cylinder with base height 100 m, depth 100 m and diameter of 500 m. The cylinder is centred on the vertical z-axis and constitutes the "effective volume" of the heat release resulting from the interaction of the plume with the boundary layer. Both heat and vapour are distributed uniformly within the source cylinder. For more details and further motivation we refer to Chapters 2 and 3. For the purpose of quantifying the relative importance of the effects of sensible heat versus latent heat, it is convenient to have the same emission rate for the two forms of waste energy. The value used is $H_s=H_l=511$ MW which is the mean of the observed rates.

The pollution effect enters the model via the specification of the cloud droplet concentration (N_c), the relative dispersion coefficient of cloud droplet distribution (ν_m), and the effective supersaturation value required for cloud condensation (S_p). Our choices for these parameters were $N_c=620$ cm^{-3}, $\nu_m=0.73$ and $S_p=0\%$ for polluted air, and 239 cm^{-3}, 0.5 and 0.4% for unpolluted air. These particular values were chosen to mimic the conditions for the Wood River conditions as outlined in Chapter 4.

Because of the lack of observational data for the rates of heat, moisture and pollution emitted from an industrial facility in tropical conditions, we have simply adopted the sources from the Wood River facility. This approach, at least,

Table 1: Definition of numerical experiments used for sensitivity studies for midlatitude and tropical conditions.

Midlat Exp	MSLP	M	MSL	MSP	MLP	MS	ML	MP
Tropic Exp	TSLP	T	TSL	TSP	TLP	TS	TL	TP
H_S (MW)	511	0	511	511	0	511	0	0
H_L (MW)	511	0	511	0	511	0	511	0
$N_c(cm^{-3})$	620	230	230	620	620	230	230	620
ν_m	0.73	0.50	0.50	0.73	0.73	0.50	0.50	0.73
S_p %	0.0	0.4	0.4	0.0	0.0	0.4	0.4	0.0

allows for easy inter-comparison of the response of midlatitude and tropical air masses affected by the same anthropogenic input.

Table 1 lists the eight numerical experiments made for each of the soundings. Each experiment is labelled with a code. If the first letter of the code is "M" the experiment is based on the midlatitude sounding, whereas the "T" denotes experiments made with the tropical sounding. The other letters of the code indicate which of the three factors (sensible heat S, latent heat L or pollution P) have been switched on.

b. Results for the Wood River sounding

Fig. 2 shows the time evolution of the domain-integrated mass of cloud water (CM) and rainwater (RM) and the accumulated mass of rainwater at the ground (AR) for experiments MSLP and M. Precise definitions of these variables

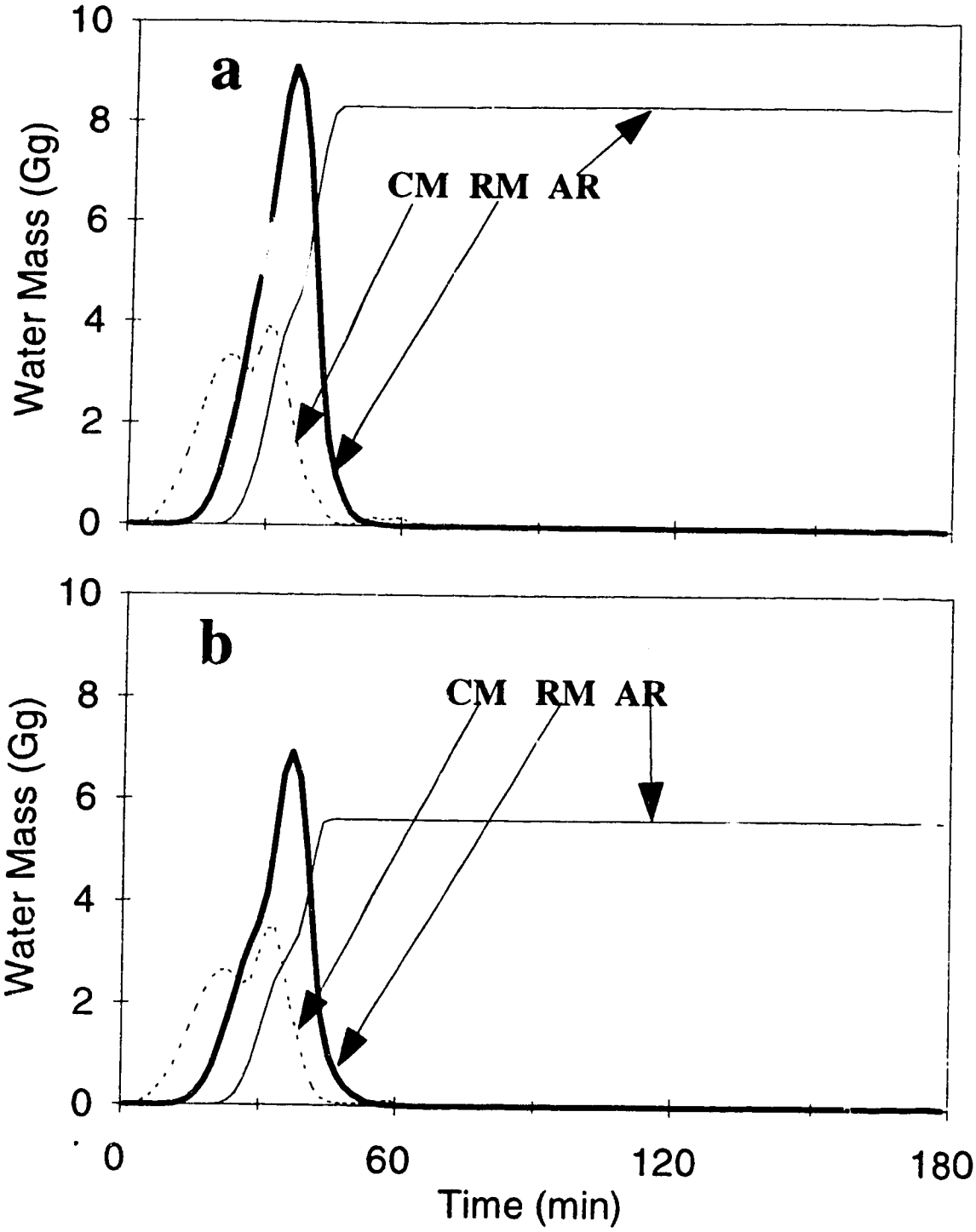

Fig. 2. The time evolution of simulation over the industrial complexes (MSLP) and simulation in the natural environment unaffected by the industrial complexes (M) depicting total cloud mass (CM), total rain mass (RM), and accumulated rainfall at the surface (AR). a. MSLP experiment, b. M experiment for the midlatitude sounding.

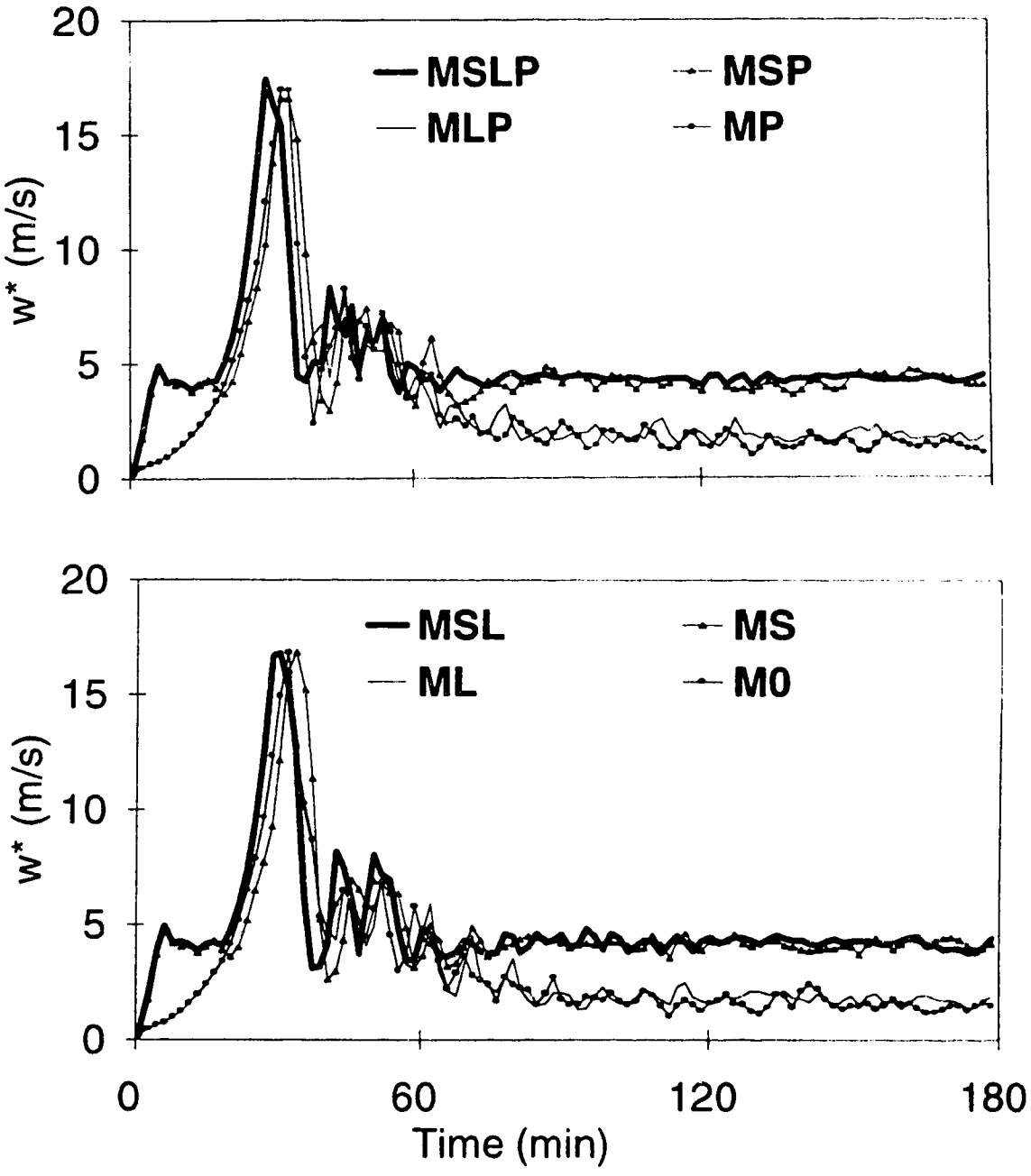

Fig. 3. Time evolution of peak vertical updraft (w^*) for the eight experiments defined in Table 1.

were given in chapter 3. MSLP is considered as the control experiment as it includes the sources for sensible heat, latent heat, and pollution, while M is the "natural" case which has none of the three factors. The development of the "industrial" and the "natural" cumulus clouds is very similar. The curves of CM indicate two local maxima in both cases. The minimum CM between the maxima results from a large rate of conversion of cloud water to rainwater. The precipitation lasts for 22 min in MSLP. The development of rain in M is slightly slower than that in MSLP. Also the peak magnitudes of the integral variables are smaller in the "natural" cloud.

Fig. 3 shows the time evolution of peak vertical updraft w^* for all eight experiments. The curves show that the presence of a source of sensible heat has a significant impact on the development of cloud convection. All the experiments including the sensible heat source (MSLP, MSL, MSP, MS) show a similar feature: w^* grows rapidly to about 5 m s^{-1} in the first 6 min, thereafter it remains fairly steady for a further period of 13 min. After the rain shower, w^* remains about 4.3 m s^{-1}. In contrast, in all experiments with the sensible heat source being switched off (M, MLP, ML and MP), w^* grows steadily and slowly; it does not reach 5 m s^{-1} until 20 min. After the rain shower, w^* remains around 1.6 m s^{-1}.

The above simulations show qualitatively that for the Wood River sounding the industrial complexes do not change the time evolution patterns of total cloud mass, rain mass, and

Table 2: Comparison of experiments for midlatitude sounding (all units are Gg).

	MSLP	M	MSL	MSP	MLP	MS	ML	MP
CM_{max}	3.90	3.46	3.75	4.12	3.79	3.76	3.45	3.81
RM_{max}	9.10	6.90	8.86	8.91	7.33	8.48	6.89	7.34
AR_{max}	8.31	5.60	8.20	6.63	5.84	6.74	5.60	5.75

accumulated rainfall at the surface but modify the maximum values of those variables; while the time evolution pattern of the peak updraft is changed by the sensible heat. Thus, to evaluate quantitatively the effect of the industrial complexes on the convective rain shower, we compare the maxima of total cloud mass, rain mass, accumulated rainfall at the surface (Table 2). Maximum values of MSLP tend to be the largest, while those of M are the smallest. Moreover, maxima of MSLP are much larger than those of M. Thus, the industrial complex intensifies the convective rain shower. The maxima of M are about the same as those of ML, i.e., the latent heat emitted by the industrial complex has little effect on cloud development for the midlatitude sounding.

Let F_S, F_l and S_P represent the pure contributions (in percentage) to the predicted value f by sensible heat, latent heat and pollution, respectively. Then (5)- (7) become

$$F_S = \frac{\hat{f}_1}{\hat{f}_0} \times 100\% = \frac{f(S) - \hat{f}_0}{\hat{f}_0} \times 100\% \qquad (12)$$

$$F_L = \frac{\hat{f}_2}{\hat{f}_0} \times 100\% = \frac{f(L) - \hat{f}_0}{\hat{f}_0} \times 100\% \quad (13)$$

$$F_P = \frac{\hat{f}_3}{\hat{f}_0} \times 100\% = \frac{f(P) - \hat{f}_0}{\hat{f}_0} \times 100\% \quad (14)$$

Similarly, the contributions due to the possible interactions between two factors F_{SL} (interaction between sensible heat and latent heat), F_{SP} (interaction between sensible heat and pollution) and F_{LP} (interaction between latent heat and sensible heat) can be expressed as:

$$F_{SL} = \frac{\hat{f}_{12}}{\hat{f}_0} \times 100\% = \frac{f(SL) - [f(S) + f(L)] + \hat{f}_0}{\hat{f}_0} \times 100\% \quad (15)$$

$$F_{SP} = \frac{\hat{f}_{13}}{\hat{f}_0} \times 100\% = \frac{f(SP) - [f(S) + f(P)] + \hat{f}_0}{\hat{f}_0} \times 100\% \quad (16)$$

$$F_{LP} = \frac{\hat{f}_{23}}{\hat{f}_0} \times 100\% = \frac{f(LP) - [f(L) + f(P)] + \hat{f}_0}{\hat{f}_0} \times 100\% \quad (17)$$

While the contribution due to interaction among three factors (F_{SLP}) is

$$F_{SLP} = \frac{\hat{f}_{123}}{\hat{f}_0} \times 100\%$$

$$= \frac{f(SLP) - [f(SL) + f(SP) + f(LP)] + [f(S) + f(L) + f(P)] - \hat{f}_0}{\hat{f}_0} \times 100\%$$

The results of the Factor Separation Method applied to the maximum values of CM, RM and AR are summarized in Table 3. Both sensible heat and pollution increase maximum of cloud

Table 3. The relative contributions (in percentage) to maxima of accumulated rainfall, total cloud water and total rainwater by the pure factors F_S, F_L, and F_P; interaction effects among two factors F_{SL}, F_{SP}, F_{LP}; the triple interaction effect F_{SPL}, and the total effect $F_{TOT}=F_S+F_L+F_P+F_{SL}+F_{SP}+F_{LP}+F_{SPL}$ for midlatitude sounding.

	F_{TOT}	F_S	F_L	F_P	F_{SL}	F_{SP}	F_{LP}	F_{SLP}
CM_{max}	12.6	8.5	-0.4	9.8	0.1	0.7	-0.0	-6.1
RM_{max}	31.8	22.9	-0.1	6.4	5.6	-0.2	-0.1	-2.7
AR_{max}	48.3	20.3	-0.0	2.7	26.0	-4.7	1.7	2.4

water. The contribution on RM_{max} due to sensible heat (without interaction with other factors) is about 3.6 times larger than that of pollution. The difference between the effects of sensible heat and pollution on accumulated rainfall at the surface is even more obvious: the pure contribution of sensible heat increases AR_{max} 7.5 times larger than the pure pollution effect. It is interesting to note that pollution has the largest effect in increasing CM_{max}, in agreement with observations of Eagan et al. (1974) that clouds formed in the plume from a paper mill had a much broader spectrum of droplet sizes and a larger concentration of droplets than those formed in the ambient air unaffected by the plume. However, the sensible heat is dominant for enhancing the rainfall. This is consistent with the conclusion of Hindman et al. (1977) that the pollution is not by itself responsible for the increased rainfall.

Comparing the pure effects of three factors, the pure

effect of sensible heat plays the most important role for rainfall. The pollutant plays a significant role in increasing total cloud mass while the latent heat has little pure effect on the convective rain shower. The contributions to the convective rain shower due to the mutual interactions among two and three factors are not negligible. The contribution to CM_{max} due to the mutual interaction among sensible heat, latent heat and pollution is comparable with pure contribution of sensible heat or pollution and is much larger than that of vapour. The contribution to RM_{max} due to the mutual interaction between sensible heat and latent heat is much larger than pure effect of vapour. In fact, this mutual contribution to AR_{max} is the largest component (26%).

c. Model results for the tropical sounding

The time evolutions of CM, RM and AR for experiments TSLP and T are shown in Fig. 4. The "industrial" cumulus development in the tropic, represented by TSLP, differs significantly from the "natural" cumulus development (T) in that the "industrial" cloud appears much earlier than the "natural" cloud. After the cloud dissipates there is a continuous regeneration of rainwater and precipitation for TSLP and no regeneration of precipitation for experiment T. Because of the regeneration the "industrial" cloud produces much larger accumulated rainfall than the "natural" cloud. Regeneration of precipitating cells occurs in all experiments

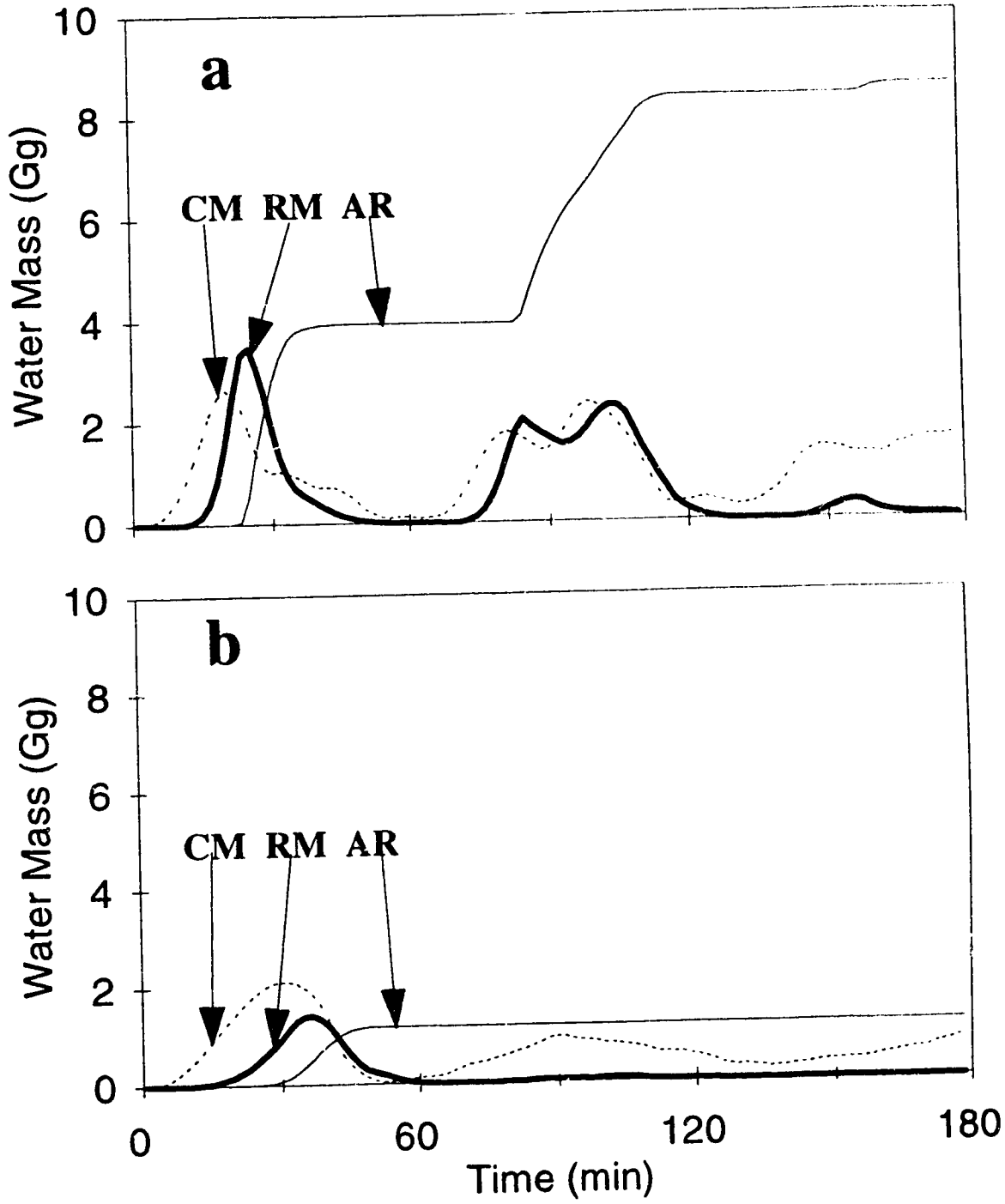

Fig. 4. Time evolution for the control experiment TSLP and the "natural" run T depicting CM, RM and AR for the tropical sounding.

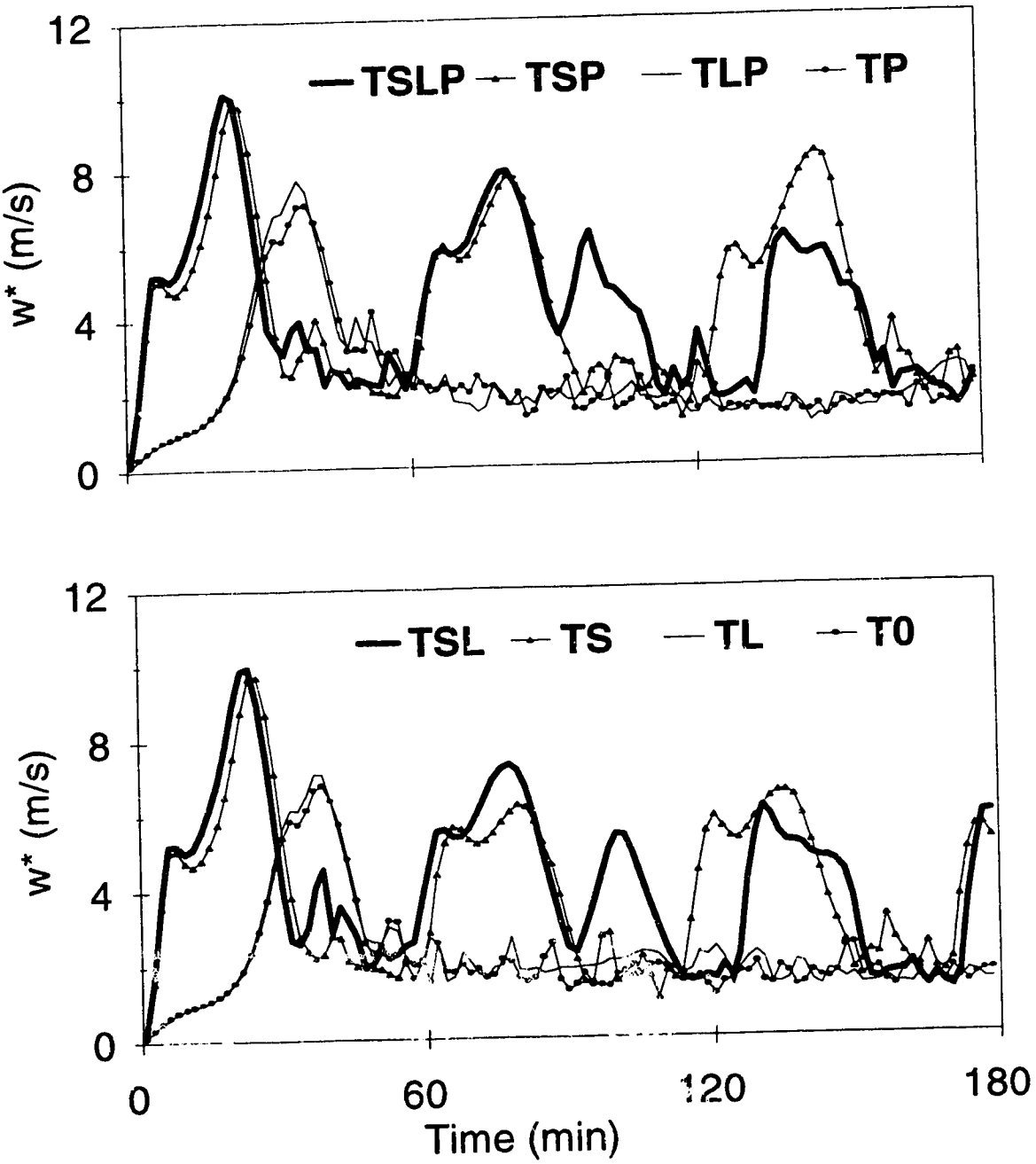

Fig. 5. Time evolution of peak vertical updraft (w^*) for the eight experiments based on the tropical sounding.

that had sensible heat being switched on, but not in the experiments that had no source of sensible heat. Thus the sensible heat source is the driving force of cumulus regeneration.

Fig. 5 shows the time evolution of peak vertical updraft w^* for all eight experiments of the tropical sounding. In the experiments including source of sensible heat (TSLP, TSL, TSP and TS) the model updraft (w^*) grows rapidly in the first 20 min and after that the peak updraft continuously oscillates between 1.5 m s^{-1} and 8.0 m s^{-1}. In contrast, in the experiments in which the sensible heat source is switched off (TLP, TL, TP and T), w^* grows slowly. After the rain shower, w^* stays around 1.6 m s^{-1}. There is only one cycle in evolution of w^* for all experiments without sensible heat and more cycles for all experiments with sensible heat.

Table 4 compares the maxima of the domain-integrated mass of cloud water, rainwater and the accumulated mass of rainfall at the surface for the model experiments using the tropical sounding. The control case (TSLP) yields the largest values of CM_{max}, RM_{max} and AR_{max} while the "natural" case (T) yields the smallest values. Similarly as for midlatitude conditions, the industrial complex enhances the convective rain shower in tropical conditions.

Table 5 compares the contributions to CM_{max}, RM_{max} and AR_{max} due to pure factors as well as the mutual interactions among factors. The pure effects of all three factors increase cloud

Table 4: Comparison of experiments for tropical sounding (all units are Gg).

	TSLP	T	TSL	TSP	TLP	TS	TL	TP
CM_{max}	2.64	2.11	2.47	2.71	2.59	2.46	2.20	2.44
RM_{max}	3.47	1.40	3.24	3.13	1.91	2.97	1.58	1.59
AR_{max}	8.55	1.16	6.03	8.36	1.77	5.30	1.43	1.32

Table 5. The relative contributions (in percentage) to maxima of accumulated rainfall, total cloud water and total rainwater by the pure factors F_S, F_L, and F_P; interaction effects among two factors F_{SL}, F_{SP}, F_{LP}; the triple interaction effect F_{SPL}, and the total effect $F_{TOT}=F_S+F_L+F_P+F_{SL}+F_{SP}+F_{LP}+F_{SPL}$ for tropical sounding.

	F_{TOT}	F_S	F_L	F_P	F_{SL}	F_{SP}	F_{LP}	F_{SLP}
CM_{max}	25.2	16.5	4.0	15.3	-3.6	-3.6	3.4	-6.8
RM_{max}	147.3	111.2	12.4	13.2	7.3	-1.6	10.2	-5.4
AR_{max}	635.0	355.5	22.8	13.3	40.1	249.8	16.0	-62.6

water, rainwater and rainfall. The pure effect of sensible heat in increasing cloud water is slightly larger than that of pollution and is about four times larger than that of latent heat. The pure contribution to increasing rainwater due to latent heat is about the same as that of pollution while the contribution of sensible heat is much larger than that of pollution or latent heat. The effect of sensible heat on accumulated rainfall at the surface is even larger. The mutual interaction effects are quite large in some cases. For example, the mutual interaction between sensible heat and

latent heat increases accumulated rainfall by 250%. This is about one order larger than the pure effect of latent heat.

5.5 Conclusions

An axisymmetric cloud model is used to study sensitivity experiments for a convective rain shower affected by an industrial complex that emits sensible heat, moisture and pollution. The Factor Separation Method is used to quantify the pure and interactive effects of sensible heat, latent heat and pollution, respectively. For both midlatitude and tropical soundings, the cloud development is affected mostly by the release of sensible heat. The peak updrafts of experiments including sensible heat increase much faster than those of experiments without the sensible heat. For the tropical sounding, there is only one cycle of cumulus convection for all experiments without a sensible heat source, but several life cycles for all experiments with sensible heat source.

For both soundings the pure contribution of the sensible heat to increasing accumulated rainfall at the surface and total rainwater is much larger than that of vapour or pollution. A tentative conclusion, based on our experiments of two soundings, is that the sensible heat is the major contributing factor toward increased rainfall. However, pollution and sensible heat play an important role in increasing cloud water.

The contributions to the convective rain shower due to

the mutual interactions among two or three factors are quite large and should not be neglected. A similar behaviour is well-known for large-scale airflow in which interactions of two forcing mechanisms can have very large synergistic effects (e.g., Mailhot and Chouinard, 1989).

REFERENCES

Auer, A. H., Jr., 1976: Observations of an industrial cumulus. J. Appl. Meteor., 15, 406-413.

Berry E. X., and R. L. Reinhardt, 1973: Modelling of Condensation and collection within clouds. Desert Res. Inst. Phys. Sci. Publ., 16.

Eagan R. C., P. V. Hobbs, and L. F. Radke, 1974: Particle emissions from a large Kraft paper mill and their effects on the microstructure of warm clouds. J. Appl. Meteor. 13, 535-552.

Hanna, S. R., and F. A. Gifford, 1975: Meteorological effects of energy dissipation at large power parks. Bull. Amer. Meteor. Soc., 56, 1069-1076.

Hill, G. E., 1974: Factors controlling the size and spacing of cumulus clouds as revealed by numerical experiments. J. Atmos. Sci., 31, 646-673.

Hindman E. E. II, P. M. Tag, B. A. Silverman, and P. V., Hobbs, 1977: Cloud condensation nuclei from a paper mill. Part II: Calculated effects on rainfall. J. Appl. Meteor. 16, 753-755.

Hobbs, P. V., L. F. Radke, and S. E. Shumway, 1970: Cloud condensation nuclei from industrial sources and their apparent influence on precipitation in Washington State. J. Atmos. Sci., 27, 81-89.

Mailhot, J., and C. Chouinard, 1989: Numerical forecasts of explosive winter storms: Sensitivity experiments with a meso-α scale model. Mon. Wea. Rev., 117, 1311-1343.

Miles, J. W., 1961: On the stability of heterogeneous shear flows. J. Fluid. Mech., 10, 496-508.

Murray, F.W., L. R. Koenig, and P. M. Tag, 1978: Numerical simulation of an industrial cumulus and comparison with observations. J. Appl. Meteor., 17, 655-668.

Ogura, Y., and N. A. Phillips, 1962: Scale analysis of deep and shallow convection in the atmosphere. J. Atmos. Sci., 19, 173-179.

Orville, H. D., P. A. Eckhoff, J. E. Peak, J. H. Hirsch, and F. J. Kopp, 1981: Numerical simulation of the effects of cooling tower complexes on clouds and severe storms. Atmos. Environ., 15, 823-836.

Reuter, G. W, and M. K. Yau, 1987: Mixing mechanisms in cumulus congestus clouds. Part II: Numerical simulations. J. Atmos. Sci., 44, 798-827.

Soong, S., and Y. Ogura, 1973: A comparison between axisymmetric and slab-symmetric cumulus cloud model. J. Atmos., Sci. 30, 879-893.

Stein U., and P. Alpert, 1993: Factor separation in numerical

simulations. J. Atmos. Sci., 50, 2107-2115.

Steiner, J. T., 1982: An axially symmetric cloud model: Development and simulations. Stormy Weather Group, Scientific Report. MW-94, McGill University, 55pp.

Stout, G. E., 1962: Cloud initiation in industrial areas. Proc. Symposium of Air Over Cities, Public Health Service, Sanitary Engineering Centre, Cincinnati, Ohio, SEC Tech. Rept. A62-5, 147-153.

Chapter 6

Conclusions and suggestions for further research

6.1 Summary and conclusions

This thesis investigates the effects of industrial complexes on convective cloud development and rain showers using a numerical cloud model. Specifically, we quantify the changes in cumulus clouds arising from sensible heat, vapour and pollution which are emitted from industrial complexes during calm wind conditions. The cloud model used is an extension of Steiner's (1982) axisymmetric model which is suitable to simulate warm rain processes and sources of external heat and vapour. The approach of using an axisymmetric model geometry is considered superior to assuming slab symmetry in that axisymmetry allows for a source region of waste energy of finite spatial dimension. Previous studies based on slab-symmetric models had the unrealistic feature of infinitely long source regions (e.g., Murray et al., 1978; Hane, 1978; Orville et al., 1981). Our approach is also novel in that our study evaluates the relative contributions of sensible heat, vapour, and pollution on a convective rain shower, whereas previous studies focused only on either the thermodynamic sources (e.g., Murray et al., 1978; Hane, 1978; Orville et al., 1981) or the pollution aspects (e.g., Hindman et al., 1977).

Two different soundings were used to provide initial

conditions for our model experiments. One of these soundings was sampled close to a major oil refinery complex in Wood River, Illinois (Murray et al., 1978). The other sounding, which represented typical conditions in the tropics, was adopted from Soong and Ogura (1973).

Aircraft observations by Auer (1976) sampled in cumulus clouds formed over the oil refinery at Wood River, Illinois served as the data set for comparison with the midlatitude model simulation. The cloud model could realistically simulate the observed cloud sizes and updraft strength suggesting that model convection bears a close resemblance to the natural case.

A series of sensitivity experiments was made to analyze the effects of heat sources on the convection and rainfall for two soundings. The major findings were:

- Without a sustained waste heat input the model convection ceased. The model convection became progressively more intense and developed more rain as the rate of total waste energy heat released from the power station was increased. Doubling the total waste energy amount from its control case value caused a 15-fold increase in 3-h rainfall values. However, reducing the control case value of total waste energy release by 20% led to much weaker convection without rain.
- The triggering of cumulus clouds was reduced when the waste energy was released as latent heat rather than

sensible heat. As the relative contribution of sensible heat increased, so did the intensity of the circulation and the rainfall.

- The cloud formation depended on the area of the heat source: a wider source tended to delay and to weaken the convection.
- The model results were only slightly sensitive to the radial distribution of the sensible and latent heat fluxes within the source region.

Our next step was to extend the model to incorporate the effects of industrial pollution on cumulus convection and rain showers. The pollution was included in the model equations by changing the cloud droplet size spectra and by lowering the supersaturation threshold required for cloud condensation. Comparison of model outputs from polluted and unpolluted clouds indicated that the pollution had only a minor impact on rain enhancement.

Stein and Alpert (1993) presented a method of factor separation in numerical simulation. The method allows to quantify the contributions arising from mutual interactions among two or more factors, which is not possible with other methods. We used the Factor Separation Method to isolate the pure contributions of changing drop size spectrum and decreasing supersaturation towards convective rainfall, as well as the contribution due to the mutual interaction between

them. The calculation showed that increases in rainfall could be attributed mainly to the mutual interaction of the supersaturation effect and the drop spectrum effect, while both the individual contributions remained small.

Finally, we investigated the combined effects of sensible heat, latent heat and pollution on a convective rain shower. Using the Factor Separation Method, we obtained the pure contributions of the three factors, as well as the contributions due to the mutual interaction among them. The pure effect of sensible heat on increasing accumulated rainfall at the surface and total rainwater was much larger than that of vapour or pollution. This result is consistent with the results of Koenig et al. (1978) indicating that sensible heat played a very important role in triggering convective clouds.

Both sensible heat and pollution effects contributed significantly in raising the total amount of cloud water within the model domain. The contributions to the convective rain shower due to the mutual interactions between these two factors were large, confirming that synergistic interactions between factors can be substantial (e.g., Uccellini et al., 1987; Mailhot and Chouinard, 1989).

6.2 Suggestions for further research

This thesis has focused on effects of industrial complexes on a convective cloud in calm wind conditions. Only

warm rain processes were considered. We recommend that our research should be extended in several ways:

1. To simulate the effects of industrial complexes in a sheared wind environment where the ambient wind varies with altitude. A high-resolution three-dimensional cloud model will be needed for this purpose.

2. To extend the cloud model to allow for ice phase cloud microphysics. We thus recommend that effects of industrial facilities on rain showers with mixed-phased microphysics should be investigated.

3. To extend this study to simulate nimbostratus clouds affected by industrial complexes.

4. To support modelling studies, field experiments on "industrial" clouds are required. Measurements from radar and research aircraft would document the precipitation structures and microphysical regime which are essential for verifying the numerical cloud simulations.

5. Because of concerns about global warming, there is growing interest in radiative properties of clouds. Research on the how industrial pollution changes radiative properties of clouds is thus relevant to the larger climate problem.

References

Auer, A. H., Jr., 1976: Observations of an industrial cumulus. J. Appl. Meteor., 15, 406-413.

Hane, E., 1978: The application of a two-dimensional convective cloud model to waste heat release from proposed nuclear energy centres. Atmos. Environ., 12, 1839-1848.

Hindman E. E. II, P. M. Tag, B. A. Silverman, and P. V., Hobbs, 1977: Cloud condensation nuclei from a paper mill. Part II: Calculated effects on rainfall. J. Appl. Meteor. 16, 753-755.

Koenig, L. R., F. W. Murray, and P. M. Tag, 1978: Differences in atmospheric convection caused by waste energy rejected in the forms of sensible and latent heats. Atmos. Environ., 12, 1013-1019.

Mailhot, J., and C. Chouinard, 1989: Numerical forecasts of explosive winter storms: Sensitivity experiments with a meso-α scale model. Mon. Wea. Rev., 117, 1311-1343.

Murray, F.W., L. R. Koenig, and P. M. Tag, 1978: Numerical simulation of an industrial cumulus and comparison with observations. J. Appl. Meteor., 17, 655-668.

Orville, H. D., P. A. Eckhoff, J. E. Peak, J. H. Hirsch, and F. J. Kopp, 1981: Numerical simulation of the effects of cooling tower complexes on clouds and severe storms. Atmos. Environ., 15, 823-836.

Soong, S., and Y. Ogura, 1973: A comparison between axisymmetric and slab-symmetric cumulus cloud model. J. Atmos., Sci. 30, 879-893.

Stein U., and P. Alpert, 1993: Factor separation in numerical

simulations. J. Atmos. Sci., 50, 2107-2115.

Steiner, J. T., 1982: An axially symmetric cloud model: Development and simulations. Stormy Weather Group, Scientific Report, MW-94, McGill University, 55pp.

Uccellini, L. W., R. A. Petersen, K. F. Brill, P. J. Kocin, and J. J. Tuccillo, 1987: Synergistic interactions between an upper level jet streak and diabatic processes that influence the development of a low-level jet and a secondary coastal cyclone. Mon. Wea. Rev., 115, 2227-2261.

Appendix 1[1]. Sensitivity experiments on different model parameters for the Wood River Sounding

a. The depth (D) of the layer receiving sensible and latent heat

Experiments S1 and S2 are run to examine the role of the depth (D) of the layer receiving the waste energy. S1 is identical with S2 (the control run) except that D is 80 m rather than 40 m (Table 1). Fig. 1 compares the time evolution of peak updraft (w^*) and total liquid water mass (LM) for S1 and S2. Increasing the depth from 40 m to 80 m terminates the formation of precipitation (S1). w^* of S1 gradually increases to near 5 m s^{-1} and remains close to this value as there is no precipitation-induced downdraft and associated cumulus decay. The total liquid water mass of S1 is much less than that of S2 after 30 min. The other cloud variables of S1 are also much smaller than those of S2 (Table 1). Therefore, increasing the effective depth of heat source from 40 m to 80 m, no precipitation takes place and the intensity of the convection is well reduced.

b. The threshold cloud water mixing ratio (β)

The threshold cloud water mixing ratio (β) is the constant in Kessler's (1969) parameterization scheme. It

---

[1] All symbols in this appendix have the same meaning as in chapter 3.

Table 1. Comparison of experiments initialized with the Wood River sounding for different input parameters: The depth of the layer receiving sensible and latent heat (D), threshold cloud water mixing ratio (β), and the ratio of the eddy mixing coefficient for scalars to that for momentum (ν_s/ν_m).

Exp	β g/kg	ν_s/ν_m	D m	w^*_{max} m s^{-1}	KE_{max} GJ	TOP_{max} km	CM_{max} Gg	RM_{max} Gg	AR_{max} Gg	LM_{max} Gg
S1	1.5	3.0	80	5.3	2.4	1.7	0.04	0.02	0.00	0.05
S2[a]	1.5	3.0	40	6.6	5.7	2.5	0.22	0.14	0.41	0.54
S3	0.5	3.0	40	6.3	4.6	2.4	0.19	0.15	0.40	0.53
S4	1.0	3.0	40	6.9	5.4	2.4	0.20	0.12	0.34	0.56
S5[a]	1.5	3.0	40	6.6	5.7	2.5	0.22	0.14	0.41	0.54
S6	1.5	2.0	40	8.0	5.8	2.7	0.25	0.22	0.81	0.97
S7[a]	1.5	3.0	40	6.6	5.7	2.5	0.22	0.14	0.41	0.54

[a] Control case simulation.

determines the autoconversion rate. Previous cloud modelling studies have used a threshold cloud water mixing ratio β = 0.5 g kg^{-1} or 1.0 g kg^{-1}. We use β = 1.5 g kg^{-1} for our control run as Hill (1977) did. Three numerical experiments (S3, S4, and S5) are run in which β is 0.5, 1.0, and 1.5 g kg^{-1}, respectively. The numerical results are summarized in Table 1 and Fig. 2. All w^* are the same during first 22 min and thereafter vary in a similar way. A small value β results in early precipitation. The time evolutions of LM for three runs are also similar. Table 1 shows that differences of maxima of the cloud variables for S3, S4, and S5 (the control run) are quite small. This indicates that the model results depend only marginally on the chosen threshold cloud water mixing ratio used in Kessler's microphysical parameterization scheme.

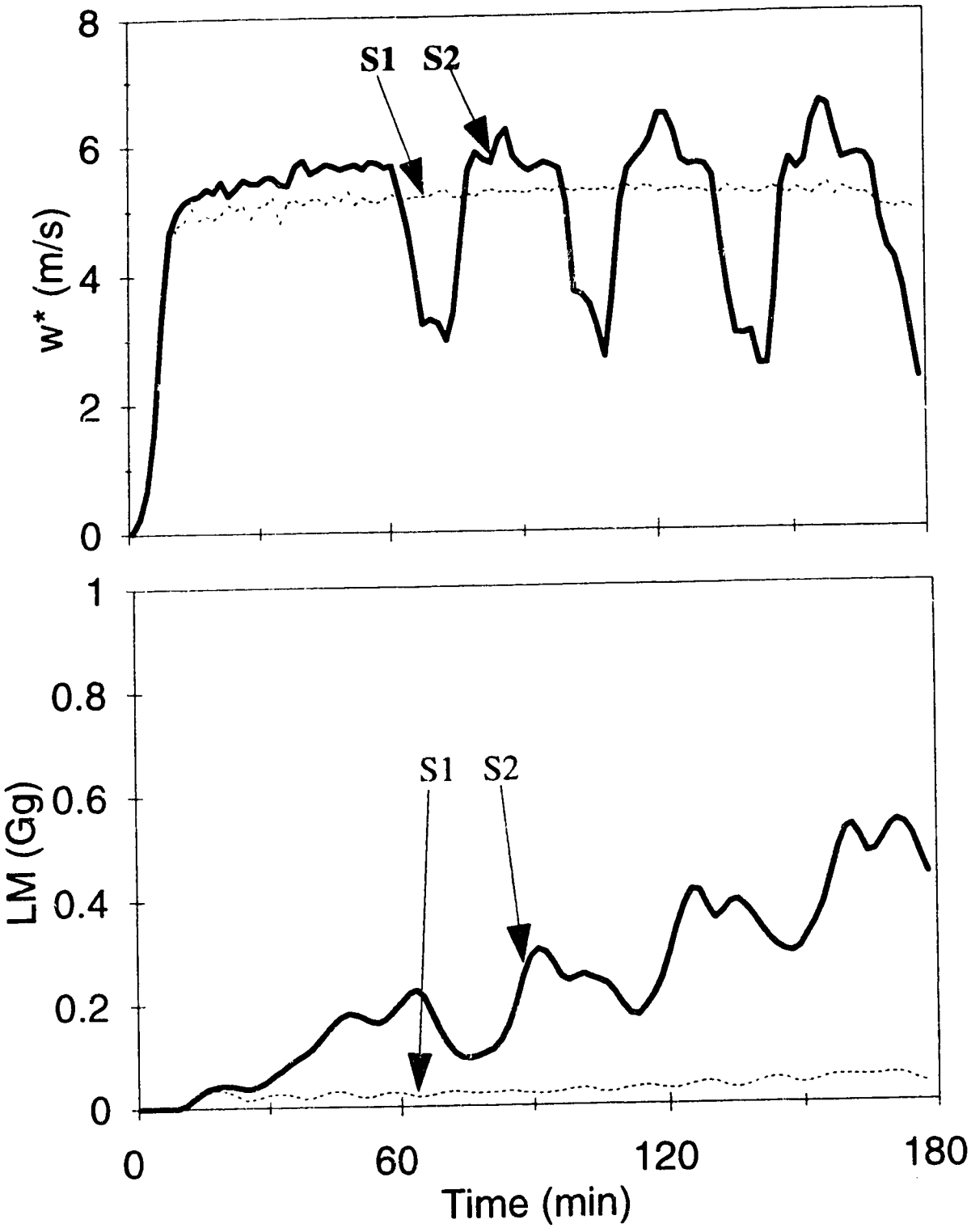

Fig. 1. Comparison of the evolution of w^* and LM for experiments S1 and S2. The depth of the layer receiving sensible and latent heat (D) is 80 m for S1 and 40 m for S2.

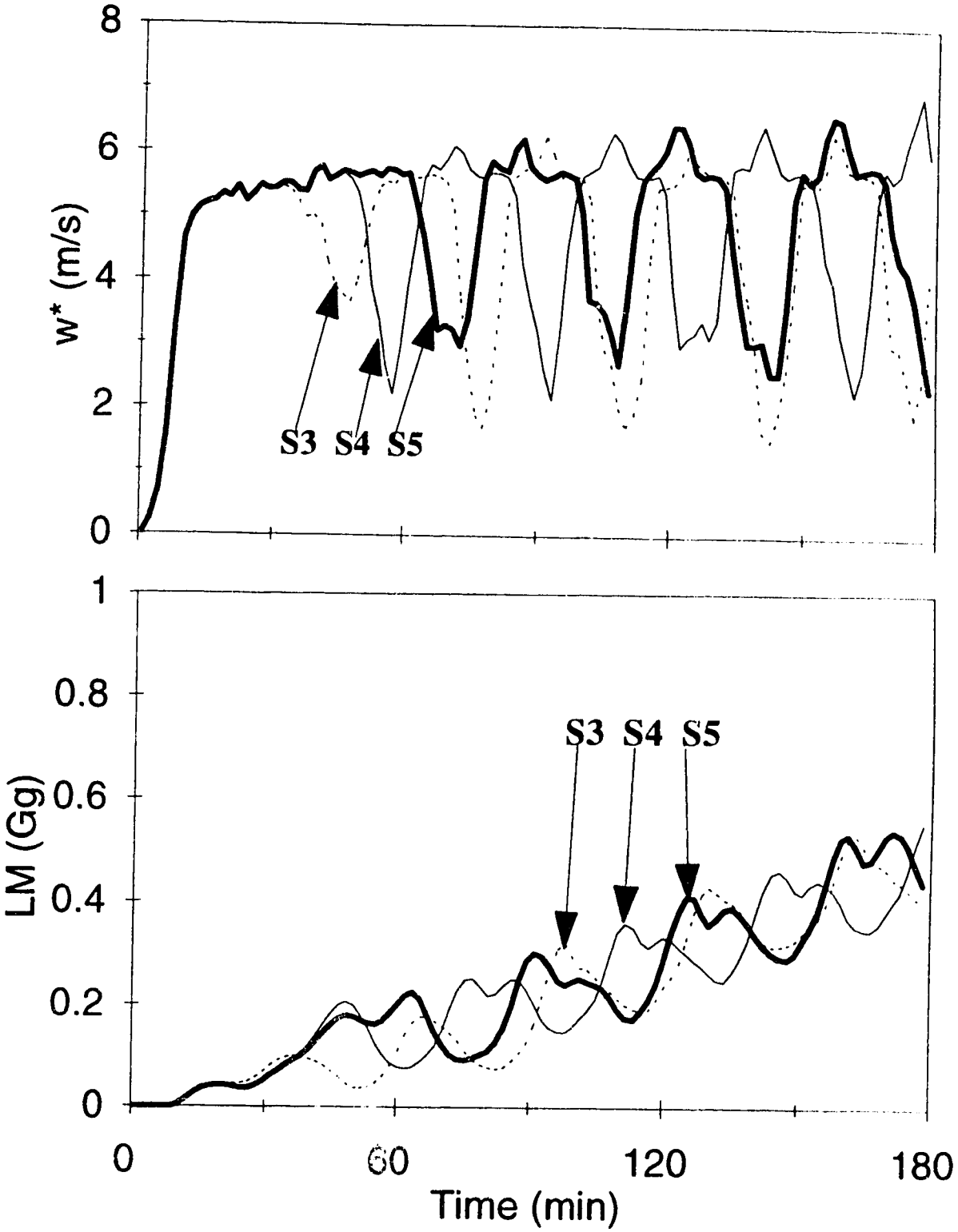

Fig. 2. Comparison of the evolution of w* and LM for experiments S3 to S5 that differed in their β values being 0.5 (S3), 1.0 (S4) and 1.5 (S5).

c. The ratio of the eddy mixing coefficient for scalars to that for momentum (ν_s/ν_m)

To test how the model responds to the magnitude of the eddy mixing coefficient for scalars, experiments S6 is run differing from the control case simulation (S7) only in that the scalar eddy mixing coefficient is smaller than that of S7. Comparison of S6 with S7 shows that the smaller scalar eddy mixing causes a stronger peak updraft and a larger total liquid water mass (Fig.3). The other cloud variables of S6 are also larger than those of S7 (Table). Clearly, the simulation results depend on the magnitude of scalar eddy mixing coefficient, but the effects are quite small compared with those of the depth of the layer receiving heat energy.

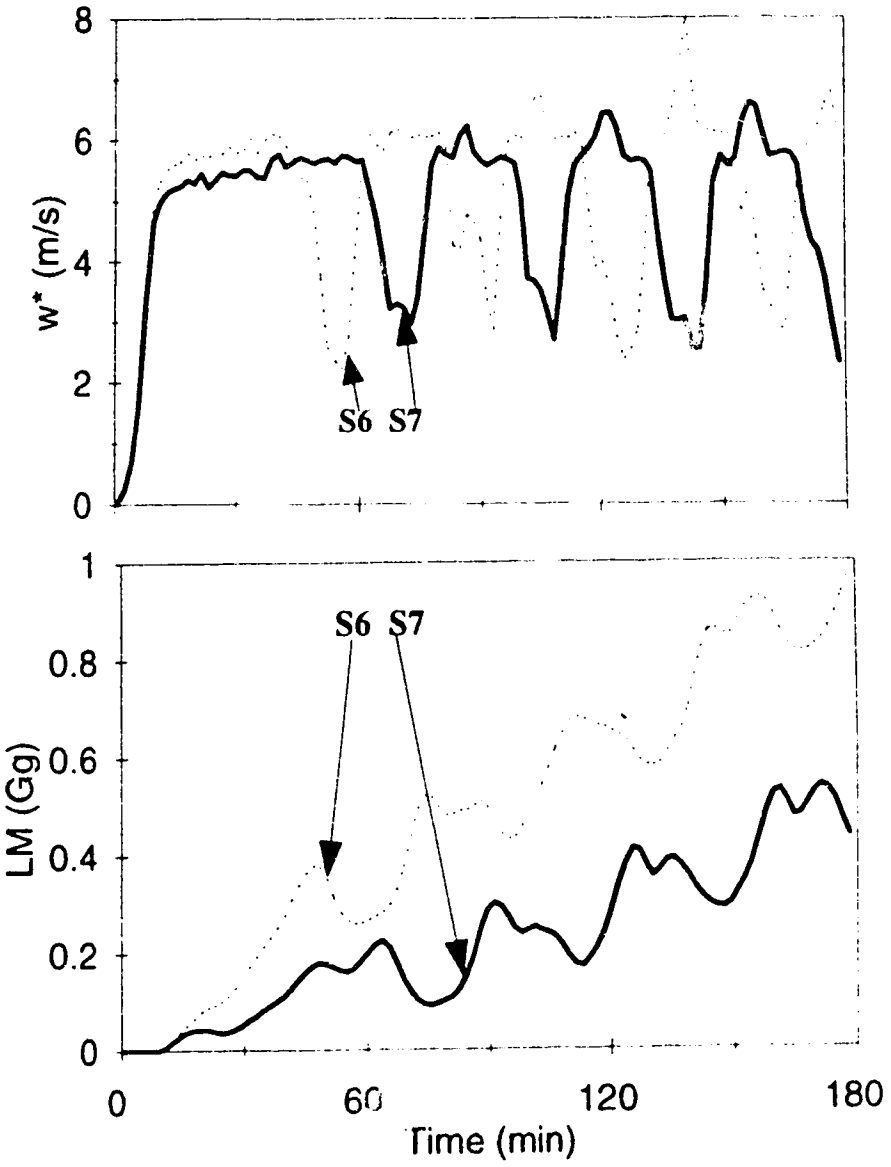

Fig. 3. Comparison of the evolution of w* and LM for the tropical experiments T5 to T9 that differed in their H_s/H_l values being 1.0 (T5), 0.8 (T6), 0.6 (T7), 0.4 (T8) and 0.2 (T9).

Appendix 2[1]. Graphs of time evolution of selected cloud parameters for the tropical sounding

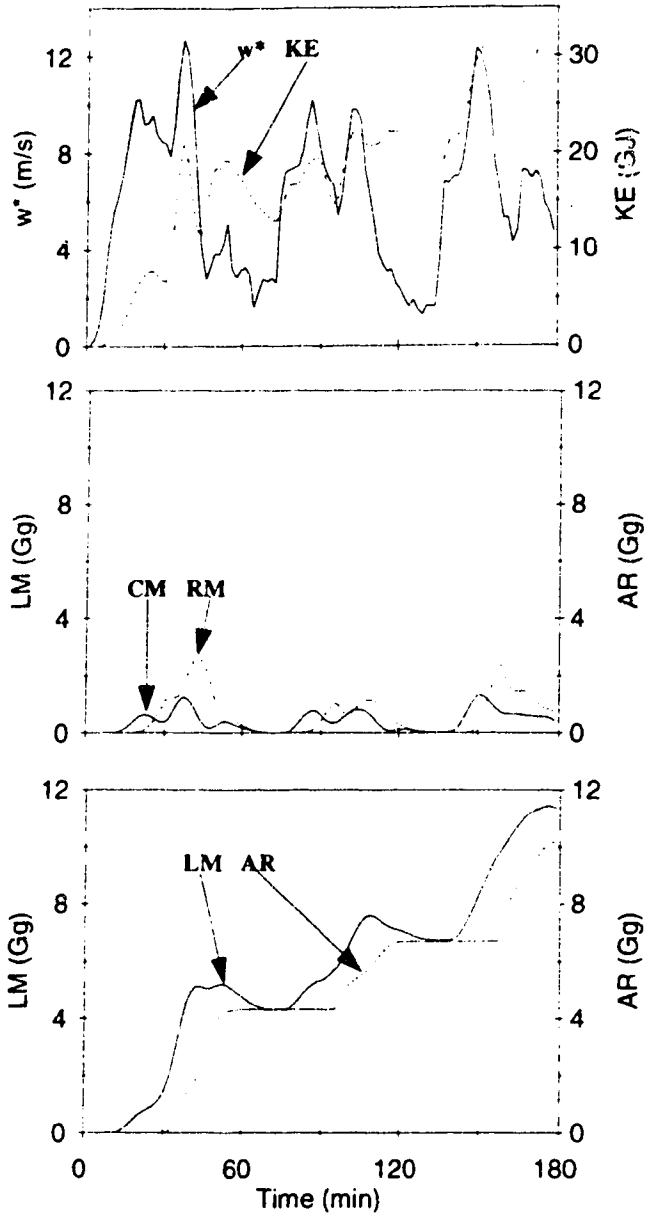

Fig. 1. Time evolution of the control run for the tropical sounding depicting peak updraft (w^*) and total kinetic energy (KE), total mass of cloud (CM) and rain (RM), and total mass of liquid water (LM) and accumulated rain at the surface (AR).

[1] All symbols in this appendix have the same meaning as in chapter 3.

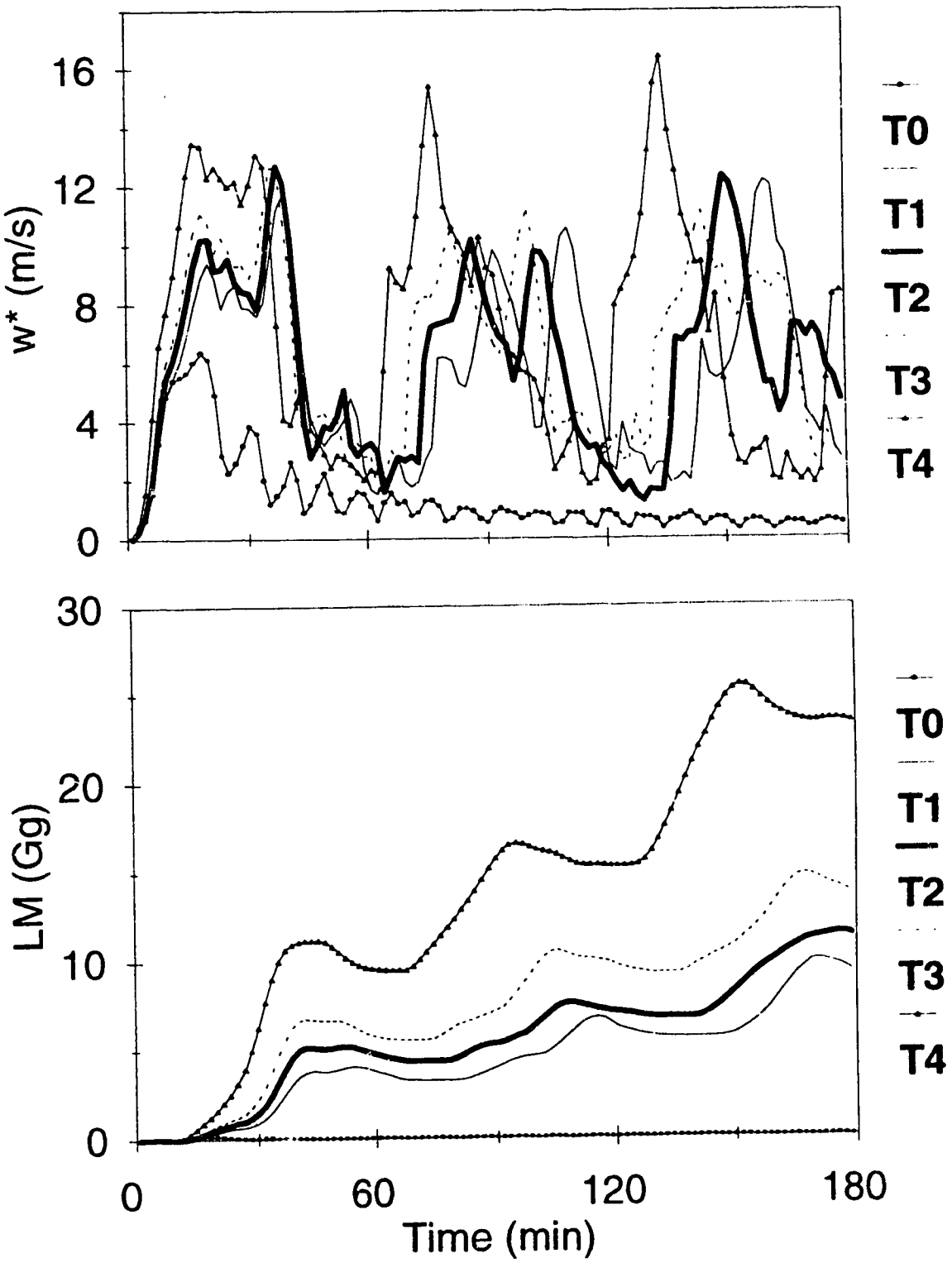

Fig. 2. Peak vertical updraft, w^*, and total liquid water mass, LM, plotted versus time for the tropical experiments T0 to T4. The H_c values were 0.0 GW (T0), 0.8 GW (T1), 1.0 GW (T2), 1.2 GW (T3) and 2.0 GW (T4).

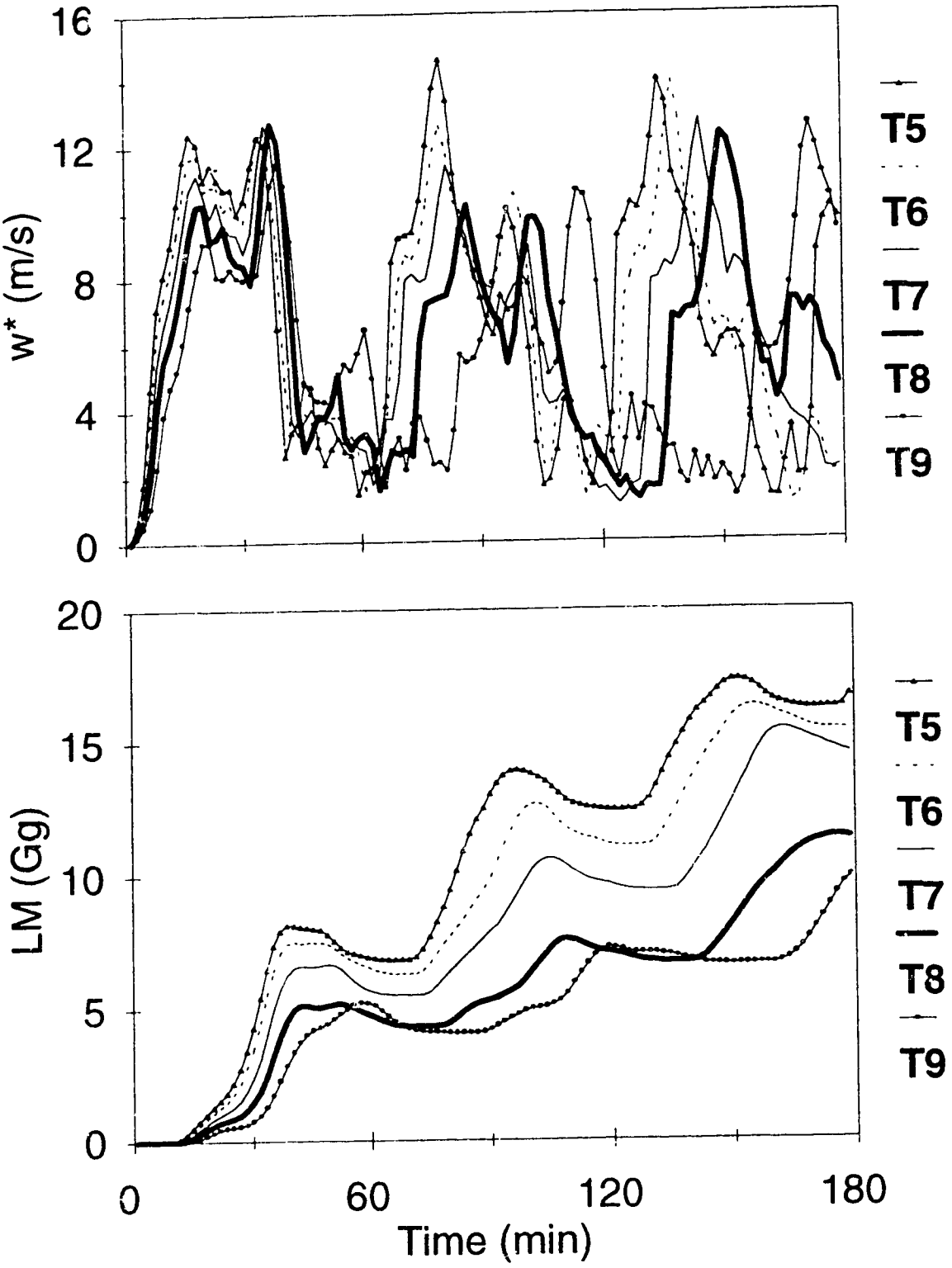

Fig. 3. Comparison of the evolution of w^* and LM for the tropical experiments T5 to T9 that differed in their H_s/H_t values being 1.0 (T5), 0.8 (T6), 0.6 (T7), 0.4 (T8) and 0.2 (T9).

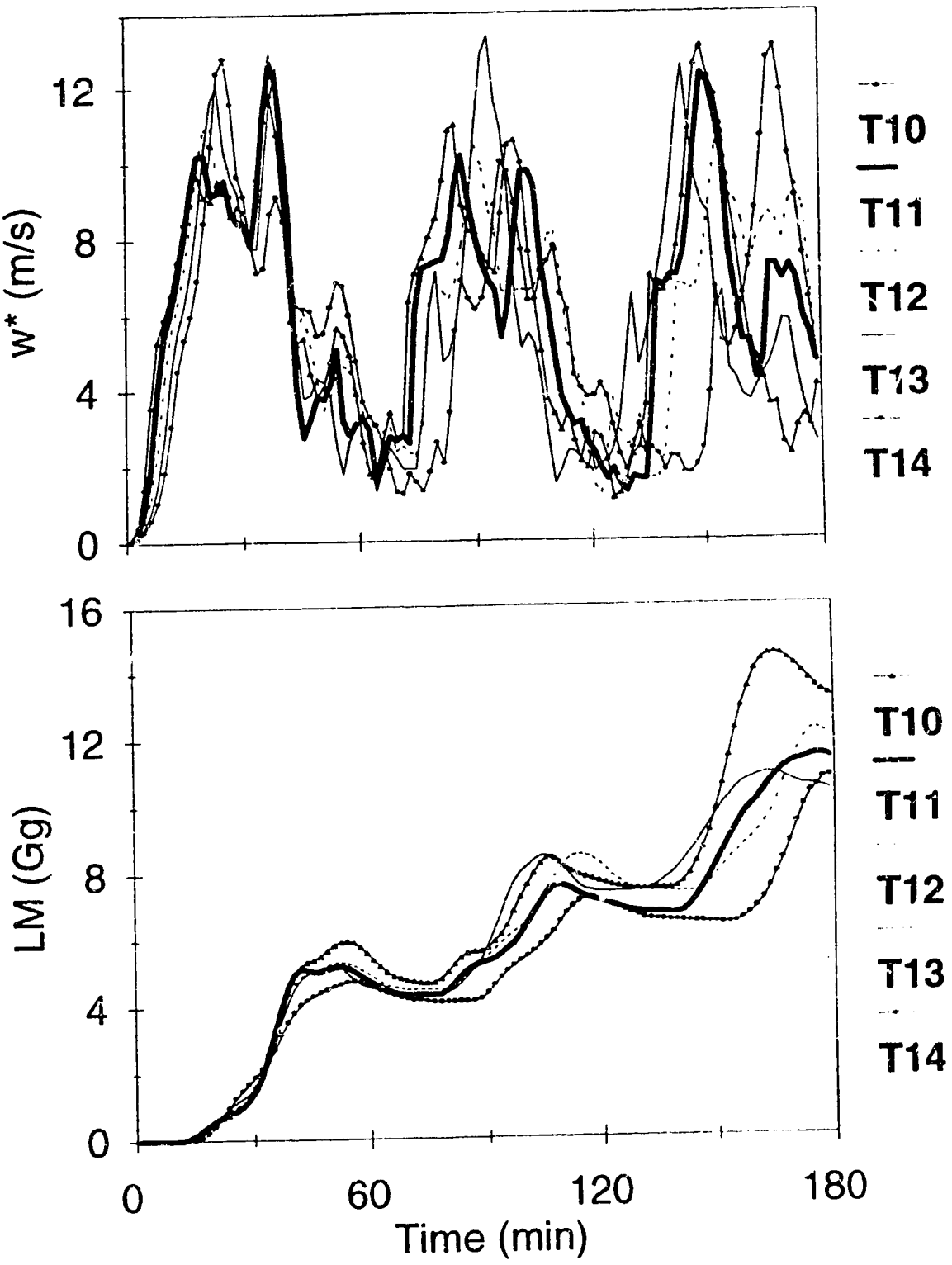

Fig. 4. Comparison of the evolution of w* and LM for the tropical experiments T10 to T14 differing in their source radius, b: 200 m (T10), 250 m (T11), 300 m (T12), 350 m (T13) and 400 m (T14).

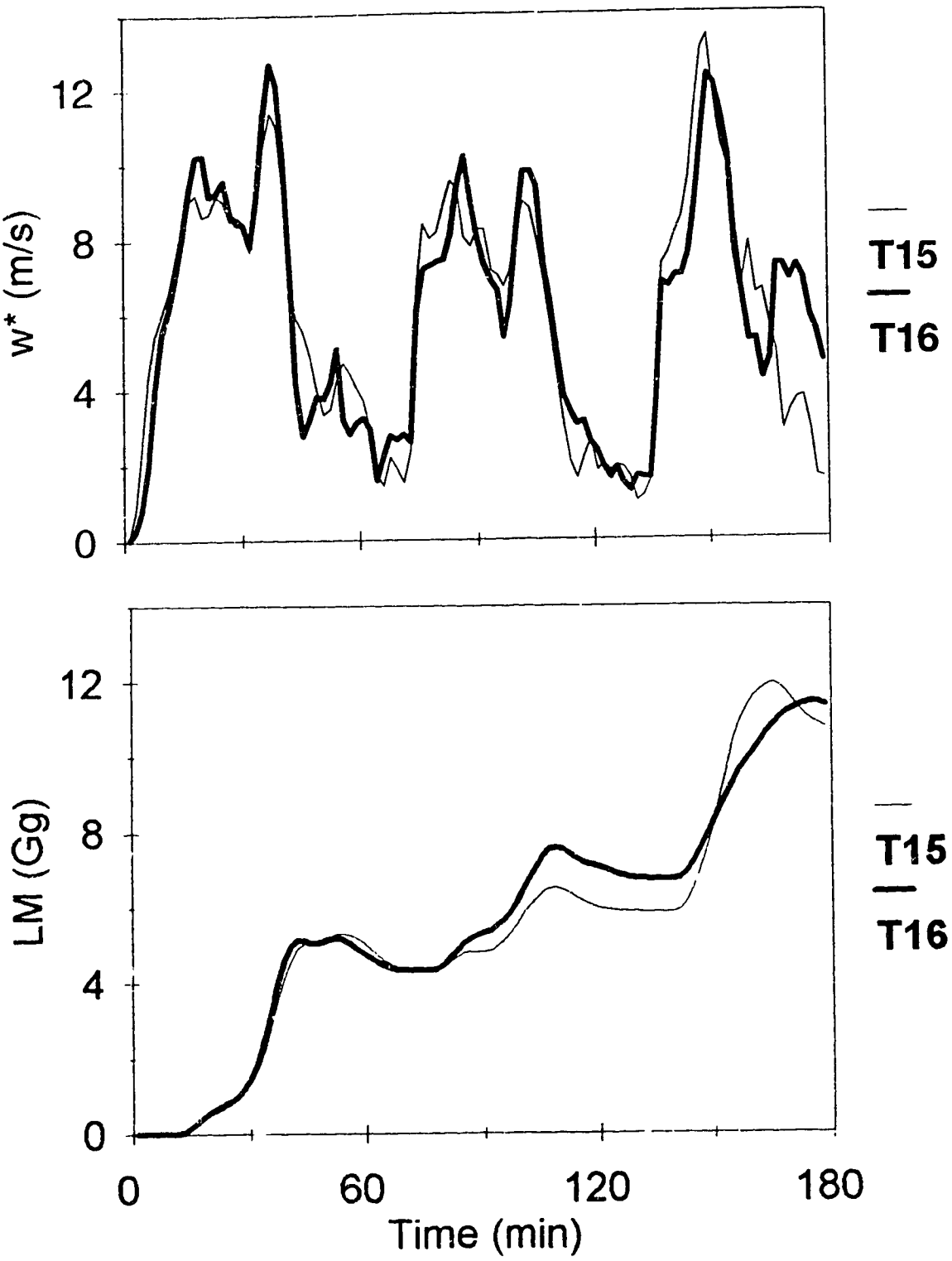

Fig. 5. Comparison of the evolution of w^* and LM for the tropical experiments T15 and T16. In T15 the sensible and latent heat fluxes were decreased linearly with increasing radius from the centre to become zero when r=b, whereas in the control case T16 the fluxes have a top-hat profile with uniform distribution for all r<b.

Appendix 3[1]. The model parameters and data from the factor analysis for the low pollution case

Table 1. Comparison of input data and selected results for sensitivity experiments of the low pollution case.

Exp	N_c cm^{-3}	ν	Sup %	AR_{max} Gg	CM_{max} Gg	RM_{max} Gg	KE_{max} GJ	w^*_{max} m s^{-1}
LP	430	0.62	0.2	8.240	3.940	9.000	179.2	17.80
NP	239	0.50	0.4	8.226	3.845	8.952	179.0	17.57
NS	430	0.62	0.4	7.855	3.825	8.673	177.1	18.16
ND	239	0.50	0.2	8.075	3.788	8.627	173.0	18.12

Table 2. Selected results of factor analysis for the low pollution case.

	f	f_D	f_S	f_M
AR_{max}	0.4	-4.5	-1.8	6.5
CM_{max}	2.5	-0.5	-1.5	4.5
RM_{max}	0.5	-3.1	-3.6	7.3
KE_{max}	0.1	-1.0	-3.3	4.5

[1] All symbols in this appendix have the same meaning as in chapter 4.